UNIVERSITÀ DEGLI STUDI DI MILANO

SCUOLA DI DOTTORATO IN SCIENZE E TECNOLOGIE CHIMICHE

DIPARTIMENTO DI SCIENZE FARMACEUTICHE

CORSO DI DOTTORATO IN CHIMICA DEL FARMACO

CICLO XXVI

TRANSDERMAL AND TRANSMUCOSAL PHARMACEUTICAL DOSAGE FORMS FOR PALLIATIVE CARE IN CANCER THERAPY

SETTORE CHIM/09 FARMACEUTICO TECNOLOGICO APPLICATIVO

dott. UMBERTO MARIA MUSAZZI

Matricola: R09050

Tutor: prof.ssa PAOLA MINGHETTI

Coordinatore del dottorato: prof. ERMANNO VALOTI

ANNO ACCADEMICO
2012/2013

Γνῶθι σεαυτόν

Table of contents

Preface

Pain is recognized as one of the most distressing cancer-related syndromes and treatment side effects and is linked to decreased quality of life among patients. Despite the improvements of pain management guidelines proposed in the last decades, therapeutic issues are still unsolved, above all in the treatment of loco-regional painful symptoms. For example, a proper pharmacological therapy to treat cisplatin-induced ototoxicity is not currently available. Pain associated to cutaneous wounds is treated by an off-label use of systemic analgesics with high incidence of related side effects. Conventional dosage forms applied in the buccal cavity are unable to achieve suitable efficacy in the case of oral mucositis.

Hence, there is a need to design novel drug delivery systems, which can be easily used in the clinical practice for an effective treatment of loco-regional painful syndromes.

This doctoral thesis aimed to investigate the critical aspects of drug delivery correlated to three loco-regional syndromes and propose technological solutions to rationalize drug delivery. In particular, the experimental work focused on:

(1) the development of a mucoadhesive microparticle suspension intended for treating oral mucositis and designed to combine the peculiarities of prolonged release mucoadhesive systems with those of an immediate release oromucosal solution;

(2) the optimization of a biodegradable nanoparticle system intended to deliver resveratrol to cochlea in the therapy of cisplatin-induced ototoxicity;

(3) the rationalization of the use of morphine derivatives, according to their chemical structure, in the management of cutaneous painful syndromes.

1 General introduction

The prevalence of cancer has been enlarged worldwide both for the increase of population age and for the diffusion of unhealthy behavior (*e.g.,* smoking). Moreover, the development of effective cancer treatments has also increased the 5-year survival of patients, since some cancer types have become chronic [1, 2]. Pain is one of the main symptoms of cancer, especially in advanced and incurable states. Indeed, more than 50% of all patients suffer for painful cancer-related syndromes [3]. Therefore, pain management is the central goal of care to ensure an acceptable patient quality of life. The etiology of pain is very wide: painful syndromes might be caused by cancer itself, cancer-related symptoms, concurrent disorder or side effects related to anticancer treatments [4]. Furthermore, pain manifestations might be systemic or loco-regional.

The World Health Organization (WHO) has introduced specific guidance for palliative care [4]. According to the WHO, "palliative care is an approach that improves the quality of life of patients and their families facing the problem associated with life-threatening illness, through the prevention and relief of suffering by means of early identification and impeccable assessment and treatment of pain and other problems, physical, psychosocial and spiritual" [5]. In order to achieve acceptable pain management, the WHO suggests that clinical protocols should be based on a 3-step "analgesic ladder" [4]. The analgesic drugs are chosen according to the scale of pain severity. NSAIDs are preferred for treating mild pain, but moderate and severe pain requires potent analgesics as opioids. Although good effectiveness in controlling acute and chronic pain, the onset of related side effects (*e.g.,* sedation, nausea, constipation and fatigue) negatively affects the risk-benefit assessment of opioid-based treatments.

In general, available therapeutic strategies for systemic drug delivery have been based on oral, transdermal and parenteral dosage forms (*e.g.,* solutions, suspensions, tablets and transdermal patches) [6]. For the management of loco-regional symptoms, the development of locally acting drug products have also been developed and marketed. However, many of them are liquid and semisolid dosage forms, which are not optimized for drug absorption through physiological barriers such as buccal mucosa and skin. Even if many analgesic drugs and dosage forms are available in the market, therapeutic failure

has been widely reported in literature [7]. In many cases, undertreated pain has been caused by low patient compliance and onset of drug side effects [8].
In particular, therapeutic failures are more frequent in the treatment of loco-regional painful symptoms. On the top of that, pharmacological solutions were often absent, based on off-label use of systemic analgesics or conventional dosage forms with unsatisfactory bioavailability.

To improve the clinical effectiveness and patient's compliance, the development of novel drug delivery systems intended for specific locoregional drug delivery might be challenging. For example, oral mucositis (OMs) are a critical side effect to treat. Induced by chemo- or radiotherapy, OMs might affect oral intake, maintenance of oral hygiene and quality of life of patient [9]. Many of the pharmacological treatments available on the market are drug solutions or other immediate release dosage forms. Such dosage forms might be ineffective for guaranteeing high drug bioavailability, since the short absorption window due to the physiological swallowing. Consequently, clinical protocols require high doses and regimen increasing the systemic side effect incidence.

On the other hand, Food and Drug Administration (FDA) and European Medicines Agency (EMA) have not yet authorized drug products for preventing or treating the ototoxicity induced by cisplatin [10]. Indeed, conventional dosage forms cannot guarantee reproducible drug concentration at the active site, because of the small distribution volume of cochlea.

Finally, cutaneous painful symptomatology (*e.g.*, post herpetic neuralgia, cutaneous lesions) are also critical. The discovery of opioid receptor in skin epidermis has increased the off-label use of topical opioids [11]. However, the effectiveness of such treatments has not been well demonstrated, especially for the empirical selection of drug and delivery systems.

1.1 Aim of the work

This doctoral thesis aimed to investigate and propose technological solutions for rationalizing drug delivery in three cancer- and treatment-related syndromes. In particular, the experimental work focused on: (1) the development of a mucoadhesive formulation intended for prolonged drug absorption in the buccal cavity; (2) the optimization of a nanoparticle system intended for drug delivery to cochlea; (3) the study of influence of chemical structure on the dermal and transdermal delivery of morphine derivatives. Such a rationalization was focused on identifying the best opioid candidate for skin penetration among the morphine derivatives used in therapy.

1.1.1 Mucoadhesive mouthwash intended for the treatment of oral mucositis induced by chemo- and radiotherapy

OMs are one of the side effects of anticancer treatment that badly affects the patient quality of life [12]. Indeed, most of the drugs used in cancer chemotherapy are toxic for rapidly dividing mucosal cells, thus inducing a loco-regional inflammation and epidermal damage. In particular, OMs are generally associated with head and neck cancer chemo- and radiotherapy. The overall incidence ranges from 40% to 76%. OMs induce pain, limitations to oral intake, high incidence of secondary infection and risk of systemic septicemia [13]. Therefore, several therapeutic protocol, including basic oral care interventions [14], administration of anti-inflammatory agents [15], antimicrobials, mucosal coating agents, anesthetics and analgesics [9], have been proposed for preventing or treating OMs.

However, few of them have been proven efficacy in reducing the severity and duration of OMs, since most of the clinical studies have been contradictory or carried out with inadequate methodologies. Moreover, the selection of drug delivery systems has not been rationalized according both the pharmacokinetic limitations of buccal cavity and the patient's compliance. For example, topical applied drug solutions (*e.g.*, lidocaine mouthwashes) were reported to ensure a very short-lived pain relief. On the other side, the use of systemic analgesic drugs (*e.g.*, fentanyl transdermal patch) is related to systemic side effects.

The development of a prolonged release dosage forms might be useful to improve the patient's compliance and treatment efficacy. For an efficient drug delivery system, the

adhesion to the mucous layer on the surface of buccal cavity should be carefully considered to improve the drug absorption. The polymer selection is critical to achieve suitable mucoadhesion, since it is a complex phenomenon that may be considered as the result of electrostatic, Van de Waal's interactions between polymer chain and mucosa proteins (*e.g.*, mucin) [16].

Therefore, prolonged release mouthwashes were designed by preparing mucoadhesive microparticles in aqueous suspension (**Chapter 2**). The feasibility was investigated by preparing different formulations containing three model drugs, namely clobetasol, flurbiprofen and delmopinol. The formers were selected for their clinical effectiveness in treating OMs and other inflammatory conditions of buccal cavity. Delmopinol was chosen to verify the effectiveness of this technological platform as supportive treatment for limiting secondary bacterial infection in OMs patients. The mucoadhesive microparticles were made by spraying polymeric solutions containing the three model drugs in a cross-linking bath. Alginates were used as functional excipient of microparticles and bivalent cations were added as cross-linking agents [17]. Poly-acrylates were added for increasing microparticle mucoadhesion. The effects of microparticle composition and manufacturing parameters on *in vitro* performances of clobetasol mucoadhesive mouthwash were evaluated using a full-factorial design (**Chapter 3**). The ability of proposed technological platforms to improve the drug penetration into the buccal mucosae were studied by a wash-off method [18]. The *in vitro* ability to avoid and/or reduce the plaque development was also assayed in case of delmopinol formulations.

1.1.2 Nano-delivery system intended for treating ototoxicity induced by chemotherapeutic agents

Cisplatin is frequently used as chemotherapeutic agent for the treatment of several cancer types. However, its clinical effectiveness has been correlated with severe side effects, such as ototoxicity [10]. The ototoxic effect of cisplatin is particularly critical in children, because of their higher susceptibility in comparison with adults [19]. In this case, the ototoxicity might seriously prejudice speech skill, language and social development of young patients [20]. For instance, great efforts have been devoted to understand the mechanism of drug-induced ototoxicity and suggest some prevention strategies. *In vivo*

and *in vitro* studies showed that cisplatin induces apoptosis in cochlear cell lines (*e.g.*, hair cells, *Strial Ganglion* cells and *Stria Vascularis* cells) [21, 22], increasing the intracellular concentration of reactive oxygen species [23]. Therefore, the efficacy of several antioxidant agents have been tested after local and systemic delivery [24, 25]. Nonetheless, the simultaneous administration of some antioxidant agents (*e.g.*, sodium thiosulfate) decreased the therapeutic effect of cisplatin due to a direct molecular interaction, thus limiting their systemic administration [10].

According to the peculiarity of the cochlear system, the development of a drug delivery has been very challenging for pharmacokinetic issues after both systemic and local administration. Indeed, the small dimension of the cochlea does not allow achieving suitable drug concentrations in the target site without increasing its systemic doses. On the other hand, the local delivery was affected by low drug bioavailability and high intra-patient variability (*e.g.*, tympanic delivery route). Moreover, high-specialized medical devices and expertise are required for intra-tympanic or intra-cochlear drug delivery [26].

The recent improvements in nanotechnology could overcome the pharmacokinetic and physicochemical drawbacks, thus delivering the drug directly to target tissues or cell lines. Therefore, the properties of nanoparticle systems should be carefully selected according to the therapeutic target. In particular, the nanoparticle morphology, the surface properties, cellular uptake mechanism, the drug release profile should be deeply investigated in order to optimize drug delivering and avoiding toxic effect induced by the nanocarrier itself [27].

Resveratrol-loaded nanoparticles were developed and optimized to obtain nanoparticle with reproducible morphology and high drug loading (**Chapter 4**). Since it was known that freeze-drying process affects the physical stability of nanosystems [28], the effect of well-known cryoprotectants was also evaluated. Finally, the toxicity of proposed nanosystems was checked *in vitro* using a model of organ of Corti cells and a S*tria Vascularis* one.

1.1.3 Dermal and transdermal delivery of morphine derivatives: a qualitative structure-penetration relationship

Opioids have been widely used for managing several kinds of acute and chronic painful syndromes [29]. Their pharmacological action (*e.g.*, central analgesia) or related side effects (*e.g.*, constipation) are related to the activation of G protein-coupled receptors widely distributed in brain, spinal cord and digestive tract.

Recently, opioid receptors were also discovered in the human skin [30]. In addition to the regulation of peripheral nociceptive signaling, cutaneous opioid receptors are involved in the keratinocyte proliferation, differentiation and the pigmentation process. These receptors might also modulate the immunity response of skin immune cells [31]. Therefore, recent clinical studies reported the efficacy of opioid in the treatment of peripheral painful syndromes, such as post herpetic neuralgia [32], regeneration of cutaneous lesions and pain controlling in wounds [33].

Although these cutaneous lesions are very painful, the use of potent analgesic is still limited. Indeed, the systemic administration of opioids is complicated by the unpredictable drug cutaneous bioavailability due to the inflammation process [34]. Therefore, topical opioids (*e.g.*, morphine gels) have been widely studied for treating cutaneous painful syndromes to guarantee high drug concentration at therapeutic site and negligible systemic absorption [34]. However, their effectiveness has been strongly affected by the drug ability to diffuse through the skin barrier [11]. In order to obtain a local effect in the skin, morphine derivatives have to permeate through the stratum corneum and concentrate in the viable epidermis.

Despite the increase of clinical interest, the cutaneous absorption of morphine and its active derivatives has not been deeply investigated. Published studies are limited to fentanyl [35, 36] and buprenorphine [37]. Moreover, the available literature reports that morphine and its derivatives poorly permeated the human epidermis. According to the results obtained by Roy et al., the *in vitro* flux of morphine, hydromorphone and codeine was lower than 0.1 µg/cm^2/h through human cadaver skin [38], where the fluxes fentanyl and buprenorphine were 40-fold higher [39].

These evidences allowed speculating that small modifications on chemical structure of morphine derivatives have a great influence on their permeation profiles. For example,

the introduction of a methoxyl group induced a 15-fold increase in the permeation profile of codeine in comparison with morphine [38]. Furthermore, Wang et al. suggested that esterification of the hydroxyl group on morphine phenolic ring could improve the drug permeation though nude/hairless mouse skin [40], because of an increase of drug lipophilicity. In particular, most of the models used have demonstrated the correlation between the drug lipophilicity (log *P*) and molecular weight to its diffusion through the human skin [41]. However, such models lost robustness in describing the permeation of a small dataset of molecules and other electrochemical descriptors have been proposed [42]. Furthermore, the drug retention in the human skin has not been widely investigated. On the best of our knowledge, only few authors tried modelling the skin retention of a specific class of molecules, like corticosteroids [43, 44].

Considering the clinical need to find effective treatments for managing loco-regional painful syndromes and for avoiding systemic side effect, the influence of chemical structure of eight well-known morphine derivatives was evaluated in terms of skin permeation and retention (**Chapter 5**). Statistical analyses were carried out to test the effect of four substituents (*i.e.*, 3-methoxyl, 6-carbonyl, 14-hydroxyl, 7,8-didehydro) on molecule penetration through human epidermis.

1.2 References

[1] Sedjo, R. L., Byers, T., Barrera, E., Jr., Cohen, C., Fontham, E. T., Newman, L. A., Runowicz, C. D., Thorson, A. G., Thun, M. J., Ward, E., Wender, R. C., and Eyre, H. J., 2007, "A midpoint assessment of the American Cancer Society challenge goal to decrease cancer incidence by 25% between 1992 and 2015," CA Cancer J. Clin., 57(6), pp. 326-340.

[2] Schottenfeld, D., Beebe-Dimmer, J. L., Buffler, P. A., and Omenn, G. S., 2013, "Current perspective on the global and United States cancer burden attributable to lifestyle and environmental risk factors," Annu. Rev. Public Health, 34, pp. 97-117.

[3] van den Beuken-van Everdingen, M. H., de Rijke, J. M., Kessels, A. G., Schouten, H. C., van Kleef, M., and Patijn, J., 2007, "Prevalence of pain in patients with cancer: a systematic review of the past 40 years," Ann. Oncol., 18(9), pp. 1437-1449.

[4] WHO, 1996, Cancer Pain Relief: with a guide to opioid availability, Geneva.

[5] WHO, 2013, "WHO definition of palliative care," http://www.who.int/cancer/palliative/definition/en/.

[6] Comerford, D., 2008, "Techniques of opioid administration," Anaesthesia & Intensive Care Medicine, 9(1), pp. 21-26.

[7] Deandrea, S., Montanari, M., Moja, L., and Apolone, G., 2008, "Prevalence of undertreatment in cancer pain. A review of published literature," Ann. Oncol., 19(12), pp. 1985-1991.

[8] Zuccaro, S., Vellucci, R., Sarzi-Puttini, P., Cherubino, P., Labianca, R., and Fornasari, D., 2012, "Barriers to Pain Management," Clin. Drug Investig., 32(1), pp. 11-19.

[9] Saunders, D. P., Epstein, J. B., Elad, S., Allemano, J., Bossi, P., van de Wetering, M. D., Rao, N. G., Potting, C., Cheng, K. K., Freidank, A., Brennan, M. T., Bowen, J., Dennis, K., and Lalla, R. V., 2013, "Systematic review of antimicrobials, mucosal coating agents, anesthetics, and analgesics for the management of oral mucositis in cancer patients," Support. Care Cancer, 21(11), pp. 3191-3207.

[10] Rybak, L. P., Whitworth, C. A., Mukherjea, D., and Ramkumar, V., 2007, "Mechanisms of cisplatin-induced ototoxicity and prevention," Hear. Res., 226(1–2), pp. 157-167.

[11] Farley, P., 2011, "Should topical opioid analgesics be regarded as effective and safe when applied to chronic cutaneous lesions?," J. Pharm. Pharmacol., 63(6), pp. 747-756.

[12] Raber-Durlacher, J. E., Weijl, N. I., Abu Saris, M., de Koning, B., Zwinderman, A. H., and Osanto, S., 2000, "Oral mucositis in patients treated with chemotherapy for solid tumors: a retrospective analysis of 150 cases," Support. Care Cancer, 8(5), pp. 366-371.

[13] Sonis, S. T., 1998, "Mucositis as a biological process: a new hypothesis for the development of chemotherapy-induced stomatotoxicity," Oral Oncol., 34(1), pp. 39-43.

[14] McGuire, D. B., Fulton, J. S., Park, J., Brown, C. G., Correa, M. E., Eilers, J., Elad, S., Gibson, F., Oberle-Edwards, L. K., Bowen, J., and Lalla, R. V., 2013, "Systematic review of basic oral care for the management of oral mucositis in cancer patients," Support. Care Cancer, 21(11), pp. 3165-3177.

[15] Nicolatou-Galitis, O., Sarri, T., Bowen, J., Di Palma, M., Kouloulias, V. E., Niscola, P., Riesenbeck, D., Stokman, M., Tissing, W., Yeoh, E., Elad, S., and Lalla, R. V., 2013, "Systematic review of anti-inflammatory agents for the management of oral mucositis in cancer patients," Support. Care Cancer, 21(11), pp. 3179-3189.

[16] Gu, J. M., Robinson, J. R., and Leung, S. H., 1988, "Binding of acrylic polymers to mucin/epithelial surfaces: structure-property relationships," Crit. Rev. Ther. Drug Carrier Syst., 5(1), pp. 21-67.

[17] Chan, L., Jin, Y., and Heng, P., 2002, "Cross-linking mechanisms of calcium and zinc in production of alginate microspheres," Int. J. Pharm., 242(1-2), pp. 255-258.

[18] Rao, K. V. R., and Buri, P., 1989, "A novel in situ method to test polymers and coated microparticles for bioadhesion," Int. J. Pharm., 52(3), pp. 265-270.

[19] Knight, K. R., Kraemer, D. F., and Neuwelt, E. A., 2005, "Ototoxicity in children receiving platinum chemotherapy: underestimating a commonly occurring toxicity that may influence academic and social development," J. Clin. Oncol., 23(34), pp. 8588-8596.

[20] Ruggiero, A., Trombatore, G., Triarico, S., Arena, R., Ferrara, P., Scalzone, M., Pierri, F., and Riccardi, R., 2013, "Platinum compounds in children with cancer: toxicity and clinical management," Anticancer Drugs, 24(10), pp. 1007-1019.

[21] Sluyter, S., Klis, S. F., de Groot, J. C., and Smoorenburg, G. F., 2003, "Alterations in the stria vascularis in relation to cisplatin ototoxicity and recovery," Hear. Res., 185(1-2), pp. 49-56.

[22] Alam, S. A., Ikeda, K., Oshima, T., Suzuki, M., Kawase, T., Kikuchi, T., and Takasaka, T., 2000, "Cisplatin-induced apoptotic cell death in Mongolian gerbil cochlea," Hear. Res., 141(1–2), pp. 28-38.

[23] Dehne, N., Lautermann, J., Petrat, F., Rauen, U., and de Groot, H., 2001, "Cisplatin ototoxicity: involvement of iron and enhanced formation of superoxide anion radicals," Toxicol. Appl. Pharmacol., 174(1), pp. 27-34.

[24] Rybak, L. P., Whitworth, C., and Somani, S., 1999, "Application of antioxidants and other agents to prevent cisplatin ototoxicity," Laryngoscope, 109(11), pp. 1740-1744.

[25] Wimmer, C., Mees, K., Stumpf, P., Welsch, U., Reichel, O., and Suckfull, M., 2004, "Round window application of D-methionine, sodium thiosulfate, brain-derived neurotrophic factor, and fibroblast growth factor-2 in cisplatin-induced ototoxicity," Otol. Neurotol., 25(1), pp. 33-40.

[26] Swan, E. E. L., Mescher, M. J., Sewell, W. F., Tao, S. L., and Borenstein, J. T., 2008, "Inner ear drug delivery for auditory applications," Adv. Drug Deliv. Rev., 60(15), pp. 1583-1599.

[27] FDA, 2011, "Investigation of Potential Toxic Effects of Engineered Nanoparticles and Biologic Microparticles in Blood and Their Biomarker Applications," http://www.fda.gov/BiologicsBloodVaccines/ScienceResearch/BiologicsResearchAreas/ucm127045.htm.

[28] Abdelwahed, W., Degobert, G., Stainmesse, S., and Fessi, H., 2006, "Freeze-drying of nanoparticles: formulation, process and storage considerations," Adv. Drug Deliv. Rev., 58(15), pp. 1688-1713.

[29] Barnett, M., 2001, "Alternative opioids to morphine in palliative care: A review of current practice and evidence," Postgrad. Med. J., 77(908), pp. 371-378.

[30] Bigliardi, P. L., Tobin, D. J., Gaveriaux-Ruff, C., and Bigliardi-Qi, M., 2009, "Opioids and the skin – where do we stand?," Exp. Dermatol., 18(5), pp. 424-430.

[31] Stein, C., and Küchler, S., 2012, "Non-analgesic effects of opioids: Peripheral opioid effects on inflammation and wound healing," Curr. Pharm. Des., 18(37), pp. 6053-6069.

[32] Philip, A., and Thakur, R., 2011, "Post herpetic neuralgia," J. Palli. Med., 14(6), pp. 765-773.

[33] Graham, T., Grocott, P., Probst, S., Wanklyn, S., Dawson, J., and Gethin, G., 2013, "How are topical opioids used to manage painful cutaneous lesions in palliative care? A critical review," PAIN, 154(10), pp. 1920-1928.

[34] LeBon, B., Zeppetella, G., and Higginson, I. J., 2009, "Effectiveness of Topical Administration of Opioids in Palliative Care: A Systematic Review," J. Pain Symptom Manage., 37(5), pp. 913-917.

[35] Roy, S. D., and Flynn, G. L., 1990, "Transdermal delivery of narcotic analgesics: pH, anatomical, and subject influences on cutaneous permeability of fentanyl and sufentanil," Pharm. Res., 7(8), pp. 842-847.

[36] Lane, M. E., 2013, "The transdermal delivery of fentanyl," Eur. J. Pharm. Biopharm., 84(3), pp. 449-455.

[37] Stinchcomb, A. L., Paliwal, A., Dua, R., Imoto, H., Woodard, R. W., and Flynn, G. L., 1996, "Permeation of buprenorphine and its 3-alkyl-ester prodrugs through human skin," Pharm. Res., 13(10), pp. 1519-1523.

[38] Roy, S. D., and Flynn, G. L., 1989, "Transdermal delivery of narcotic analgesics: Comparative permeabilities of narcotic analgesics through human cadaver skin," Pharm. Res., 6(10), pp. 825-832.

[39] Roy, S. D., Roos, E., and Sharma, K., 1994, "Transdermal delivery of buprenorphine through cadaver skin," J. Pharm. Sci., 83(2), pp. 126-130.

[40] Wang, J.-J., Sung, K. C., Huang, J.-F., Yeh, C.-H., and Fang, J.-Y., 2007, "Ester prodrugs of morphine improve transdermal drug delivery: a mechanistic study," J. Pharm. Pharmacol., 59(7), pp. 917-925.

[41] Potts, R. O., and Guy, R. H., 1992, "Predicting skin permeability," Pharm. Res., 9(5), pp. 663-669.

[42] Abraham, M. H., Chadha, H. S., and Mitchell, R. C., 1995, "The Factors that Influence Skin Penetration of Solutes," J. Pharm. Pharmacol., 47(1), pp. 8-16.

[43] Roberts, M. S., Cross, S. E., and Anissimov, Y. G., 2004, "Factors affecting the formation of a skin reservoir for topically applied solutes," Skin Pharmacol. Physiol., 17(1), pp. 3-16.

[44] Cross, S. E., and Roberts, M. S., 2008, "Use of in vitro human skin membranes to model and predict the effect of changing blood flow on the flux and retention of topically applied solutes," J. Pharm. Sci., 97(8), pp. 3442-3450.

2 A novel oromucosal prolonged release mucoadhesive suspension by one step spray coagulation method

2.0 Abstract

An oromucosal suspension of mucoadhesive microparticles (MMS) able to combine the peculiarities of prolonged release mucoadhesive microparticles with those of an immediate release oromucosal solution is described. Microparticles were obtained by ionotropic gelation of alginate blended with another mucoadhesive material in a one-step process where the cross-linking bath constituted the suspension vehicle. The effects of formulation and processing conditions on MMS performances were measured *in vitro* determining the enhancement of drug penetration in buccal porcine mucosa and inhibition of tooth plaque formation using flurbiprofen and delmopinol as model drugs, respectively. Well-formed and spherical microparticles were obtained combining alginate with carbomer; linear dependence of particle size from the feed composition, viscosity and atomization pressure was found. As demonstrated by using FITC-labelled microparticles, the system remained onto the buccal mucosa at least for a six-hour period. Consequently, 0.1% flurbiprofen MMS guaranteed a concentration of flurbiprofen into buccal porcine mucosa over 6 hours comparable to 0.25% flurbiprofen reference solution, allowing a potential reduction of the 60% administered dose. The use of in-house made artificial mouth revealed that the once-a-day administration of 0.1% delmopinol MMS was as effective in plaque inhibition as the 0.2% delmopinol reference solution product given twice a day. These results suggested that the development of bioadhesive oromucosal suspensions, localizing the drug into buccal cavity, can reduce regimen and administrated dose.

The formulative studies were carried out in the laboratory directed by prof. Luisa Montanari, Department of Pharmaceutical Sciences, University of Milan, via G. Colombo, 71 – 20133, Milan (Italy).

The in vitro evaluation of plaque development was carried out by in the laboratory directed by dr. Cristiano Rumio, Department of Medical Biotechnology and Translational Medicine, Humanitas Clinical and Research Center, via Manzoni, 56 – 20089, Rozzano (Italy)

The contents of this chapter was published in Current Drug Delivery (Cilurzo et al.; Cur. Drug. Del.; 2013, 10, 251-260)

2.1 Introduction

Oromucosal formulations are intended for administration in the oral cavity and/or the throat to achieve mainly a local effect. They are usually immediate release dosage forms, such as mouthwashes and sprays, which are easily swallowed and are unable to maintain efficacious drug levels for a prolonged period. Mucoadhesive preparations designed to retain the active ingredient in the oral mucosal epithelium by adhesion, may prolong drug absorption at the site of application [1, 2]. Nevertheless, the slow drug release can delay the drug onset of action. Thus, the main objective of this study was to develop an oromucosal formulation, which can guarantee both fast onset of action and prolonged release. The basic idea was to prepare an oromucosal suspension of mucoadhesive microparticles (MMS) combining peculiarities of an oromucosal solution with those of prolonged release mucoadhesive microparticles, guaranteeing uniform distribution of the drug into the mouth because of their high surface.

However, the main critical issue in MMS was related to the physical stability of the microparticulate systems. Suspension should be easy to disperse by shaking after long period of storage and enough stable to deliver correct dose and to assure drug release. Indeed, mucoadhesive microparticles have to exhibit a narrow particle size distribution and a mean diameter suitable to be delivered by using a spray device that allows the uniform distribution of the preparation in the mouth.

In order to produce such MMS by a one-step process, spray coagulation method was tested using alginates as the main microparticles constituents. Alginates were chosen considering their ability to form stable reticulated structure in presence of alkali earth ions, like calcium. This feature has been extensively exploited to produce beads by ionotropic/external gelation process [3, 4]. Cross-linking of alginates is mainly achieved by exchanging sodium ions from the guluronic acids with bivalent cations and stacking these guluronic groups to form the characteristic egg-box structure [5]. Considering poor mucoadhesive properties of calcium alginates [6], the effect of blending with several mucoadhesive polymers, namely hydroxypropyl methylcellulose [7], carboxymethylcellulose [8], poly-(sodium methacrylate, methylmethacrylate) [9, 10] or carbomer [11], on microparticles properties was investigated in the current work.

The feasibility of using this approach for designing MMS was evaluated *in vitro* by using two different active ingredients with different charges and water solubilities, namely delmopinol and flurbiprofen. The former is a cationic freely soluble active ingredient able to inhibit plaque and gingivitis [12-15]; the latter is an anionic insoluble drug, commonly locally administered to treat inflammatory processes of oral cavity, such as ulcers and aphtous stomatitis, postsurgical dental pain, gingivitis, laryngopharyngitis, and sore throat [16-19].

The mucoadhesion strength of microparticles was determined estimating the interaction with mucin by a colorimetric assay. Furthermore, the residence time of the microparticles onto the buccal porcine mucosae was *in vitro* determined by wash off method using placebo MMS prepared with FITC-labelled alginate.

The performances of the proposed drug delivery systems were evaluated by a) measuring flubiprofen amount penetrated into porcine cheek mucosal segment as well as effused from the mucosa surface by a falling liquid technique and b) checking the ability to inhibit plaque development, using an in-house made artificial mouth appositely developed.

2.2 Materials and Methods

2.2.1 Materials

Sodium alginate (Protanal® LF210M) was kindly gifted by FMC Biopolymer (Cork, Ireland). Carboxymethylcellulose (CMC; 400-600 mPas) and hydroxyl propyl methyl cellulose K4M (HPMC) were obtained from Chimitex (Milan, Italy), and Colorcon (Gallarate, Italy), respectively. Sodium poly-(methyl methacrylate) (NaPMM) was obtained as previously described [20]. Carbopol® 974P (carboxypolymethylene cross-linked with allyl sucrose; CP) was provided from Lubrizol Co. (Wickliffe, USA). Porcine mucin, fluorescein isothiocyanate (FITC), N-(3-dimethylaminopropyl)-N'-ethylcarbodiimide (EDC), N-hydroxysulfosuccinimide sodium salt (NHSS), and diamino-hexane (DAH) were purchased by Sigma Aldrich Co. (Milan, Italy). Cremophor® RH was kindly gifted from BASF (Ludwigshafen, Germany). Flurbiprofen, sodium saccharine, sorbitol, calcium chloride bihydrate, methyl-paraben and long articulated throat adapter were purchased from Farmalabor (Canosa di Puglia, Italy). Hyaluronic acid sodium salt was obtained from Therapo (Basel, Switzerland). Glycerol

was purchased from Carlo Erba Reagenti (Milan, Italy). Mint flavor was kindly gifted by Kerry Group (Tralee, Ireland). Delmopinol hydrochloride was kindly obtained from Sinclair Pharma S.r.l. (Milan, Italy). All solvents were of analytical grade unless specified.

2.2.2 Preparation of FITC-labelled alginate

The alginate-FITC derivative was synthesized adapting a process previously described in literature [21]. Briefly, 12 g sodium alginate solution 1% w/w were mixed in 1.5 mL pH 4.9 sodium acetic buffer and mixed with 50 mg EDC and 30 mg NHSS for 30 min; then 60 mg DAH were added and the system was stirred for 4 h. Finally, 12 mL isopropanol were added to the blend to remove the excess of DAH and precipitate the alginate-amine derivative. The latter was reacted with 14.03 mg FITC in pH 9 sodium bicarbonate for 4 h and precipitated with 5 mL acetone. Alginate-FTIC was assayed by an HPLC coupled with a spectrofluorimeter (HP 1100 ChemStations, Agilent, Santa Clara, USA) using a SEC column (BioSuit 125, 4 µm UHR SEC 4.6x300 mm, Waters Co., Dublin, Ireland) to assure the absence of unreacted FITC and/or FITC-labelled alginate degraded by the reaction process.

2.2.3 Preparation of oromucosal microparticle suspension

In order to evaluate the influence of formulation variables and experimental parameters, placebo MMS were preliminarily prepared starting from mixtures of alginate and several mucoadhesive polymers. The feed was made mixing aqueous dispersion of sodium alginate and secondary mucoadhesive polymer in 3:1 ratio. The best feed in terms of microparticles formation was remade according to the ratios reported in **Table 2.1.** Afterwards, feed was pumped at the rate of 15 mL/min into a standard two-way nozzle (0.8 mm inner diameter, Schlick Atomizing Technologies, Düsen-Schlick GmbH, Untersiemau, Germany) and sprayed into a 2% w/w calcium chloride solution, under magnetic stirring. The air pressure ranged from 450 mbar to 550 mbar. Microparticles were cured into the cross-linking bath for 1 h at room temperature before filtering throughout a 710 µm sieve. The final placebo MMS were stored in 50 mL blue PE bottle at 25°C until use. Drug-loaded MMS were similarly prepared. Since cross-linking baths constituted product vehicles, all constituents, including active ingredients, were dissolved

before spraying (**Table 2.1**). In the control formulations D_{0a}, D_{0b} and F_0 (**Table 2.1**), microparticles and cross-linking agent were not present.

2.2.4 Viscosity measurements

The feed viscosity was determined using a rotational viscometer (HAAKE VT500, Gemini B.V., Apeldoorn, Netherlands) equipped with a recirculating bath to maintain sample at 20.0±0.1 °C. The sample temperature in the rheometer was stabilized 15 min before taking the measurement. The shear rate (D) was in the 0-300 s^{-1} range. Reproducibility of the data was assessed in triplicate. The obtained rheograms were analyzed and adjusted to the Ostwald model, then the viscosity (η) was calculated at D = 250 s^{-1}.

2.2.5 Determination of microparticle size

The particle size of suspension (1 mL) was measured by an Accusizer 770 granulometer (PSS Inc., Santa Barbara, USA). Particle size was expressed as undersize cumulative percentages and the population dispersion was referred as SPAN and calculated as reported in the **Eq. 2.1**:

$$SPAN = \frac{d_{90} - d_{10}}{d_{50}} \qquad \textbf{Eq. 2.1}$$

where d_{90}, d_{10}, and d_{50} are the mean diameters at the 90%, 10% and 50% of the population distribution, respectively.

2.2.6 Uniformity of Mass Delivered

The uniformity of mass delivered from the device was assayed according to the Ph. Eur. method (2.9.27). Moreover, since a variation in the amount of delivered microparticles might cause differences in the drug release, the number of microparticles suspended in aliquots of 10 mL and 20 mL were also counted by an Accusizer 770 granulometer (PSS Inc., Santa Barbara, USA). The results were expressed as the mean of three determinations.

Table 2.1 *– Compositions of placebo MMS (Formulations P_0-P_3), Delmopinol MMS (Formulations D_0-D_2) and Flurbiprofen MMS (Formulations F_0-F_3). The Ratio phase A/phase B was fixed at 1/10 (%, w/v) for Formulations P_0-P_3, F_1-F_2 and D_1, 1.5/10 (%, w/v) for Formulation D_2 and 1/5 (%, w/v) for Formulation F_3.*

	Ingredients	**Formulations**											
		P_0	P_{0a}	P_1	P_2	P_3	D_{0a}	D_{0b}	D_1	D_2	F_0	F_1	F_2	F_3
Phase A (microparticles)	Flurbiprofen			-	-	-	-	-	-	-	-	0.10	0.10	0.05
	Delmopinol hydrochloride			-	-	-	-	-	0.1	-	-	-	-	-
	Sodium alginate	3.00	2.00	2.25	1.80	1.50	-	-	2.25	1.80	-	1.50	2.25	1.50
	Carbopol® 934P			0.75	1.20	1.50	-	-	0.75	1.20	-	1.50	0.75	1.50
	Purified water	97.00	98.00	97.00	97.00	97.00	-	-	97.00	97.00	-	96.90	96.90	96.95
Phase B (aqueous vehicle)	Flurbiprofen			-	-	-	-	-	-	-	0.25	0.10	0.10	0.05
	Delmopinol hydrochloride			-	-	-	0.20	0.10	0.10	0.11	-	-	-	-
	Glycerol			-	-	-	-	-	-	-	10.00	10.00	10.00	10.00
	Sodium saccharine			-	-	-	0.01	0.01	-	0.01	0.15	0.15	0.15	0.15
	Sorbitol			-	-	-	-	-	-	-	7	7	7	7
	Sodium hyaluronate			-	-	-	-	-	-	0.02	-	-	-	-
	Cremophor® RH			-	-	-	-	-	-	-	2.40	2.40	2.40	2.40
	Sodium methyl-paraben			-	-	-	-	-	-	-	0.12	0.12	0.12	0.12
	Mint flavor			-	-	-	0.02	0.02	0.02	0.02	0.20	0.20	0.20	0.20
	Calcium chloride bihydrate	2.00	2.00	2.00	2.00	2.00	-	-	2	2	-	1.00	1.00	1.00
	Water	98.00	98.00	98.00	98.00	98.00	98.27	99.27	96.28	95.37	69.88	69.03	69.03	69.08
	Ethanol			-	-	-	1.50	1.50	1.50	1.50	10	10	10	10

2.2.7 Mucoadhesive properties

The mucoadhesive properties of placebo and drug-loaded microparticles were determined after filtering MMS through a 90 μm sieve. Aliquots of 100 mg microparticles were suspended in 2.5 mL purified water. Afterwards, same volume of 0.05% w/v mucin solution was added. Samples were shaken at 100 rpm for 5 min in a shaker incubator (Sartorius Stedim, Antella, Italy) at 37±1 °C and then centrifuged at 1000 × *g* by a Hettich Universal centrifuge 30F (Andreas Hettich GmbH & Co. KG, Tuttlingen, Germany). After discharging the supernatant, 5 mL fresh purified water was added to each tube to remove mucin not adsorbed on the microparticle surface. This water was discharged and the microparticles were re-suspended in 2.5 mL deionized water. Aliquots of each suspension (200 μL) were incubated for 30 min at 37±1 °C by using a micro BCA Protein Assay Reagent (Euroclone, Pero, Italy) following a method adapted from Shi and Caldwell [22]. The amount of bound mucin was determined by spectrophotometer at the wavelength of 562 nm (DU®-640 spectrophotometer, Beckman Coulter, Brea, USA).

2.2.8 Drug content

Microparticles recovered by filtration through a 0.45 μm membrane were washed with methanol to remove the drug absorbed on their surface and dried at room temperature till constant weight. 50 mg samples were digested in 10 mL 5% w/v sodium chloride solution/methanol (50/50 %, v/v) under sonication for 2 h. Then, samples were filtered and the contents of flurbiprofen and delmopinol were determined using the HPLC methods reported below. The drug content of the aqueous vehicle was also determined after dilution 1:10 with water.

2.2.9 HPLC assay

The drug content in microparticles and vehicles was determined by an HP 1100 Chemstations (Agilent, Santa Clara, USA). The results were expressed as mean of three determinations. The experimental conditions were set up in order to avoid interferences of the other components.

Flurbiprofen - Column: Symmetry Shield™, ODS HYPERSIL, 100 x 4.6 mm ID, particle size 3 μm (Waters Co., Dublin, Ireland); mobile phase: methanol/pH 2.5 0.01 M Na_2HPO_4 (66/34 %, v/v);. flow rate: 1.2 mL/min; temperature: 40°C wavelength: 254

nm; injection volume: 10 μL; retention time: 4 min. The standard curve was constructed in the concentration range from 0.05 to 50 μg/mL (R^2 = 0.99999).

Delmopinol - Column: Symmetry Shield™ RPC-18, 150 x 4.6 mm ID, particle size 5 μm (Waters Co., Dublin, Ireland); mobile phase: methanol/pH 7.0 PBS (80/20 %, v/v); flow rate: 1 mL/min; wavelength: 210 nm; temperature: 25°C; injection volume: 10 μL; retention time: 5 min. The standard curve was constructed in the concentration range from 15 to 500 μg/mL (R^2 = 0.99921).

2.2.10 In vitro drug release

The release profile of flurbiprofen from microparticles was determined using the USP 26 paddle dissolution apparatus, using 500 mL of PH 6.4 PBS at 37.0±0.5 °C and 25 rpm. MMS was filtered in order to remove suspension medium and washed with fresh water. Samples of microparticles were exactly weighed to achieve an amount of flurbiprofen corresponding to 50 mg. Drug concentration in the release medium was determined at 249 nm.

The results were expressed as mean of three samples. In order to understand drug release mechanism, release profiles were fitted with the Higuchi model (**Eq. 2.2**).

$$M_t/M_\infty = Kt^{1/2} \qquad \textbf{Eq. 2.2}$$

where M_t was the amount of drug released at time t, M_∞ was the drug loading in the microparticles, and K was the release rate constant expressed as h^{-1} [23].

2.2.11 In vitro mucosa penetration study

The *in vitro* mucosa penetration study was performed adapting the falling liquid technique described by Rao and Buri [24] by using fresh porcine cheek mucosa obtained by a local slaughterhouse. Specimens of mucosa were dipped in pH 7.4 PBS at 70°C for 1 min in order to isolate mucosa epithelium.

In-house equipment of three components was built up: (a) six in-series mucosa supports set at an acute angle of 30°; (b) peristaltic pump and (c) collector of fractions. Apparatus was designed in order to mimic both the effusion of the preparations from the surface of buccal mucosa and flurbiprofen penetrated amount.

A dose of the selected MMS was sprayed twice onto a 2.5x1.0 cm mucosal surface corresponding to a total amount of about 40 mg. Then, porcine cheek epithelium membrane was placed on the sample support and pH 6.4 PBS was dropped at the rate of 1 mL/min to simulate the buccal environment and the saliva swallowing.

This system was used either for qualitatively estimating the residence time of microparticles onto the buccal mucosa by testing MMS, made with 30% of FTIC-labelled alginate, or determining the penetration of flurbiprofen in the porcine cheek epithelium membrane. In the former case, porcine sample sheet was dismounted at predetermined intervals of time and fluorescent microparticles applied onto the mucosa segments were observed by using an Eclipse 80i Microscope (Nikon Instruments S.p.A, Firenze, Italy). In the case of flurbiprofen formulations, portions of the effused buffer were collected at predetermined intervals and drug concentration was determined by HPLC.

At predefined times (*i.e.*, 1, 3 and 6 h), the applied test sample was peeled away by means of an adhesive tape strip and the mucosa was stored at -40°C for 24 h. Finally, mucosa samples were homogenized and the amount of the penetrated drug was extracted with 5 mL methanol and assayed.

2.2.12 In vitro evaluation of plaque development

In order to investigate antiplaque efficacy of different formulations, an *in vitro* system called "artificial mouth", assuring high standardization and repeatability, was developed. This testing system was composed by an array of six glass holding intact human grinders reassembling in independent artificial oral cavities. The artificial oral cavities were surrounded by thermostated jacket at 35±1 °C. The upper part of the artificial oral cavity was firmly closed by a lid equipped with three atomizers connected to working solutions which acted as drop collectors for bacterial suspension and the testing product. The functionality of each atomizer was independently programmable. Each artificial oral cavity was equipped with a discharge system for the rinsing liquids. Prior insertion in the artificial mouth to use, each tooth was thoroughly cleaned with a rubber cup and pumice, immersed in physiologic solution and sterilized by saturated steam under pressure at 121°C for 15 min.

At the beginning of the experiments, sterilized teeth were inserted into the artificial mouth. The drop collectors for bacteria suspension and the test solution were adjusted at a position of 8 cm straight above the tooth specimen. The solutions of tested plaque-inhibiting compounds were supplied (6 mL/dose) onto the tooth specimen once a day over a 10 day period. For guaranteeing formation and development of plaque, it was essential that any contamination occurred. Therefore, equipment coming into direct contact with the bacterial suspension, nutrient broth or tooth specimen were sterilized and all procedures were carried out in aseptic conditions. Moreover, a standard protocol was established for the sterilization of artificial oral cavities at the beginning and the end of each testing. Soft plaque collected from healthy human subjects was cultured in a nutrient broth and bacteria were harvested in the logarithmic growth phase. The nutrient broth containing bacteria was used at a bacterial density of 10^6-10^7 cells/mL. The suspension of bacteria was supplied onto the tooth specimen at a flow rate of 5 mL/h over a 10-day period, at 5 s per hour, once an hour. The suspension of bacteria was daily tested for pH and number of cells per volume unit. During the experimental procedure, the suspension of bacteria was kept at 4±1 °C under continuous stirring to avoid undesired bacterial growth.

At the end of the testing period (10 days), the plaque formed on the tooth surface was stained with 0.05% w/v basic fuchsine. To estimate plaque-inhibiting effect of the tested product, the amount of plaque formed on the tooth surfaces was quantified according to a Visual Index as well as a semi-automatic image analyzer (NAIS Elements) on defined area of the tooth surface.

The Visual Index was made up by the following scale:

- 0: no plaque formation;
- 1: slight plaque formation, when less than 1/3 of the tooth surface was covered by plaque;
- 2: moderate plaque formation, when 1/3-2/3 of the tooth surface was covered by plaque;
- 3: heavy plaque formation, when more then 2/3 of the tooth surface was covered by plaque.

In addition, the percentage of the tooth surface covered by plaque was calculated by computerized planimetric measurements and the plaque inhibiting effect of the tested substance was classified as following:

- very good: less than 10% tooth surface covered by plaque;
- good: 10-20 % tooth surface covered by plaque;
- moderate: 20-50 % tooth surface covered by plaque
- slight: 50-80 % tooth surface covered by plaque;
- no effect: more than 80% tooth surface covered by plaque.

To assess ability to the reduce plaque formation, following formulations were tested: formulation D_{0a} (the conventional solution containing 0.2% w/w delmopinol as the marketed product), D_{0b} (the conventional solution of delmopinol at the same concentration as the MMS) and D_2 (0.1% w/w delmopinol MMS) (**Table 2.1**). Sterile water was also supplied onto control tooth specimens for comparison with plaque inhibitors-treated teeth.

2.2.13 Preliminary evaluation of MMS stability

The stability of drug-loaded MMS was investigated over six months in terms of re-suspendability, pH of aqueous vehicle and drug content. Volumes of 100 mL of the Formulations D_2 and F_1 were filled in 120 mL blue polyethylene terephthalate bottles and stored at 25°C/60 % and 40°C/75 % relative humidity (RH).

2.3 Results

2.3.1 Preparation of oromucosal mucoadhesive suspensions

Spraying alginate/NaPMM mixtures into the aqueous vehicle containing $CaCl_2$, formation of irregular and solid particles occurred probably due to the strong interaction between NaPMM and calcium ions [25]. The suspension of microparticles made of CMC/alginate and HPMC/alginate mixtures resulted not stable overtime, since aggregation was evident after few days of storage.

Well-formed and spherical microparticles were obtained only combining alginate with CP. **Table 2.2** reports the feed viscosities and the particle size distribution of suspensions

of designed formulations using such polymeric blends. Considering that obtained microparticles should guarantee a prolonged drug release and be deployed from the device by spraying, SPAN and d_{90} were considered the most critical parameters to evaluate in particle size distribution. As far as the former parameter was concerned, the atomization of the feed, during the preparation process, at 550 mbar allowed lower values and narrower particle size distribution than 450 mbar; increasing atomization pressure up to 550 mbar did not allow suitable microparticle formation.

A linear dependence of d_{90} from the feed composition, viscosity (η) and atomization pressure (P) was found as shown by **Eq. 2.3** (R^2=0.894):

$$d_{90} = +0.238 \pm 0.005\ \eta - 1.323 \pm 0.229\ P - 1.039 \pm 0.247\ CP \qquad \textbf{Eq. 2.3}$$

where all independent variables were significant ($p<0.01$). The amount of alginate was excluded from the equation due to co-linearity with CP.

Both the total amount of mass delivered (average value 160 mg) and the number of microparticles sprayed from the device filled with 30 mL MMS of Formulation P_2 atomized at 450 mbar resulted not statistically different during the draining: 38000±5000 microparticles were sprayed, 36000±5000 after the deployment of one third of the MMS and 35000±6000 after the deployment of two third of the preparation from the same container. Therefore, the selected spray device was considered adequate for the delivery of the MMS. The measured pH in all vehicles resulted 4.5.

The mucoadhesive data are reported in **Table 2.2**. As expected, MMS made of alginate and CP showed mucoadhesive properties statistically higher than cross-linked alginate ($p<0.05$) and the following rank order was found: $P_0 < P_1 \approx P_2 < P_3$. Moreover, the encapsulation and/or adsorption of both drugs did not affect the mucoadhesive properties of all formulations ($p>0.80$).

In all MMSs, sedimentation of microparticles occurred within few hours leading to a clear vehicle. The preliminary stability data indicated suitability of the proposed system to produce oromucosal suspensions. Indeed, the sediment of microparticles could be easily re-suspended by manual agitation. No aggregates were observed up to six months from preparation, indicating that the selected active ingredients did not affect the physical

stability of formulation. These observations were also confirmed by results of mass delivered as the number of microparticles sprayed from the device after 6 months of storage at 25°C and 40°C results comparable to those obtained at time 0 (data not shown). On bases of these evaluations, the atomization pressure of 550 mbar was selected and the upper limit of viscosity was established at 50 cps for drug-loaded MMS.

Table 2.2 *– Particle size distribution and mucoadhesive properties of placebo MMS.*

Form.	**Feed viscosity (mPa/s)[#]**	**Pressure (mbar)**	**d_{10}**	**d_{50}**	**d_{90}**	**SPAN**	**mg bound-mucin/g microparticles**
P_0	96,500	450	18	67	143	1,81	-*
		550	10	26	71	2,28	1.33 ± 0.12
P_{0a}	50,748	450	10	29	55	1,53	-*
		550	8	23	47	1,69	-*
P_1	43,936	450	17	41	84	1,66	-*
		550	15	33	64	1,52	1.79 ± 0.20
P_2	38,118	450	5	29	77	2,50	-*
		550	17	40	68	1,26	2.01 ± 0.18
P_3	28,866	450	17	40	74	1,41	-*
		550	13	36	78	1,80	2.76 ± 0.15

[#] standard deviation less than 2%; *not performed

The loading of flurbiprofen affected neither particle size distribution nor the particle morphology (**Table 2.3**). Delmopinol addition in the feed of Formulation D_1 (**Table 2.1**) did not allow the formation of spherical microparticles.

This evidence might be explained hypothesizing that its surfactant properties affected droplet surface energy and modified droplet penetration into the cross-linking bath. Indeed, spraying of this formulation led to the formation of a film on the surface of $CaCl_2$ solution. To solve this limitation, delmopinol was dissolved only in the aqueous vehicle and the placebo microparticles were maintained in the drug-loaded vehicles in order to favor the partition of the active ingredient from the vehicle to the microparticles until equilibrium between the two phases was reached.

The drug content assayed in the vehicle and microparticles of Formulation D_1 indicated that encapsulation efficiency was higher than 100% (**Table 2.3**). This evidence may be due to interaction among delmopinol amine and carboxylic moieties of CP and/or alginates. The same phenomenon was not evident in the presence of hyaluronic acid (Formulation D_2, **Table 2.1**). Indeed, it is possible to speculate that this compound was able to limit the drug migration from the external phase towards the microparticles.

Table 2.3 *– Particle size distribution and drug content.*

Form.	**Particle size (µm)**			**Drug content (% w/w)**	
	d_{10}	d_{50}	d_{90}	Microparticles	Aqueous vehicle
F_1	45	65	85	0.10 ± 0.00	0.10 ± 0.00
F_2	44	90	124	0.10 ± 0.01	0.10 ± 0.01
F3	45	77	117	0.06 ± 0.01	0.05 ± 0.00
D_1	43	71	103	0.18 ± 0.03	0.09 ± 0.01
D2	42	95	99	0.12 ± 0.02	0.10 ± 0.01

The percentages of delmopinol or flurbiprofen recovered in the vehicle and in microparticles showed no significant changes over the considered period of storage as reported in **Table 2.4**. Moreover, at the end of the scheduled period of storage, the measured pH resulted 4.5, independently of the tested formulation and the storage conditions.

Table 2.4 *– Drug content (%, w/w) in D_2 and F_1 MMS formulations after six months of storage in normal (25°C/ 60 % RH) and accelerated (40°C/60 % RH) conditions.*

Form.	**25°C/ 60 % RH**		**40°C/60 % RH**	
	Microparticles	Aqueous vehicle	Microparticles	Aqueous vehicle
D_2	0.13 ± 0.00	0.09 ± 0.00	0.12 ± 0.01	0.09 ± 0.00
F_1	0.10 ± 0.02	0.10 ± 0.00	0.11 ± 0.01	0.10 ± 0.01

2.3.2 In vitro mucosa Flurbiprofen penetration studies

Preliminary, residence time of the microparticles which were visually detected by using the formulation P_3 prepared with 30% of FITC-labelled alginate. As expected, continuous

washing determined a progressive decrease of microparticle number adhered onto the porcine mucosae. In every case, they were detectable over at least 6 h (**Figure 2.1**) confirming the mucoadhesive properties of MMS.

The experiments aiming to determine the amount of flurbiprofen retained into the porcine mucosa were performed with drug-loaded formulations over the same period. One hour after the sample application onto the mucosa sheets, the drug amount penetrated into the mucosa was significantly higher for the reference solution (Formulation F_0) with respect to flurbiprofen MMSs (**Figure 2.1**) according to the higher drug content (**Table 2.3**). Nevertheless, after 3 h the flurbiprofen amount retained into the mucosa was reduced of about 3-fold and further decreased over time.

The use of MMS allowed improving drug concentration into the porcine buccal mucosa over time. Indeed, Formulation F_2 exhibited a pattern similar to formulation F_0 even if the flurbiprofen retained into the mucosa was only halved between 1 and 3 h. No statistically differences in drug levels were evident over 3 h and 6 h period for Formulation F_3 and F_1, respectively.

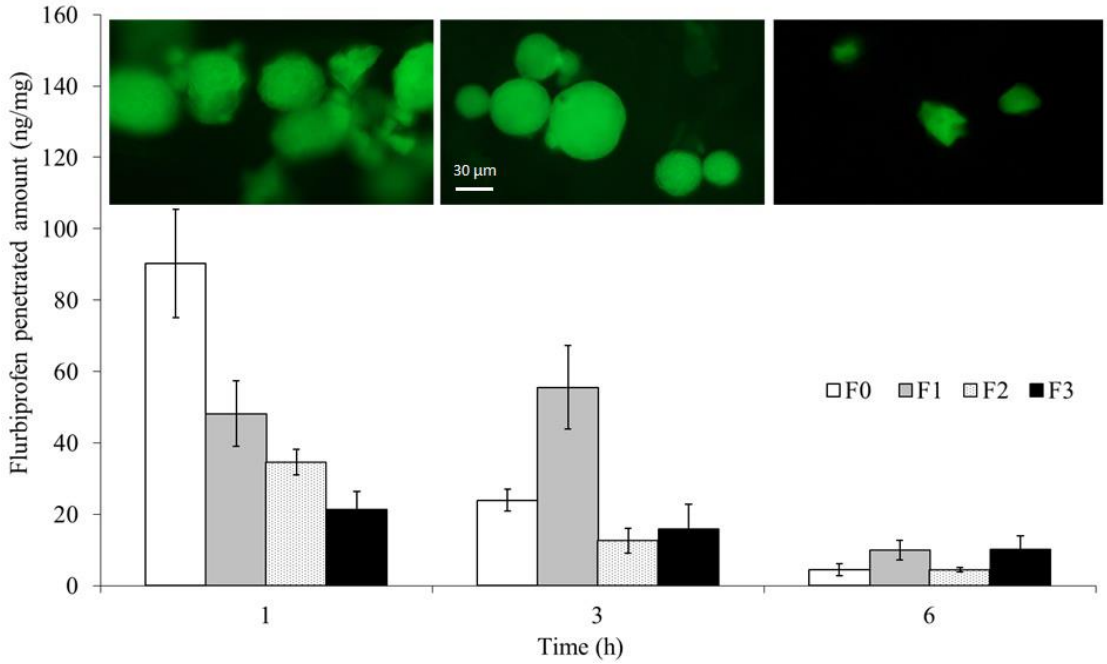

***Figure 2.1** – Amount of flurbiprofen penetrated into porcine cheek mucosal segments, 1, 3 and 6 hours after the application of Formulations F_0-F_3. The images reports the mucoadhesive microparticles of formulation F_2 taken by fluorescent microscope at the three different times. The irregular shape of the microparticles represented at time 1 h and 6 h is an artefact related to their drying during the observation by microscope.*

After 6 hours, the drug concentrations for Formulations F_0 and F_2 were not statistically different ($p=0.47$) and were lower than those obtained with Formulations F_1 and F_3 ($p<0.02$). A higher reduction of drug concentration after 6 hours was observed for Formulations F_1 than F_3, since a lower amount of mucoadhesive microparticles was present in aqueous vehicle of such formulation (**Table 2.1**).

Independently to the tested formulation, the recovery of flurbiprofen in the eluted washing medium revealed that unabsorbed drug was completely washed off within one hour and the maximum concentration was achieved within 15 min (**Figure 2.2**). As a matter of fact, the drug was not quantifiable over periods of time longer than 1 h in the eluted washing medium. The drug amount eluted from the mucosa surface was in agreement with the drug concentration in the oral spray formulations and was closed to the theoretical amount of drug sprayed onto the mucosae. The different pattern of Formulation F_2 with respect to Formulations F_1 and F_3 was attributed to the lower mucoadhesive properties (**Table 2.2**), which favored an easier washing off microparticles.

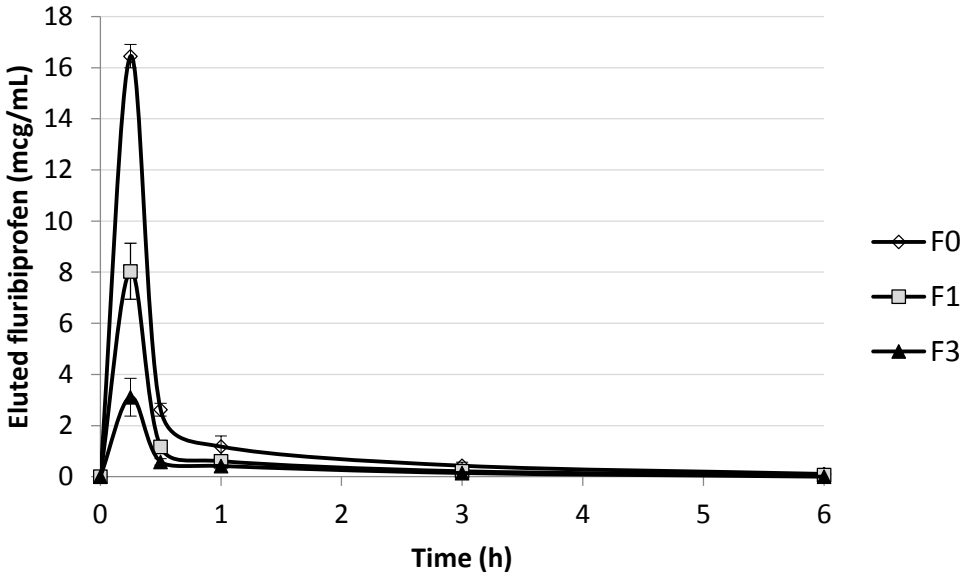

Figure 2.2 *– Elution profiles determined by in vitro falling technique of flurbiprofen after the application of Formulations F_0-F_3.*

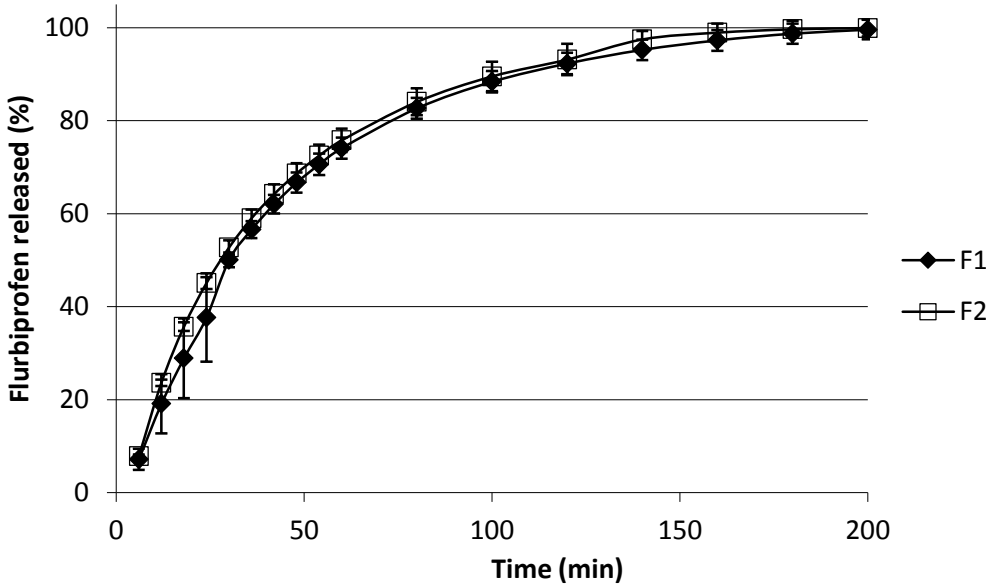

Figure 2.3 *– Drug release profile of flurbiprofen from microparticles contained in Formulations F_1 and F_2.*

This hypothesis was confirmed by the comparison of the drug release profiles, which resulted superimposable (**Figure 2.3**). Furthermore, the release rate constants (K) calculated according the Higuchi model were not statistically different (K_{F1} = 1.07±0.06 h^{-1}; K_{F2} = 1.06±0.04 h^{-1}; p=0.7487) and the good sound of correlation (R^2>0.9940) supported the hypothesis that the drug release was mainly controlled by diffusion. This result suggests that Formulations F_1 and F_3 retained the drug in the buccal mucosa for longer period with respect to Formulation F_2 because of its higher mucoadhesive properties rather than to a different ability to control drug release.

2.3.3 In vitro evaluation of plaque development

The in-house made artificial mouth and selected operative conditions allowed to discriminate the effect of the formulative variables of the oromucosal preparations on antiplaque effect of delmopinol. Indeed, results obtained by computerized planimetry with a semi-automatic image analyzer on definite areas of tooth surface (**Figure 2.4**) substantially confirmed evaluation by Visual Index: antiplaque performance of reference solutions, containing the highest drug amount (Formulation D_{0a}) was considered "very good".

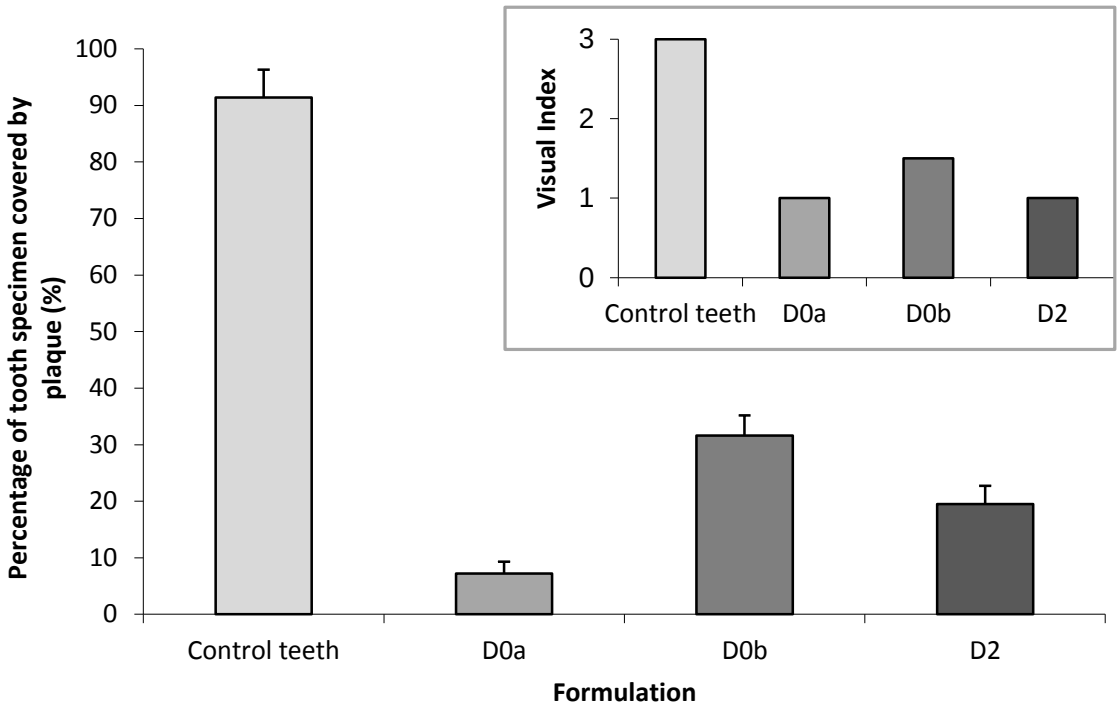

Figure 2.4 *– Percentage of tooth surface covered by plaque, as obtained by computerized planimetry with a semi-automatic image analyzer after application of Formulations D_0, diluted D_0 and D_2 and Visual Index for plaque formation after application of Formulations D_{0a}, D_{0b} and D_2 (insert).*

The reduction of drug concentration from 0.2% w/w to 0.1% w/w (Formulation D_{0b}) led a reduction of the anti-plaque effect which can be considered, in the proposed score system, moderate. Since Formulation D_2 was delivered once-a-day while Formulations D_{0a} and D_{0b} twice-a-day, the former could be considered the most efficacious in the prevention of plaque formation, with less than 20% of tooth surface covered by the plaque.

2.3.4 Preliminary stability evaluation

The stability data for formulations D_2 and F_1 are reported in **Table 2.4**.

The additives present in the oromucosal formulations were not detected in the chromatograms and therefore did not interfere with the drug determination. No degradation products were detectable in the chromatograms of both the tested formulations. The drug content showed no significant changes during storage indicating that both drugs resulted stable in MMS over considered time.

Moreover, at the end of the scheduled period of storage, the measured pH resulted 4.5, independently of the tested formulation and the storage conditions.

2.4 Discussion

The feasibility of obtaining a drug controlled release by preparing microparticles comprising alginate and CP was already reported in several papers [26]. Nevertheless, the final goal was to obtain mucoadhesive microparticles suitable for oral administration. In all cases, mucoadhesive microparticles were obtained by adding dropwise an aqueous polymeric dispersion comprising sodium alginate and CP to a cross-linking bath. Afterwards, the resulting suspension was filtered, dried and the microparticles derived by collapsing the hydrated beads [26, 27].

The production by using a standard nozzle, instead of a syringe equipped with a needle having a diameter generally comprised in the range 24-27G, allowed to obtain hydrated microparticles with an average particle size of 100 μm, which did not require further processing, such as drying. Such microparticles had no tendency to aggregation and, at the same time, high surface area and satisfactory mucoadhesive properties.

As underlined by the results concerning the multiple regression (**Eq. 2.3**), the particle size of microparticles could be easily set by changing polymer concentrations, which determined the feed viscosity, and atomization pressure. In particular, CP concentration might be considered the most critical formulative parameter since it determined the microparticle mucoadhesive properties and, therefore, drug retention into mucosa.

The proposed system resulted also flexible and versatile, in terms of encapsulation, since active ingredients with different characteristics could be loaded. The final drug loading might be adjusted by adding different amount of active ingredient in the feed and/or in the aqueous vehicle, or appropriate excipients. As verified in the case of delmopinol, the active ingredient could be added only in the cross-linking bath ant then uptaken by microparticles after their formation. The data obtained by flurbiprofen MMS suggested that when specific interaction between drug and swelled polymers used to obtain microparticles did not occur, the drug release was mainly controlled by the physically cross-linked alginate rather than the CP content.

The quantification of flurbiprofen penetrated into porcine buccal mucosa and the inhibition of plaque formation on teeth induced by delmopinol suggested that use of prolonged release oromucosal bioadhesive suspensions, such as those proposed in the current study, might decrease both the administered dose and the frequency of administration. Indeed, these formulations permitted to obtain performances comparable to those obtained by administering a traditional flurbiprofen oromucosal spray and delmopinol conventional product at dose reduced of about 60% and 50%, respectively.

The proposed drug delivery systems present also several advantages with respect to other mucoadhesive preparations intended for the treatment of pathologies localized in the oral cavity. With respect to buccal tablets and patches, the delivery of formulation by means a spray permitted to cover easily the entire oral mucosa or to localize active ingredient mainly on the throat. Furthermore, since mucoadhesive microparticles were suspended in a medium containing the drug, it could be assumed that designed MMS allowed to a fast onset of action associated to subsequent prolonged drug release.

2.5 Conclusion

The alginate/CP binary blend might be used for producing such MMS by ionotropic gelation using a one step process. The mucoadhesive microparticles exhibited a narrow particle size distribution and a mean diameter suitable to be delivered by using a spray device. The proposed MMS could assure a prolonged release of both cationic and anionic active ingredients. Finally, results of *in vitro* experiments suggested that development of MMS, localizing the drug into buccal cavity, could reduce the administrated dose and regimen.

2.6 References

[1] Cilurzo, F., Gennari, C. G. M., Selmin, F., Epstein, J. B., Gaeta, G. M., Colella, G., and Minghetti, P., 2010, "A new mucoadhesive dosage form for the management of oral lichen planus: Formulation study and clinical study," Eur. J. Pharm. Biopharm., 76(3), pp. 437-442.

[2] Kellaway, I. W., Ponchel, G., and Duchene, D., 2003, "Oral Mucosal Drug Delivery," Modified-Release Drug Delivery Technology, M. J. Rathbone, J. Hadgraft, and M. S. Roberts, eds., Marcel Dekker, Inc., New York, pp. 349-364.

[3] Schoubben, A., Blasi, P., Giovagnoli, S., Rossi, C., and Ricci, M., 2010, "Development of a scalable procedure for fine calcium alginate particle preparation," Chem. Eng. J., 160(1), pp. 363-369.

[4] Scocca, S., Faustini, M., Villani, S., Munari, E., Conte, U., Russo, V., Riccardi, A., Vigo, D., and Torre, M. L., 2007, "Alginate/polymethacrylate copolymer microparticles for the intestinal delivery of enzymes," Curr. Drug Deliv., 4(2), pp. 103-108.

[5] Gombotz, W. R., and Wee, S., 1998, "Protein release from alginate matrices," Adv. Drug Deliv. Rev., 31(3), pp. 267-285.

[6] Wittaya-areekul, S., Kruenate, J., and Prahsarn, C., 2006, "Preparation and in vitro evaluation of mucoadhesive properties of alginate/chitosan microparticles containing prednisolone," Int. J. Pharm., 312, pp. 113-118.

[7] Rahman, M. R., Jahan, S. T., Sadat, S. M. A., and Jalil, R.-u., 2010, "Preparation and evaluation of mucoadhesive hydrophilic hydroxy propyl methyl cellulose based extended release matrix tablets of Niacin (Nicotinic acid)," Am. J. Sci. Ind. Res., 1, pp. 558-564.

[8] Burjak, M., Bogataj, M., Velnar, M., Grabnar, I., and Mrhar, A., 2001, "The study of drug release from microspheres adhered on pig vesical mucosa," Int. J. Pharm., 224(1-2), pp. 123-130.

[9] Cilurzo, F., Selmin, F., Minghetti, P., Rimoldi, I., Demartin, F., and Montanari, L., 2005, "Fast-dissolving mucoadhesive microparticulate delivery system containing piroxicam," Eur. J. Pharm. Sci., 24(4), pp. 355-361.

[10] Cilurzo, F., Selmin, F., Minghetti, P., Gennari, C. G., Demartin, F., and Montanari, L., 2008, "Characterization and physical stability of fast-dissolving microparticles containing nifedipine," Eur. J. Pharm. Biopharm., 68(3), pp. 579-588.

[11] Singla, A. K., Chawla, M., and Singh, A., 2000, "Potential applications of carbomer in oral mucoadhesive controlled drug delivery system: a review," Drug. Dev. Ind. Pharm., 26(9), pp. 913-924.

[12] Collaert, B., Attstrom, R., De Bruyn, H., and Movert, R., 1992, "The effect of delmopinol rinsing on dental plaque formation and gingivitis healing," J. Clin. Periodontol., 19(4), pp. 274-280.

[13] Hase, J. C., Soder, P. O., Soder, B., Kulstad, S., and Kelty, E., 1995, "Development of plaque and gingivitis after mouthrinsing with 0.2% delmopinol hydrochloride," Eur. J. Oral. Sci., 103(3), pp. 172-178.

[14] Hase, J. C., Ainamo, J., Etemadzadeh, H., and Astrom, M., 1995, "Plaque formation and gingivitis after mouthrinsing with 0.2% delmopinol hydrochloride, 0.2% chlorhexidine digluconate and placebo for 4 weeks, following an initial professional tooth cleaning," J. Clin. Periodontol., 22(7), pp. 533-539.

[15] Moran, J., Addy, M., Wade, W. G., Maynard, J. H., Roberts, S. E., Astrom, M., and Movert, R., 1992, "A comparison of delmopinol and chlorhexidine on plaque regrowth over a 4-day period and salivary bacterial counts," J. Clin. Periodontol., 19(10), pp. 749-753.

[16] Heasman, P. A., Offenbacher, S., Collins, J. G., Edwards, G., and Seymour, R. A., 1993, "Flurbiprofen in the prevention and treatment of experimental gingivitis," J. Clin. Periodontol., 20(10), pp. 732-738.

[17] Procaccini, M., Palazzo, V., Mastroianni, L., and Orefici, M., 1996, "[Flurbiprofen collutory in oral surgical pathology]," Minerva Stomatol., 45(9), pp. 421-425.

[18] Ahmad, N., Grad, H. A., Haas, D. A., Aronson, K. J., Jokovic, A., and Locker, D., 1997, "The efficacy of nonopioid analgesics for postoperative dental pain: a meta-analysis," Anesth. Prog., 44(4), pp. 119-126.

[19] Roszkowski, M. T., Swift, J. Q., and Hargreaves, K. M., 1997, "Effect of NSAID administration on tissue levels of immunoreactive prostaglandin E2, leukotriene B4, and (S)-flurbiprofen following extraction of impacted third molars," Pain, 73(3), pp. 339-345.

[20] Cilurzo, F., Minghetti, P., Selmin, F., Casiraghi, A., and Montanari, L., 2003, "Polymethacrylate salts as new low-swellable mucoadhesive materials," J. Control. Release, 88(1), pp. 43-53.

[21] Liu, J., Zhang, Y., Yang, T., Ge, Y., Zhang, S., Chen, Z., and Gu, N., 2009, "Synthesis, characterization, and application of composite alginate microspheres with magnetic and fluorescent functionalities," J. Appl. Polym. Sci., 113(6), pp. 4042-4051.

[22] Shi, L., and Caldwell, K. D., 2000, "Mucin Adsorption to Hydrophobic Surfaces," J. Colloid Interface Sci., 224(2), pp. 372-381.

[23] Cilurzo, F., Alberti, E., Minghetti, P., Gennari, C. G. M., Casiraghi, A., and Montanari, L., 2010, "Effect of drug chirality on the skin permeability of ibuprofen," Int. J. Pharm., 386(1–2), pp. 71-76.

[24] Rao, K. V. R., and Buri, P., 1989, "A novel in situ method to test polymers and coated microparticles for bioadhesion," Int. J. Pharm., 52(3), pp. 265-270.

[25] Cilurzo, F., Gennari, C. G., Selmin, F., and Vistoli, G., 2010, "Effects of metal ions on entero-soluble poly(methacrylic acid-methyl methacrylate) coating: a combined analysis by ATR-FTIR spectroscopy and computational approaches," Mol. Pharm., 7(2), pp. 421-430.

[26] Thorat, Y. S., Modi, V. S., and Dhavale, S. C., 2009, "Use of carbomers to design mucoadhesive microspheres for anti-H. Pylori drug, Clarithromycin," Int. J. Pharm. Tech. Res., 7, pp. 421-430.

[27] Sambathkumar, R., Venkateswaramurthy, N., Vijayabaskaran, M., and Perumal, P., 2011, "Formulation of clarithromycin loaded mucoadhesive microspheres by emulsification-internal gelation technique for anti-helicobacter pylori therapy," Int. J. Pharm. Pharm. Sci., 3(2), pp. 173-177.

3 An oromucosal bioadhesive suspension for prolonged release of clobetasol propionate

3.0 Abstract

The study aimed to develop a buccal delivery system designed for having both fast onset of drug action and prolonged release, combining the peculiarities of aqueous solution and prolonged release mucoadhesive microparticles. Clobetasol propionate (CP) was chosen as model drug since it is currently administered to treat inflammatory diseases of the oral cavity. CP loaded mucoadhesive microparticles were prepared in one-step process by spray coagulation method. Sodium alginate (ALG) and two different grades of acrylic acid-based polymers (PAA) were selected as encapsulating and bioadhesive polymers, respectively. The effects of PAA type, PAA concentration in microparticle (25% or 50%, w/w) and spraying pressure (450 or 550 mbar) were investigated on microparticle morphology and CP penetration into porcine cheek mucosa by 2^3 factorial design. Microparticles were characterized in terms of morphology, micrometrics, mucoadhesion. Well-formed and spherical microparticles were obtained combining ALG with both types of PAA. The microparticle micrometrics was mainly influenced by spraying air pressure. The amount of mucin bounded to ALG/PAA microparticles was significantly higher ($p<0.05$) than those made of the pure ALG. The drug amount penetrated into the mucosa was significantly higher after 6 hours from administration of CP-loaded microparticles in comparison with the reference drug solution. The PAA type was critical to achieve high amount of drug penetration, especially when ALG/PAA were in the 1/1 ratio.

In conclusion, the proposed oromucosal mucoadhesive prolonged release suspension might be advantageously used to reduce the administration frequency of CP in the oral cavity.

The experimental work was carried out in the laboratory directed by prof. Luisa Montanari, Department of Pharmaceutical Sciences, University of Milan, via G. Colombo, 71 – 20133, Milan (Italy).

3.1 Introduction

Oral mucositis is one of the most critical complication of chemo- and radiotherapy [1]. Because of the high impact on life quality and care cost, several therapeutic protocols have been proposed for prevention and treatment. In general, they consisted in the basic oral care, topical administration of antimicrobials, mucosal coating agent, anesthetics, or systemic administration of high potent analgesics. Moreover, anti-inflammatory agents were tested, since oral mucositis are also correlated to an activation of inflammatory mechanism [2]. However, few of them were proven efficacy in reducing the severity and duration of oral mucositis.

Since buccal dosage forms used in the treatment of oral mucositis are based on solutions and semisolid preparations for skin application, the clinical failure might also be correlated to an ineffective drug delivery. Therefore, to improve the patient's compliance, the development of a prolonged release dosage forms might be challenging.

In a previous work, Cilurzo et al. proposed an oromucosal suspension of mucoadhesive microparticles (MMS) able to combine the peculiarities of prolonged release systems with those of an immediate release oromucosal solution [3]. The MMS was made by one-step spray coagulation method using sodium alginate (ALG) and poly-acrylate acids (PAA) as main microparticle constituents. The former was selected for the ability to form stable reticulate structure in presence of bivalent cations [4], the latter to conferee suitable mucoadhesive properties of microparticle. The *in vitro* effectiveness of MMS was demonstrated by loading flurbiprofen and delmopinol. However, the effect of polymeric feed composition and process conditions on the MMS residence time on buccal mucosa was not investigated in detail.

Therefore, the present study aimed to study the effect of these variables on clobetasol propionate (CP)-loaded MMS aiming to assure the presence of the drug into the buccal mucosae over six hours. CP was selected as model drug since its effectiveness in the treatment of oral mucositis and oral *lichen planus* [5]. Furthermore, two types of PAA were selected among those authorized for oral delivery according to the different crosslinking pattern: Carbopol® 974P is cross-linked with allyl ethers of pentaerythritol (APE), whereas Noveon® AA-1 is cross-linked with divinyl glycol (DVG). The effect of

the PAA types was evaluated in term of microparticle mucoadhesion and MMS *in vitro* performances.

A 2^3 full factorial design was built in to investigate the influence of formulation variables (*i.e.*, PAA type, ALG/PAA) and manufacturing parameter (*i.e.*, spraying air pressure) on the microparticle micrometrics the CP amount of penetrated in porcine mucosa after 6 h.

3.2 Materials and methods

3.2.1 Materials

Clobetasol propionate was purchased from Sicor SpA (Rho, Italy). Protanal® LF 120 M was supplied by FMC BioPolymer (Philadelphia, USA). Carbopol® 974P (APE-PAA), Noveon® AA-1 (DVG-PAA) were purchased from Lubrizol Corporation (Wickliffe, USA). Cremophor® RH 40 was kindly gifted by BASF (Ludwigshafen, Germany). Polyethylene glycol 400, sorbitol, saccharin sodium, methyl-paraben sodium, calcium chloride dehydrate were supplied by Farmalabor (Canosa di Puglia, Italy). Glycerol and ethanol were purchased form Carlo Erba Reagenti (Milan, Italy). Mint flavor was purchased from Kerry Group (Tralee, Ireland). Mucin type II was purchased from Sigma-Aldrich Co. (Milan, Italy). All other reagents and solvents were used as received without further purification.

3.2.2 Mouthwash preparation

The placebo feed solutions were made mixing aqueous dispersion of ALG and mucoadhesive polymers (*i.e.*, APE-PAA, DVG-PAA) in the 1/1 ratio. The feed solution was pumped at the rate of 15 mL/min into a standard two-way nozzle (0.8 mm inner diameter; Schlick Atomizing Technologies, Düsen-Schlick GmbH, Untersiemau, Germany) and sprayed into a 1% w/w calcium chloride solution, under magnetic stirring. The spraying air pressure ranged was set at 450 mbar. Microparticles were cured into the cross-linking bath for 1 h at room temperature before filtering throughout a 710 µm sieve. The final MMS were stored in 50 mL blue PE bottle at 25°C until use. The ratio between feed and aqueous vehicle were set up to achieve a final microparticle concentration of 10% w/w.

The CP-loaded MMS were prepared adding drug in both feed solution and vehicle solution to achieve final concentration of 0.025% w/v in microparticle and aqueous

vehicle. The PAA type, its concentration in microparticles and spraying air pressure were set up according 2^3 full factorial design (**Table 3.1** and **Table 3.2**). In order to compare the effectiveness of MMS with a marketed mouthwash containing 0.025% w/v CP, other excipients were added to aqueous vehicles as reported in **Table 3.3**.

***Table 3.1** - Factor and responses used in the 2^3 full factorial design of CP-loaded MMS and response specification.*

Factors	**Low level**	**High level**
PAA type (X_1)	APE-PAA	DVG-PAA
% PAA (X_2)	25	50
Air pressure (X_3, mbar)	450	550
Responses	**Goals**	
Particle mean diameter (Y_1)	None	
SPAN (Y_2)	Minimize	
Retained amount at 6h (Y_3)	Maximize	

3.2.3 Mucoadhesive properties

Although mucoadhesion of microparticles have been also investigated previously [3], the effect of DVG-PAA have not been evaluated on microparticle mucoadhesion yet. According that, three placebo MMS were made containing ALG only (P_0), ALG/APE-PAA (P_1) and ALG/DVG-PAA (P_2) (**Table 3.3**). The ratio between ALG and PAA was set up at 1/1 for maximize the mucoadhesion differences. The mucoadhesion properties of three formulation was determined after filtering microparticles through a 90 µm sieve. Aliquots of 100 mg microparticle were suspended in 2.5 mL purified water and known volume of 0.05% w/v mucin solution was added. Then, samples were shaken at 100 rpm for 5 min in a shaker incubator (Sartorius Stedim, Bagno a Ripoli, Italy) at 37±1 °C and centrifuged at 1000 x g by a Hettich Universal centrifuge 30F (Andreas Hettich GmbH & Co. KG, Tuttlingen, Germany). After discharging the supernatant, microparticles were washed by 5 mL fresh purified water to remove mucin not adsorbed on the surface. Afterwards, microparticles were re-suspended in 2.5 mL deionized water. Aliquot of each suspension (200 µL) were incubated with a micro BCA Protein Assay Reagent (Euroclone, Pero, Italy) for 30 min at 37±1 °C, as modified from Shi and Caldwell [6]. The amount of bound mucin was determined by spectrophotometer at the wavelength of

562 nm (DU®-640 spectrophotometer, Beckman Coulter, Brea, USA). The results were expressed as milligrams of bound mucin normalized for grams of microparticles. The data was reported as mean values ± SEM (n=3).

3.2.4 Design of experiments

A 2^3 full factorial design was built in to screen formulation and manufacturing parameter influencing the effectiveness of proposed CP-loaded OMS in mucosal drug penetration. Type of bioadhesive polymer (APE-PAA, DVG-PAA; X_1), theoretical PAA concentration in dried microparticles (X_2), and spray air pressure (X_3) were selected as independent variables (factors). The particle mean diameter (Y_1), particle size dispersion (SPAN; Y_2) and drug penetrated amount into mucosa after 6 h (Y_3) were used as dependent variables (responses; **Table 3.1**). Statistical analyses of the formulations design were performed using JMP® software version 10 (SAS Institute; Cary, USA).

3.2.5 Statistical analyses

Linear correlations were made from the response values of the Y_1, Y_2, Y_3 of results of 8 runs (**Table 3.2**). Analyses of variance (ANOVA) were performed to ensure the model fit. Factors and their interaction that significantly influenced Y_1, Y_2 and Y_3 were identified by stepwise backward analyses. Theoretical optimum condition was obtained by setting the maximum desirability of minimum Y_2 and maximum Y_3 (**Table 3.1**). Any optimal condition was set up for Y_1, considering that microparticle size was not a critical parameter for oromucosal delivery. Results were considered statistically significant at $p<0.05$ using the Fisher's t-test.

3.2.6 Microparticle size and distribution

The particle size of suspension (1 mL) was measured by an Accusizer 770 granulometer (PSS Inc., Santa Barbara, USA). Particle size was expressed as undersize cumulative percentages and the population dispersion was expressed as SPAN, according to the following equation (**Eq. 3.1**):

$$SPAN = \frac{d_{90} - d_{10}}{d_{50}} \times 100 \qquad \textbf{Eq. 3.1}$$

where d_{90}, d_{10} and d_{50} were the mean diameters at the 90%, 10% and 50% of the distribution of microparticle population, respectively.

3.2.7 Drug content

Microparticles recovered by filtration through 45 µm membrane were washed with acetonitrile to remove the drug absorbed on the surface and dried at room temperature till constant weight. Microparticle samples (50 mg) were digested in 10 mL of 5% w/v sodium chloride solution/acetonitrile (50/50, % v/v) under sonication for 2 h. Then, samples were 45 µm filtered and the CP content was quantified by HPLC as reported below. The CP content of aqueous vehicle was also determined after dilution 1:10 with HPLC-grade water. The analyses were carried out in triplicate.

3.2.8 HPLC analysis

The concentration of CP was determined by HPLC (HP 1100, Chemstations, Agilent Technologies, Santa Clara, USA). Compound separation was carried out using reverse-phase column (Water Spherisorb®, ODS2, 3 µm, 150x4.6 mm, Waters Co., Dublin, Ireland) and HPLC-grade water/acetonitrile (50/50, % v/v) as mobile phase. The flow rate was 1.0 mL/min and the injection volume of 20 µL. The drug concentration was determined at 240 nm from calibration curves in the range of 0.05-5 µg/mL (R^2>0.999).

3.2.9 In vitro mucosa penetration study

The *in vitro* mucosa penetration study was performed according the falling liquid technique described by Cilurzo et al. [3]. Briefly, the fresh porcine cheek mucosa was obtained by a local slaughterhouse. Specimens of mucosa were dipped in pH 7.4 PBS at 70°C for 1 min to isolate the mucosa epithelial layer. In-house equipment was composed by six in series mucosa supports set at an acute angle of 30°, the peristaltic pump and the liquid fraction collector. Tested MMS was sprayed twice onto a 2.5x1.0 cm mucosa surface corresponding a total amount of about 40 mg MMS. Then, porcine cheek epithelial layer was placed on the sample support and pH 6.4 PBS was dropped at the 1 mL/min rate to simulate the buccal environment and the saliva swallowing. At predefined times (*i.e.*, 1, 3 and 6 h), the applied test sample was peeled away by means of an adhesive tape strip and the mucosa was stored at -40°C for 24 h. Finally, mucosa samples were homogenized and penetrated drug amount was extracted in acetonitrile (2.5 mL) and then

quantified by HPLC. The amount of CP retained after a defined time (Q_{ret}) was expressed as micrograms of drug in micrograms of epithelial layer.

Table 3.2 *- Experimental matrix and observed responses from randomized runs in the 2^3 full factorial. In particular, PAA type (X_1), concentration (X_2) and air pressure setting (X_3), microparticle size (Y_1), SPAN (Y_2) and amount retained in the mucosa after 6 h (Y_3) are reported. The experimental results are expressed as mean values ± SEM (n=3).*

Form	**X_1**	**X_2 (%)**	**X_3 (mbar)**	**Y_1 (µm)**	**Y_2**	**Y_3** ***(µg/mg mucosa)***
C_1	DVG-PAA	25	450	172.2	0.78	1.01 ± 0.06
C_2	DVG-PAA	25	550	58.0	1.40	2.15 ± 0.29
C_2	DVG-PAA	50	450	178.6	0.77	0.67 ± 0.15
C_4	DVG-PAA	50	550	50.0	1.56	1.52 ± 0.36
C_5	APE-PAA	25	450	133.2	1.11	1.79 ± 0.50
C_6	APE-PAA	25	550	44.7	1.10	1.25 ± 0.01
C_7	APE-PAA	50	450	128.2	1.14	3.04 ± 0.35
C_8	APE-PAA	50	550	66.0	0.71	1.98 ± 0.56

Table 3.3 *– Composition of placebo mouthwashes (P_0-P_2), Reference (R) and optimal CP-loaded MMS (CP-MMS) according the results of 2^3 full factorial design. The ratio between Phase A and Phase B was fixed at 1/10.*

Ingredients		**Formulation composition (%)**				
		P_0	P_1	P_2	R	*CP-MMS*
Phase A (microparticles)	Clobetasol propionate	-	-	-	-	0.025
	Sodium alginate	3.00	1.50	1.50	-	1.50
	Carbopol® 974P	-	1.50	-	-	-
	Noveon® AA-1	-	-	1.50	-	1.50
	Purified water	97.00	97.00	97.00	100.00	97.00
Phase B (aqueous vehicle)	Clobetasol propionate	-	-	-	0.025	0.025
	Glycerol	-	-	-	10.00	10.00
	Ethanol	-	-	-	10.00	10.00
	Sorbitol	-	-	-	7.00	7.00
	Cremopohor® RH 40	-	-	-	2.40	2.40
	$CaCl_2$	1.00	1.00	1.00	1.00	1.00
	Mint Flavor	-	-	-	0.20	0.20
	Sodium saccharin	-	-	-	0.15	0.15
	Sodium methyl-paraben	-	-	-	0.10	0.10
	Purified water	89.00	89.00	89.00	69.125	69.125

3.3 Results and discussion

As expected, the addition of bioadhesive polymer to the feed solution conferred mucoadhesive properties to microparticles. In particular, the results showed that bound mucin increased from 1.33±0.07 mg/g for P_0 to 2.23±0.09 for P_1 (p=0.001) and 1.97±0.16 for P_2 (p=0.019). No significant differences were observed comparing the results of two types of PAA (p=0.225), showing that different cross-linker used did not significantly affect mucoadhesion.

CP could be added to feed solution and its final concentration in microparticles ranged from 0.029 to 0.032 % w/w. The drug loading caused an increase in particle size from about 50 µm of placebo microparticles [3] to 150 µm of CP-loaded MMS (**Table 3.2**). Furthermore, the step stepwise analyses highlighted that microparticle dimension were mainly affected by spraying air pressure (X_3). In particular, the microparticle size (Y_1) was inversely correlated to X_3, as shown in **Eq. 3.2** (p=0.016; R^2=0.64; F Ratio=10.90).

$$Y_1 = 496.17 - 0.76X_3 \qquad \textbf{Eq. 3.2}$$

On the contrary, the SPAN was influenced by the interaction of X_1 and X_3 (p=0.016). In particular, the higher the air pressure used to spray (X_3), the higher the values of Y_2. The linear correlation, valid only for MMS containing DVG-PAA, was shown by **Eq. 3.3** (p=0.012; R^2=0.97; F Ratio=77.35).

$$Y_2 = -2.39 + 0.01X_3 \qquad \textbf{Eq. 3.3}$$

This evidence suggested that cross-linked nature of PAA was critical for microparticle polydispersion. In general, cross-linking increased the rigidity of polymer structure. Therefore, it is possible that DVG-PAA chains affected the ALG reorganization in microparticles more strongly than APE-PAA, producing a high particle dispersion.

The *in vitro* penetration studies showed a high inter-sample variability (CV% > 30) due to high heterogeneity of epithelial layer of porcine mucosa [7]. However, the results showed different performances of tested formulation in drug retention into mucosa epithelial layer (**Figure 3.1**).

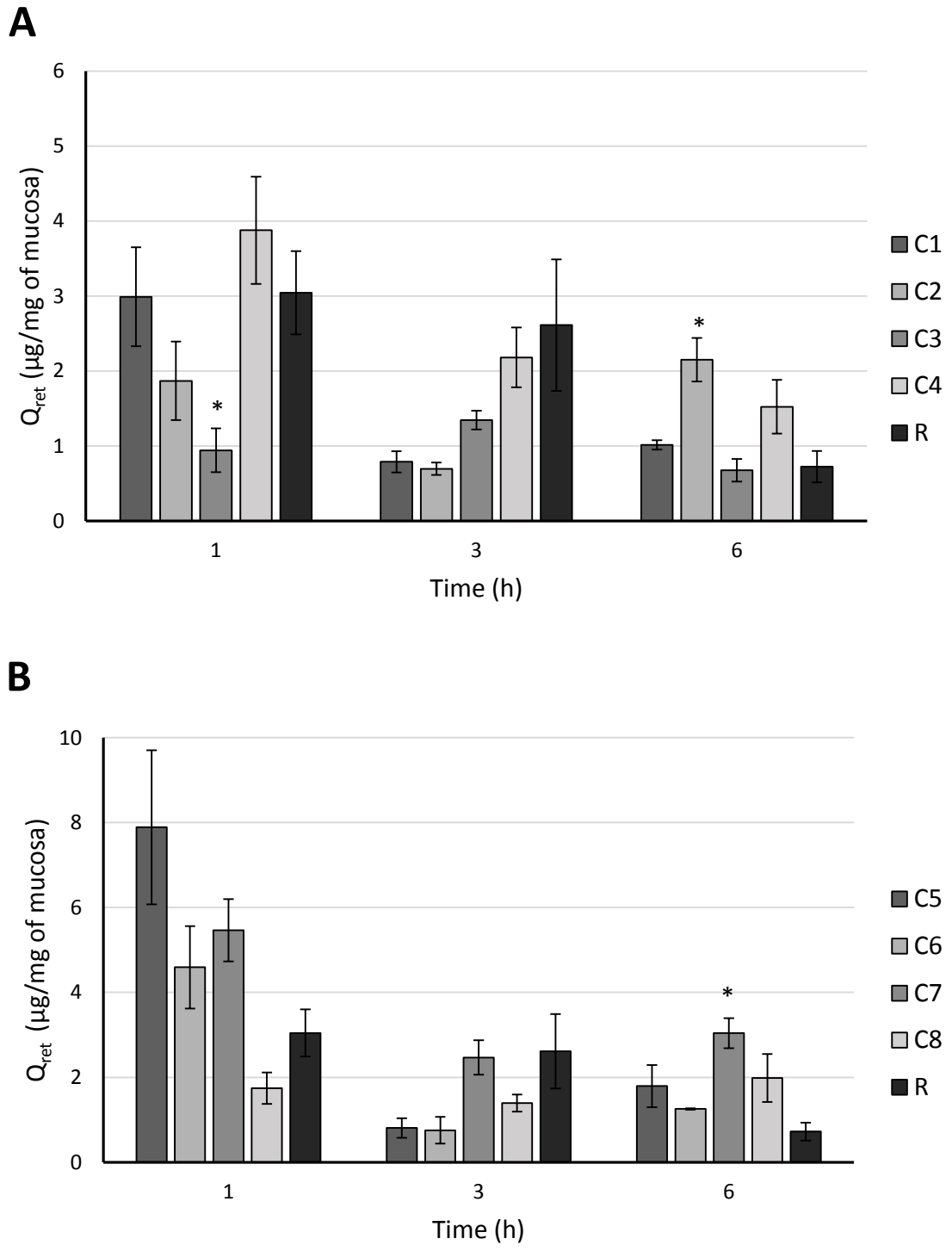

Figure 3.1 *– Q_{ret} of reference (R) and MMS formulations of 2^3 factorial design (**Table 3.2**) containing DVG-PAA (A) and APE-PAA (B) after 1, 3 and 6 h. Data are represented as average mean values ± SEM (n=3). *p<0.05 when compared with control by Student's t-test.*

Q_{ret} decreased over time both for reference mouthwash and for all MMS formulations. In the case of reference mouthwash, CP retained amounts decreased from 3.04±0.55 to 0.72±0.21 µg/mg of mucosa after 1 and 6 h, respectively. The CP- loaded MMS retention trends were influenced by design factors. Comparing **Figure 3.1 A** and **B**, it is noteworthy that Q_{ret} was higher for MMS containing APE-PAA than for those with DVG-PAA. For example, Q_{ret} were 0.94±0.29 and 5.47±0.73 µg/mg of mucosa after 1 hour from the application of C_3 and C_7, respectively ($p<0.01$). The statistical analyses also suggested that Q_{ret} after 6 h (Y_3) was significantly influenced by the PAA type (X_1; $p=0.017$), interaction of the PAA type with ALG/PAA ratio (X_1*X_2; $p=0.013$) and with air pressure (X_1*X_3; $p=0.006$).

Since the linear multiple regression fitted well with experimental results ($p=0.0068$; $R^2=0.94$; F Ratio=20.54), **Eq. 3.4** was applied to describe the factor influence on MMS made with APE-PAA.

$$Y_3 = 3{,}56 + 0.03X_2 - 0.01X_3 \qquad \textbf{Eq. 3.4}$$

According to that, the Y_3 was positively influenced by increase of APE-PAA and its concentration in the dried microparticle (X_2), whereas it was negatively affected by increase of spraying air pressure (X_3). The former observation might be justified considering that the APE-PAA concentration in microparticle was correlated to the improvement of microparticle mucoadhesion [3]. Therefore, the higher the mucoadhesive properties of microparticles the longer the resistance time on the buccal mucosa, prolonging the CP released at penetration site.

In the second case, the air pressure on Y_3 induced the presence of smaller microparticles on the mucosa surface as expressed by **Eq. 3.3**. These evidences might be explained considering that drug retention was related to microparticle residence time on the mucosa.

The falling film technique uses liquid flow on an inclined plane to simulate the physiological swallowing [8]. In these conditions, the liquid flow forces microparticles to roll on the mucosa surface. Therefore, microparticle movement might be simplified as sphere movement on the inclined plane.

The tendency to roll was directly correlated to the force applied on the sphere by liquid flow (F_L) and indirectly correlated to the rolling resistance (F_r). As reported by

Ketterhagen and coworkers, the force of rolling resistance has been directly related to the sphere weight (W) by the coefficient of rolling resistance (C_{rr}) [9]. Since F_L was constant during the experiment, the microparticle residence time on the mucosa was directly correlated to F_r. Furthermore, an increase of mucoadhesion produced higher C_{rr} due to the higher interaction between microparticle surface and mucosa layer. Therefore, at elevated PAA concentrations (X_2), C_{rr} increased because of stronger mucoadhesion and therefore the tendency of the microparticles to roll away to the mucosa resulted decreased.

On the other side, the negative effect of spraying air pressure (X_3) on Q_{ret} might be justified considering that size can be correlated to microparticle weight. At constant density: the smaller the size, the lower the microparticle weight and the lower F_r.

Moreover, statistical model allowed identifying optimal formulation and condition to achieving satisfying retention after 6 h. As shown in **Figure 3.2**, the optimal conditions were APE-PAA (X_1), 50% w/w of PAA (X_2) and 450 mbar (X_3; Desirability: 0.83).

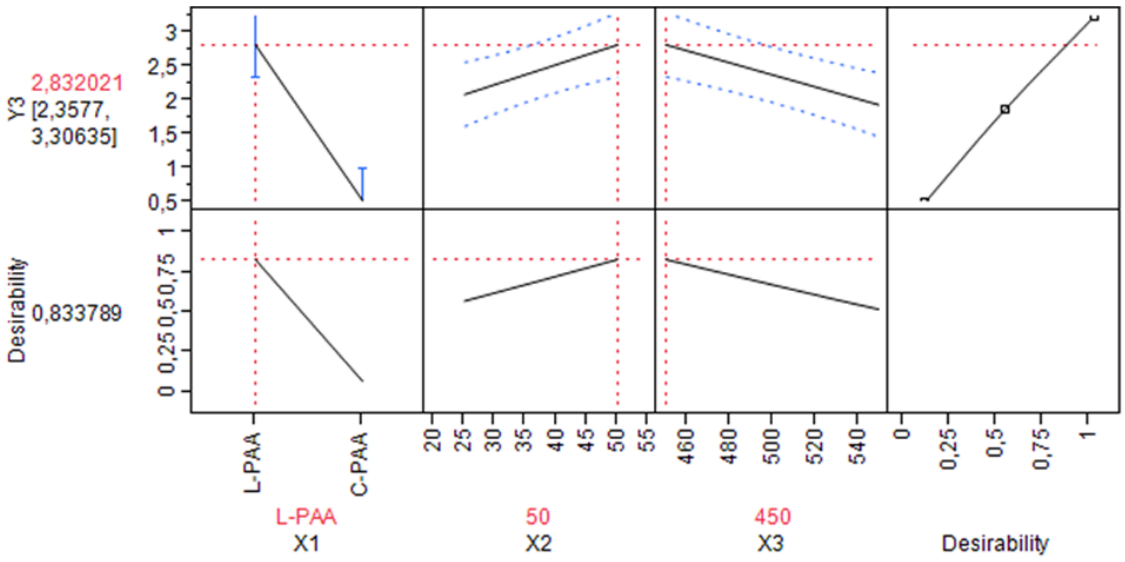

Figure 3.2 *– Prediction and desirability plot showing the effect of factors on Y_3 of 2^3 full factorial design.*

3.4 Conclusion

The experimental work confirmed that MMS was a suitable technological platform for oromucosal delivery of drugs. The current study demonstrated that MMS were also able to increase the mucosal penetration of clobetasol propionate. The 2^3 full factorial design showed which formulation and manufacturing process affect mainly the microparticles performances. Moreover, optimal conditions for high CP retention after 6 hours were obtained using APE-PAA as bioadhesive polymer in the 50% w/w of microparticle concentration. Finally, the spraying air pressure had to be set at 450 mbar in order to limit the particle size dispersion during the production process.

3.5 References

[1] Saunders, D. P., Epstein, J. B., Elad, S., Allemano, J., Bossi, P., van de Wetering, M. D., Rao, N. G., Potting, C., Cheng, K. K., Freidank, A., Brennan, M. T., Bowen, J., Dennis, K., and Lalla, R. V., 2013, "Systematic review of antimicrobials, mucosal coating agents, anesthetics, and analgesics for the management of oral mucositis in cancer patients" Support Care Cancer, 21(11), pp. 3191-3207.

[2] Nicolatou-Galitis, O., Sarri, T., Bowen, J., Di Palma, M., Kouloulias, V. E., Niscola, P., Riesenbeck, D., Stokman, M., Tissing, W., Yeoh, E., Elad, S., and Lalla, R. V., 2013, "Systematic review of anti-inflammatory agents for the management of oral mucositis in cancer patients" Support Care Cancer, 21(11), pp. 3179-3189.

[3] Cilurzo, F., Gennari, C. G. M., Selmin, F., Musazzi, U. M., Rumio, C., and Minghetti, P., 2013, "A Novel Oromucosal Prolonged Release Mucoadhesive Suspension by One Step Spray Coagulation Method," Curr. Drug Deliv., 10(3), pp. 251-260.

[4] Gombotz, W. R., and Wee, S., 1998, "Protein release from alginate matrices," Adv. Drug Deliv. Rev., 31(3), pp. 267-285.

[5] Cilurzo, F., Gennari, C. G. M., Selmin, F., Epstein, J. B., Gaeta, G. M., Colella, G., and Minghetti, P., 2010, "A new mucoadhesive dosage form for the management of oral lichen planus: Formulation study and clinical study," Eur. J. Pharm. Biopharm., 76(3), pp. 437-442.

[6] Shi, L., and Caldwell, K. D., 2000, "Mucin Adsorption to Hydrophobic Surfaces," J. Colloid Interface Sci., 224(2), pp. 372-381.

[7] Kulkarni, U., Mahalingam, R., Pather, I., Li, X., and Jasti, B., 2010, "Porcine buccal mucosa as in vitro model: Effect of biological and experimental variables," J. Pharm. Sci., 99(3), pp. 1265-1277.

[8] Rao, K. V. R., and Buri, P., 1989, "A novel in situ method to test polymers and coated microparticles for bioadhesion," Int. J. Pharm., 52(3), pp. 265-270.

[9] Ketterhagen, W. R., Bharadwaj, R., and Hancock, B. C., 2010, "The coefficient of rolling resistance (CoRR) of some pharmaceutical tablets," Int. J. Pharm., 392(1–2), pp. 107-110.

4 Resveratrol-loaded nanocarriers: formulation optimization, characterization and *in vitro* toxicity on cochlear cells

4.0 Abstract

The present work aimed to investigate polymeric nanoparticles (NPs) loaded with resveratrol (RES)-loaded nanoparticles (NPs) as suitable drug delivery system to cochlear cells. RES-loaded NPs were prepared by solvent-diffusion technique without surfactant. Box-Behnken design was used to study the effect of formulation variables on particle mean diameter, polydispersity index (PDI), zeta-potential, and percent drug encapsulation efficiency (EE%) and ratio between NPs size before and after freeze-drying (S_f/S_i). Furthermore, the physicochemical stability of the colloidal suspension was improved using different types and concentrations of cryoprotectants. Finally, the *in vitro* toxicity of the synthesized NPs was evaluated in two cochlear cell lines: organ of Corti (HEI-OC1) and *Stria Vascularis* (SVK-1) cells. The optimal formulation (desirability: 0.86) corresponded to NPs with mean diameter of 135.5±37.3 nm, PDI of 0.126±0.080, zeta-potential of -26.84±3.31 mV, EE% of 99.83±17.59% and S_f/S_i of 3.30±0.92. The particle mean diameter and PDI of RES-loaded NPs were maintained within the model space only when trehalose was used at concentrations higher than 15% w/v. The *in vitro* studies showed that blank NPs did not alter the viability of both cells lines, except for concentrations higher than 600 µg/mL. On the other hand, the cell viability decreased at high concentrations of native RES (>50µM) in both cell lines, whereas RES-loaded NPs influenced only HEI-OC1 cell viability.

The formulative and in vitro toxicity studies were carried out in the Laboratory of Future Nanomedicines and Theoretical Chronopharmaceutics directed by prof. Bi-Botti C. Youan, Division of Pharmaceutical Sciences, University of Missouri Kansas City, 2464 Charlotte St., Kansas City, MO 64108, USA.

The Powder X-ray diffraction analyses were carried out in the laboratory directed by prof. James B. Murowchick, Department of Geosciences, University of Missouri-Kansas City, 420 Flarsheim Hall, 5110 Rockhill Rd., Kansas City, MO, 64110, USA.

*The contents of this chapter have been submitted for publication to an. international peer-reviewed journal. Furthermore, the results of ancillary in vivo biodistribution study were presented as posters at the 2013 AAPS Annual Meeting and Exposition (**Appendix 4.1**).*

4.1 Introduction

Cisplatin (cis-diaminedichloroplatinum (II)) is one of the most frequently used chemotherapeutic agents for the treatment of several varieties of tumors, including ovarian, testicular, breast, hematologic, lung, cervical, and head and neck cancers. However, its clinical effectiveness is often correlated with severe side effects such as ototoxicity [1]. Cisplatin-induced ototoxicity generally manifests as ear pain, tinnitus, sensorial hearing loss and deafness. In particular, around 60% of treated patients have exhibited elevated hearing threshold with a higher incidence in children than in adults [2].

Cisplatin has been demonstrated to trigger *in vitro* activation of apoptosis in cochlear cell lines (*i.e.*, outer hair, *Strial Ganglion* and *Stria Vascularis* cells) through the generation of reactive oxygen species (ROS) [3, 4]. Therefore, the efficacy of several antioxidant agents, including α-lipoic acid, D-methionine, ebselen, L-carnitine, N-acetylcysteine, has been tested *in vitro* and *in vivo* after local and systemic delivery [1, 5]. However, there are no FDA/EMA-approved medicines for the treatment of hearing impairment caused by cisplatin.

Recently, resveratrol (RES) has been proposed as a protective agent since its effectiveness was proven after systemic administration in guinea pigs and rats [6, 7]. RES (3,5,4'-trihydroxystilbene) is a non-flavonoid poly-phenolic compound abundant in grapes, peanuts and other foods. In humans, RES has been correlated with several pharmacological effects, including cardio-protection, cancer prevention, anti-inflammatory activity, antioxidant effects, improvement of cellular stress resistance and longevity [8]. However, the use of RES in clinics remains limited due to its low oral bioavailability (70%), rapid metabolism and elimination [9]. Several delivery systems including microparticles, ultra-fine fiber, nanosponges, liposomes, and nanoparticles (NPs) have been proposed as alternative solutions to bypass the pharmacokinetic limitations [9].

In the present study, RES was loaded in polymeric NPs, made of two biodegradable polymers. Poly-(lactic-co-glycolic) acid (PLGA) was selected as a biodegradable polymer considering its well-known safety and ability to control drug release. On the other hand, the poly-(caprolactone)–poly-(ethylene glycol) (PCL–PEG) di-block was

used for taking advantage of its amphiphilic nature for stabilizing nanoparticle surface and improving drug loading.

Recently, experimental approaches based on design of experiment (DoE) have been widely applied in the academic research and pharmaceutical development of new drugs [10, 11]. Hence, Box-Behnken design (BBD) was selected, requiring fewer number of runs (12 plus 3 center points) and only three levels of each independent variable than other response surface designs [12]. The BBD allowed to deeply investigate the influence of formulation variables (*i.e.*, RES, PLGA and PCL-PEG amounts) on the selected responses, namely particle mean diameter, PDI, Zeta-potential, percent drug encapsulation efficiency (EE%) and physicochemical changes after freeze-drying.

The optimal formulation was also characterized by powder X-ray diffraction (PXRD), scanning electron microscopy (SEM) and *in vitro* drug release. Furthermore, the effect of well-known cryoprotectants was investigated to minimize physical instability of nanoparticle system during freeze-drying.

Since no information has been available in literature about the pharmacology/toxicology of RES in cochlear cells, its toxicity was evaluated *in vitro* in two different cochlear cell lines: organ of Corti cells (HEI-OC1) and a *Stria Vascularis* one (SVK-1) [13, 14]. The toxicity of blank and RES-loaded NPs was also tested in HEI-OC1 and SVK-1 cells.

4.2 Materials and Methods

4.2.1 Materials

RES was obtained from AK Scientific Inc. (Union City, USA). Poly-(D,L-lactide-co-glycolide) with a L/G ratio of 50/50 and inherent viscosity of 0.39 dL/g was supplied from Birmingham Polymers Inc. (Pelham, USA). Poly-(ε-caprolactone)–poly-(ethylene glycol) di-block was obtained from Advanced Material Polymers Inc. (Montréal, Canada). Sucrose, trehalose, acetone, methanol were supplied from Sigma Aldrich (Saint-Louis, USA). Lactose and Mannitol were obtained from Fisher Scientific Inc. (Pittsburgh, USA). All other chemicals used in the study were of analytical grade and were used without further purification.

4.2.2 Preparation of resveratrol-loaded nanoparticles

RES-loaded NPs were prepared by solvent-diffusion technique without surfactant adapted from published method [15]. NPs were prepared by varying the amounts of RES and PCL-PEG/PLGA ratio (**Table 4.1**). Briefly, a known amount of PLGA and PCL-PEG was dissolved in 1 mL of acetone containing a known amount of RES. The resulting solution was added dropwise into 10 mL of purified water (Direct-Q 3 UV system, Millipore SAS, Molsheim, France) under constant mechanical stirring at 1,100 rpm (stirrer model RO 15, IKA-WerkeGmbh& Co, Staufen, Germany). The organic phase was evaporated (BUCHI Labor technik AG, Flawil, Switzerland) at 25°C for 2 h. Finally, the RES-loaded NPs were isolated by centrifugation at 15,000 rpm, 4°C for 20 min (VWR International Micro 18R, Darmstadt, Germany), washed twice and re-suspended in purified water. Then, the suspension was frozen at -196°C in liquid N_2 and dried at -47°C, 0.01 mbar, for 24 h (Labconco Corporation, Kansas City, USA). The powdered RES-loaded NPs were stored at 4°C until use. Blank NPs were similarly prepared without active substance.

4.2.3 Preparation of resveratrol nanocrystals

RES nanocrystals were produced according to a published method [16] using acetone and water as solvent and anti-solvent, respectively. The organic solution and the anti-solvent were mixed rapidly to assure fast nucleation and thereby forming small particles. RES nanocrystals were collected by centrifugation (10,000 rpm for 20 min at 5°C), washed twice and freeze-dried.

4.2.4 Design of experiments

4.2.4.1 Experimental design

The BBD was used as experimental design for response surface methodology to optimize the NP formulation. RES (X_1), PLGA (X_2), and PCL–PEG amount (X_3) were selected as independent variables (factors). The particle mean diameter (Y_1), polydispersity index (PDI; Y_2), zeta-potential (Y_3), percent drug encapsulation efficiency (EE%; Y_4), and ratio between NP diameter before (S_i) and after (S_f) freeze-drying (Y_5) were used as dependent variables (responses, **Table 4.1**). A statistical model incorporating interactive and polynomial terms was utilized to evaluate the formulation responses (**Eq. 4.1**).

$$Y_i = b_0 + b_1X_1 + b_2X_2 + b_3X_3 + b_{1,2}X_1X_2 + b_{1,3}X_1X_3 + b_{2,3}X_2X_3 + b_{1,1}{X_1}^2 + b_{2,2}{X_2}^2 + b_{3,3}{X_3}^2 \quad \textbf{Eq. 4.1}$$

where Y_i is the dependent variable, b_0 is the arithmetic mean response of the 15 runs, b_i is the estimated coefficient for each factor and X_i represents the independent variables.

Table 4.1 *- Variables used in the Box-Behnken Design of RES-loaded NPs engineering and response specification of Monte Carlo simulation.*

Factors	**Levels**		
	Low	*Medium*	*High*
X_1 (Resveratrol amount, mg)	3	6	9
X_2 (PLGA amount, mg)	3	6	9
X_3 (PCL-PEG amount, mg)	3	6	9
Responses	**Goals**	**Simulation specification**	
Y_1 (particle mean diameter; nm)	Minimize	< 200 nm	
Y_2 (PDI)	Minimize	< 0.2	
Y_3 (Zeta-potential; mV)	None	< - 15 mV	
Y_4 (EE%)	Maximize	85 – 125%	
Y_5 (S_f/S_i)	Minimize	None	

Statistical analysis of the formulation design was performed using JMP® software version 10 (SAS Institute, Cary, USA). Furthermore, the robustness of the optimal formulation was tested using the Monte Carlo simulation (15,000 runs) [17]. The Monte Carlo simulation allowed to evaluate the influence of casual changes in factors on reproducibility of model responses. After simulation, each tested parameter was associated with defect rate value, which indicated how many runs of simulation were out of the targeted response specifications (**Table 4.1**).

4.2.4.2 Checkpoint analysis

The resulting statistical model was checked in triplicate with two random points with respective (X_1, X_2 and X_3) values of (−0.5, −0.5, −0.5) and (+0.5, +0.5, +0.5), in addition to the theoretically optimal formulation R_{16} (+1.4, −1, −0.7; **Table 4.2**). Biases percentage (**Eq. 4.2**) between predicted and observed values were calculated for all dependent

variables. The experimental responses (Y_i) were compared with those predicted by the model using the Student's t-test.

$$Bias\ \% = \frac{(predicted\ value - observed\ value)}{observed\ value} x100 \quad \textbf{Eq. 4.2}$$

4.2.4.3 Statistical analysis

Polynomial equations were made by the significant response values of Y_1, Y_2, Y_3, Y_4 and Y_5 of 15 run results. One-way analysis of variance (ANOVA) and the analysis of lack of fit were performed to ensure the model fitting. The formulation variables that significantly affected Y_1, Y_2, Y_3, Y_4 and Y_5 were identified and shown through a Pareto chart. The theoretical optimum condition was obtained by setting the maximum desirability of minimum Y_1, Y_2, Y_5 and maximum Y_4. Since Y_3 was not critical for the proposed formulation, the desirability was not set up (**Table 4.1**). Results were considered statistically significant at $p<0.05$ using the Fisher's t-test.

4.2.5 Physiochemical characterization of resveratrol-loaded nanoparticles

4.2.5.1 Particle mean diameter, polydispersity index and zeta-potential measurements

The particle mean diameter, PDI, and zeta-potential were measured at 25°C by dynamic light scattering method (DLS; Zetasizer Nano ZS, Malvern Instruments Ltd, Worcestershire, UK). According to the National Institute of Standards and Technology, a sample with a PDI < 0.05 is considered monodisperse [18].

4.2.5.2 Percent drug encapsulation efficiency of resveratrol-loaded nanoparticles

The percent drug encapsulation efficiency (EE%; Y_4) was evaluated according to a previous method described by Youm et al. [19] with a slight modification. Briefly, the powdered RES-loaded NPs (1 mg) were dissolved in 0.02 mL of acetone and diluted (1:74, v/v) in a mixture of 1% v/v acetic acid aqueous solution and methanol (40:60). The suspension was centrifuged at 15,000 rpm, 4°C for 20 min and then the supernatant was collected for analysis. The amount of RES in the supernatant was determined by high performance liquid chromatography (HPLC, Milford, USA) equipped with UV detector at 305 nm. An isocratic flow of mobile phase composed of 1% v/v acetic acid aqueous

solution/methanol (40:60, v/v) was employed at a flow rate of 1 mL/min with an injection volume of 10 µL. The separation of RES was carried out using a Waters Spherisorb ODS2 Column, 80 Å, 5 µm, 4.6 x 250mm (Waters Corporation, Milford, USA) [20]. The calibration curves were constructed in the range of 0.002 to 0.05mg/mL (R^2=0.9982) and 0.05 to 1.00 mg/mL (R^2=0.9993). The experimental loading of RES was quantified using the peak area of each NP formulation. Theoretical RES loading (DL) and EE% were calculated according to **Eq. 4.3** and **Eq. 4.4**:

$$DL\% = \frac{Drug\ amount}{Amount\ of\ polymer+drug} x100 \qquad \textbf{Eq. 4.3}$$

$$EE\% = \frac{Experimental\ drug\ loading}{Theoretical\ drug\ loading} x100 \qquad \textbf{Eq. 4.4}$$

4.2.5.3 Powder X-ray diffraction analysis of resveratrol-loaded nanoparticles

PXRD analyses of the powdered RES-loaded NPs were performed using a MiniFlex automated X-ray diffractometer (Rigaku, The Woodlands, USA) at room temperature. Ni-filtered Cu Kα radiation was used at 30 kV and 15 mA. The diffraction angle covered from 2θ = 10° to 2θ = 50° with a step size of 0.05°/step, and a count time of 2.5 sec/steps (effectively 1.2 °/min). The samples were tested for 38 min. The diffraction patterns were processed using Jade 8+ software (Materials Data, Inc., Livermore, USA).

4.2.6 Effect of cryoprotectants on resveratrol-loaded nanoparticle changes during freeze-drying

In order to minimize unexpected physical changes of RES-loaded NPs, lactose, mannitol, sucrose, and trehalose were tested to achieve suitable cryoprotection. Cryoprotectant aqueous solutions were made at various concentrations (2%, 10%, 20%, 30%, 40%, w/v) and mixed with aliquots of RES-loaded NP suspension before freeze-drying, to obtain the final concentration of 1%, 5%, 10%, 15%, and 20% w/v. The suspensions were frozen at -196°C in liquid N_2 and dried at -47°C, 0.01 mbar for 24 h.

The particle mean diameter and PDI were measured by DLS before and after freeze-drying at 25°C. The former analyses were carried out after diluting the mother suspension (1:50, v/v) in HPLC-grade water (Fisher Scientific Inc., Pittsburgh, USA) and sonicating the latter for 1 min. On the other hand, the particles dispersibility was optimized in

suspending 1 mg of the powdered RES-loaded NPs in HPLC-grade water (dilution 1:50, v/v). The colloidal supension was sonicated for 1 min with a probe-sonicator (Sonicator 300, Misonix Inc., Farmingdale, USA) and analyzed by DLS. The initial and final particle mean diameter and PDI ratios (S_f/S_i; PDI_f/PDI_i) were calculated as end points of the freeze-drying process. The variabilities accepted by BBD for Y_1 and Y_2 were utilized as references to evaluate the physical stability of the particles after freeze-drying. Therefore, S_f/S_i and PDI_f/PDI_i values up to 1.27 and 1.59 were considered out of the model space.

4.2.7 Morphological analysis of resveratrol-loaded nanoparticles

Mixtures of RES-loaded NPs and cryoprotectant (15%, w/v) were analyzed by scanning electron microscopy (SEM). For this purpose, a small amount of the powdered RES-loaded NP/cryoprotectant mixture was put into a grid and visualized under a Philips SEM 515 microscope (Philips/FEI, Eindhoven, USA).

4.2.8 In vitro drug release from resveratrol-loaded nanoparticles

In vitro drug release from RES-loaded NPs was performed using a dialysis method [19]. Specifically, a known amount of the powdered RES-loaded NPs (2 mg) was suspended in an inner dialysis bag (Spectra/Por Float-A-Lyzer G_2, MWCO 3.5-5 kD, Spectrum Laboratories Inc. Rancho Dominguez, USA) containing 4 mL of 5% w/v ethanol aqueous solution. Considering the poor water solubility of RES [9], ethanol medium was chosen to achieve sink condition. In turn, the inner bag containing the RES-loaded NP suspension was placed in a tube filled with 15 mL of 5% w/v ethanol solution. The system was placed in a shaking water bath (BS-06, Lab. Companion, Des Plaines, USA) at 25°C, under constant agitation (speed 50 rpm). At several times (1, 8, 24, 48, 72, and 96 h), aliquots of 300 μL were withdrawn and replaced with the same volumes of fresh medium to maintain constant the volume. The percent of RES released (%) from the NPs was calculated at each time point as a percentage of total entrapped drug. RES nanocrystals were used as a reference.

4.2.9 In vitro cell culture study of resveratrol-loaded nanoparticles

4.2.9.1 Cell culture

The toxicity studies were performed using cochlear cell lines as previously described [21]. Briefly, HEI-OC1 and SVK-1 cells, obtained from the House Research Institute (formerly

House Ear Institute, Los Angeles, USA), were cultured under permissive conditions (33°C, 10% CO_2) in 75 cm^2 culture flasks containing high-glucose Dulbecco's Modified Eagle's Medium (DMEM; Gibco BRL, Gaithersburg, USA) and 10% v/v fetal bovine serum (FBS; Gibco BRL, Life Technologies, Carlsbad, USA).

4.2.9.2 In vitro toxicity of native resveratrol and resveratrol-loaded nanoparticles

The *in vitro* toxicity of RES, blank NPs and RES-loaded NPs was investigated by the cell viability and cellular membrane integrity assays after 24 h incubation.

The cell viability was determined by methyl tetrazolium salt (MTS) assay following the manufacturer protocol. The assay was optimized for the cell lines used in the experiments. Briefly, cells were transferred to 96-well plates to ensure $1x10^4$ cells per well until 80% confluence. Then, each well was filled with 100 µL of increasing concentrations of native RES, RES-loaded NPs (RES concentration: 0.005, 0.05, 0.5, 5, 50, 500 µM) and blank NPs (NPs concentration: 200, 400, 600, 800, 1000 µg/mL) for 24 h of incubation at 37°C with 5% CO_2. The fresh medium and 1% of Triton X-100 were used as the control and positive control, respectively. After incubation, 20 µL of CellTiter 96® Aqueous One Solution Reagent (Promega, Madison, USA) was added to each well for 3 h. After the completion of exposure period, 96-well plates were placed on a DTX 800 multimode microplate reader (Beckman Coulter, Brea, USA) and absorbance of the formazan product was read at 490 nm. The cell viability was determined using **Eq. 4.5**:

$$Cell\ viability\ (\%) = \frac{ABS_{Test}}{ABS_{Control}} \times 100 \qquad \textbf{Eq. 4.5}$$

where ABS_{Test} and $ABS_{Control}$ represent the absorbance of formazan detected in viable cells treated with NPs and the culture medium alone, respectively.

The cellular membrane integrity was determined by the release of lactate dehydrogenase (LDH) following the manufacturer protocol. Briefly, cells were seeded in a 96-well plate and incubated with native RES, blank NPs and RES-loaded NPs using the same condition as the MTS assay. After 24 h of incubation, the medium was removed and the cells were washed twice with phosphate buffered saline (PBS). Then, 100 µL of CytoTox-One™ reagent (Promega, Madison, USA) was added in each well. The microplate was maintained at room temperature for 10 min and 50 µL of stop solution was added to each

well. The fluorescence was detected using the microplate reader at an excitation wavelength of 560 nm and emission wavelength of 590 nm. For this assay, the samples of both supernatant and cell lysate were determined in order to correct any endogenous LDH activity in mammalian cells. The percent cell death for a given treatment is expressed through **Eq. 4.6**:

$$Cytoxicity\ (\%) = \frac{Experimental - Background}{Positive - Background} x100 \qquad \textbf{Eq. 4.6}$$

where Experimental, Background, and Positive represent the fluorescence of the NPs treated, not treated, and cells treated with 1% of Triton X-100, respectively.

4.3 Results

4.3.1 Optimization of resveratrol-loaded nanoparticles

RES-loaded NPs were successfully formulated and optimized using BBD. The effect of independent variables (X_1, X_2, and X_3) on Y_1, Y_2, Y_3, Y_4 and Y_5 were thoroughly investigated. As showed in **Table 4.2**, RES-loaded NPs had Y_1 and Y_2 ranging from 119.1 to 329.5 nm and from 0.089 to 0.334, respectively. The Y_3 was ranged from -35.2 to -12.83 mV, Y_4 from 31.11% to 141.35% and Y_5 from 1.69 to 5.84. The effect of formulation variables on the NPs physicochemical properties is shown in **Figure 4.1** and **Figure 4.2**.

Pareto charts show that a positive increase of Y_1 can influence X_1 (*e.g.,* R_3 versus R_5; **Table 4.2**) and X_2 (*e.g.,* R_7 versus R_{10}). On the other hand, X_3 did not have any significant effect on Y_1 (p=0.8687).

Table 4.2 *– Experimental matrix, observed responses from randomized runs, optimal formulation (R_{16}), and checkpoint formulation (R_{17}, R_{18}) in the BBD (**Table 4.1**).*

Form.	**X_1 (mg)**	**X_2 (mg)**	**X_3 (mg)**	**Y_1 (d-nm)**	**Y_2**	**Y_3 (mV)**	**Y_4 (%)**	**Y_5**
R_1	6	9	3	203.4	0.089	-33.00	104.18	3.55
R_2	3	3	6	128.0	0.152	-29.03	31.11	4.07
R_3	3	9	6	152.7	0.129	-35.20	47.43	4.68
R_4	3	6	9	138.5	0.147	-30.83	43.95	5.84
R_5	9	9	6	329.5	0.334	-26.00	103.08	3.01
R_6	6	3	3	152.7	0.129	-28.50	98.52	4.68
R_7	6	3	9	119.1	0.194	-21.15	138.45	2.34
R_8	9	6	3	212.5	0.157	-31.77	107.5	4.62
R_9	6	6	6	164.8	0.137	-28.77	77.62	3.79
R_{10}	6	9	9	178.4	0.215	-26.93	116.82	3.89
R_{11}	9	6	9	289.4	0.520	-12.83	141.35	1.69
R_{12}	6	6	6	164.6	0.133	-27.20	95.04	3.50
R_{13}	3	6	3	167.6	0.162	-22.33	63.99	2.73
R_{14}	6	6	6	177.7	0.202	-23.93	90.15	2.67
R_{15}	9	3	6	161.5	0.180	-22.97	100.18	2.45
R_{16}	7.4	3	5.3	136.2	0.127	-26.80	100.09	3.30
R_{17}	7.5	7.5	7.5	236.70	0.289	-24.47	100.65	2.46
R_{18}	4.5	4.5	4.5	136.10	0.137	-27.20	75.32	4.31

Furthermore, the interactions between X_1 and X_2, and the intermolecular interaction of X_1 was shown to have a significant effect on Y_1 (p=0.0223; p=0.0410, respectively). The following polynomial equation was found to represent adequately Y_1 variation (p=0.001, R^2 = 0.88; **Eq. 4.7**):

$$Y_1 = 165.81 + 50.76X_1 + 37.83X_2 + 35.82X_1X_2 + 31.64X_1^2 \quad \textbf{Eq. 4.7}$$

In contrast, Y_2 was mainly influenced by X_1 and X_3 and the interaction between X_1 and X_3 and intramolecular interaction of X_1, (p=0.0006, R^2=0.84; **Eq. 4.8**):

$$Y_2 = 0.16 + 0.08X_1 + 0.07X_2 + 0.09X_1X_3 + 0.06X_1^2 \quad \textbf{Eq. 4.8}$$

Sorted Parameter Estimates — A

Term	Estimate	Std Error	t Ratio	Prob>|t|
X1(3,9)	50,7625	7,760475	6,54	0,0013*
X2(3,9)	37,8375	7,760475	4,88	0,0046*
X1*X2	35,825	10,97497	3,26	0,0223*
X1*X1	31,245833	11,42311	2,74	0,0410*
X1*X3	26,5	10,97497	2,41	0,0605
X2*X2	-7,354167	11,42311	-0,64	0,5481
X2*X3	2,15	10,97497	0,20	0,8524
X3(3,9)	-1,35	7,760475	-0,17	0,8687
X3*X3	1,7208333	11,42311	0,15	0,8861

Sorted Parameter Estimates — B

Term	Estimate	Std Error	t Ratio	Prob>|t|
X1(3,9)	0,075125	0,016713	4,50	0,0064*
X3(3,9)	0,067375	0,016713	4,03	0,0100*
X1*X3	0,0945	0,023635	4,00	0,0103*
X1*X1	0,0655833	0,0246	2,67	0,0446*
X1*X2	0,04425	0,023635	1,87	0,1201
X2*X2	-0,024167	0,0246	-0,98	0,3710
X3*X3	0,0235833	0,0246	0,96	0,3818
X2(3,9)	0,014	0,016713	0,84	0,4404
X2*X3	0,01525	0,023635	0,65	0,5472

Sorted Parameter Estimates — C

Term	Estimate	Std Error	t Ratio	Prob>|t|
X1*X3	6,86	0,976257	7,03	0,0009*
X3(3,9)	2,9825	0,690318	4,32	0,0076*
X1(3,9)	2,9775	0,690318	4,31	0,0076*
X2(3,9)	-2,435	0,690318	-3,53	0,0168*
X2*X2	-2,310833	1,016121	-2,27	0,0721
X3*X3	1,5491667	1,016121	1,52	0,1879
X1*X2	0,785	0,976257	0,80	0,4579
X1*X1	0,6441667	1,016121	0,63	0,5540
X2*X3	-0,32	0,976257	-0,33	0,7564

Sorted Parameter Estimates — D

Term	Estimate	Std Error	t Ratio	Prob>|t|
X1(3,9)	33,20375	3,66335	9,06	0,0003*
X3*X3	22,818333	5,392305	4,23	0,0082*
X1*X1	-21,22417	5,392305	-3,94	0,0110*
X1*X3	13,4725	5,180759	2,60	0,0482*
X3(3,9)	8,2975	3,66335	2,27	0,0729
X2*X3	-6,8225	5,180759	-1,32	0,2450
X2*X2	4,0708333	5,392305	0,75	0,4843
X1*X2	-3,355	5,180759	-0,65	0,5458
X2(3,9)	0,40625	3,66335	0,11	0,9160

Figure 4.1 *– Pareto Charts showing standardized effect of formulation variables (X_1, X_2, X_3) and their interaction on Y_1 (A), Y_2 (B), Y_3 (C), Y_4 (D): x-axis showing the t ratio. Bars extending past the vertical line indicate values reaching statistical significance.*

The results also indicated that X_1 (*e.g.*, R_3 versus R5) and X_3 (*e.g.*, R_1 versus R_{10}) induced the significantly increase of Y_3, whereas an increase of X_2 leads to a decrease of Y_3 (*e.g.*, R_7 versus R_{10}). The interaction between X_1 and X_3 influenced significantly Y_3 ($p=0.0009$). The **Eq. 4.9** reports all significant effects on Y_3 ($p=0.0002$, $R^2=0.87$):

$$Y_3 = -26.69 + 2.98X_1 - 2.44X_2 + 2.98X_3 + 6.86X_1X_3 \qquad \textbf{Eq. 4.9}$$

Y_4 increased with an increase of X_1 (*e.g.*, R_3 versus R_5; **Table 4.2**) and X_3 (*e.g.*, R_4 versus R_{13}). Moreover, the increases of X_2 did not have any significant influence on Y_4 ($p=0.9160$). The data showed a significant interaction of X_1 ($p=0.0110$), X_3 ($p=0.0082$). The interaction between X_1 and X_3 ($p=0.0482$) had a significant effect on Y_4. The following polynomial equation represents Y_4 variation ($p<0.0001$, $R^2 = 0.94$; **Eq.4.10**):

$$Y_4 = 90.11 + 33.20X_1 + 8.30X_3 + 13.47X_1X_3 - 21.53X_1^2 + 22.50X_3^2 \qquad \textbf{Eq. 4.10}$$

Finally, Y_5 results showed that the modification of the formulation composition was not able to prevent the instability of the freeze-dried nanoparticles ($Y_5 > 1$; **Table 4.2**). Furthermore, the Pareto chart shows that Y_5 was mainly influenced by X_1 ($p=0.0153$; data not shown).

Table 4.3 *– Biases (%) between predicted and observed values for all dependent variables (**Table 4.1**) of three checkpoint formulations.*

Responses	Bias (%)		
	R_{16}	R_{17}	R_{18}
Y_1	-6.02	2.50	8.16
Y_2	0.81	6.29	-2.21
Y_3	-8.08	-7.71	-2.07
Y_4	0.46	12.74	-9.97
Y_5	7.52	14.70	-16.71

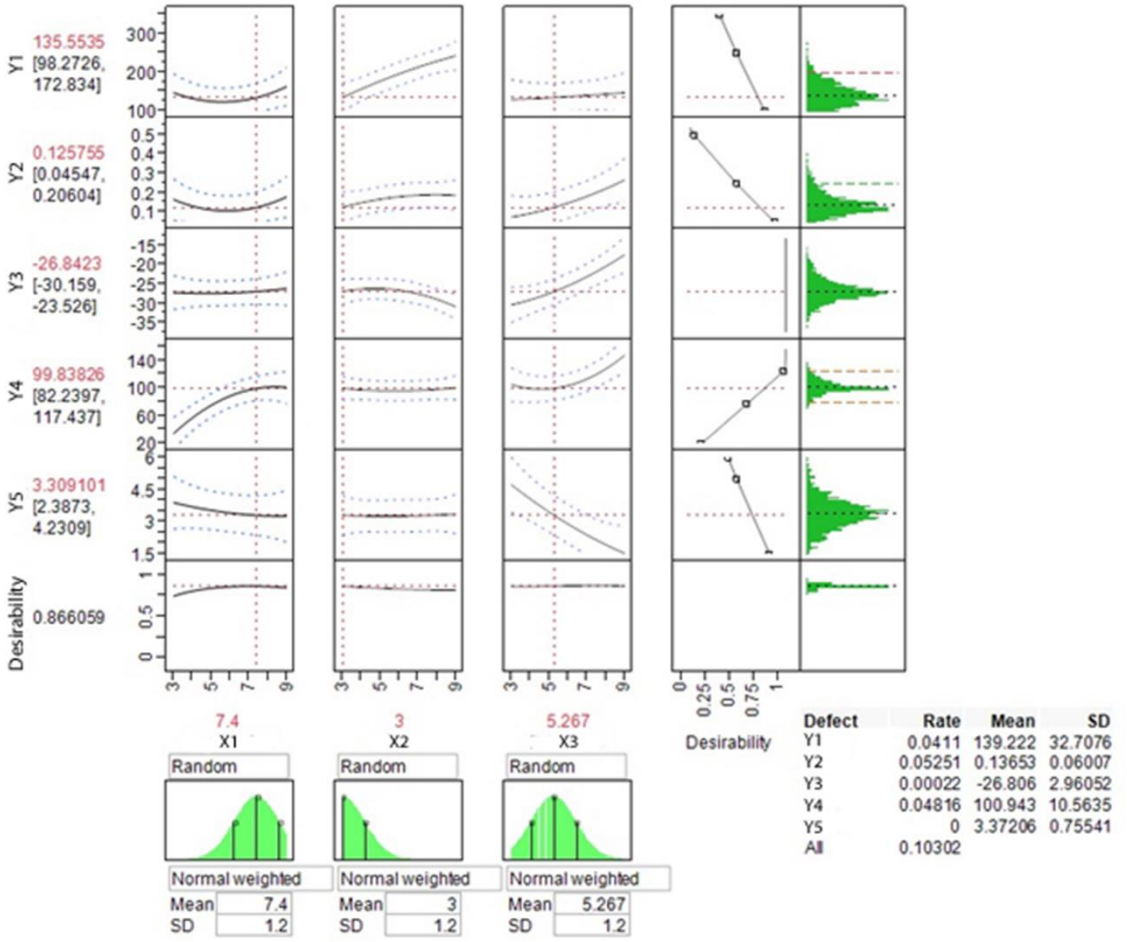

Figure 4.2 *– Prediction, desirability, and simulation plot showing the effect of factors on the responses (**Table 4.1**).*

As showed in **Figure 4.2**, the BBD optimal formulation was R_{16} (desirability 0.86). The predicted responses of the optimal formulation were Y_1: 135.5±37.3 nm, Y_2: 0.126±0.080, Y_3: -26.84±3.31 mV, Y_4: 99.83±17.59 %, and Y_5: 3.30±0.92 (**Table 4.2**).

A checkpoint analysis was performed with two random points R_{17}, R_{18} and R_{16} (**Table 4.2**). The differences between predicted and measured Y_i values were not statistically significant ($p>0.10$). Moreover, Y_i biases (%) were lower than 10%. The only exceptions were Y_5 values of R_{17} and R_{18} (**Table 4.3**). It might be explained by the fact that the model lost accuracy predicting stochastic events such as physical changes that occurred during freeze-drying [22].

According to the Monte Carlo simulation, the cumulative defect rate was near to 0.10, indicating that less than 10% runs were discarded. This indicated a good robustness of model prediction (**Figure 4.2**). Furthermore, the simulation showed Y_1 (defect rate: 0.04), Y_2 (defect rate: 0.05), and Y_4 (defect rate: 0.05) as the most sensitive responses to casual errors.

4.3.2 Powder X-ray diffraction pattern analysis of resveratrol-loaded nanoparticles

Representative PXRD patterns of the native RES, polymers, physical mixture (RES+PLGA+PCL-PEG, 1:1:2, w/w/w; RES+blank $R_{16,}$ 1:1, w/w) and three RES-loaded NPs (R_2, R_{11}, R_{16}) are reported in **Figure 4.3**. As shown, native RES exhibited major diffraction peaks at 16°, 19°, 22°, 23°, 25°, and 28°, which were consistent with previous RES crystallography [23, 24]. PEG-PCL exhibited four characteristic peaks at 19°, 21°, 22°, and 24° as reported previously [19].

The RES and PEG-PCL diffraction peaks were present in the PXRD pattern of the physical mixture. In contrast, these peaks disappeared in both blank NPs and RES-loaded NPs, suggesting its presence in amorphous state. RES diffraction peaks were detected in the physical dispersion with blank R_{16} and in RES-loaded NPs (R_{11}, R_{16}), but not in the formulation R_2

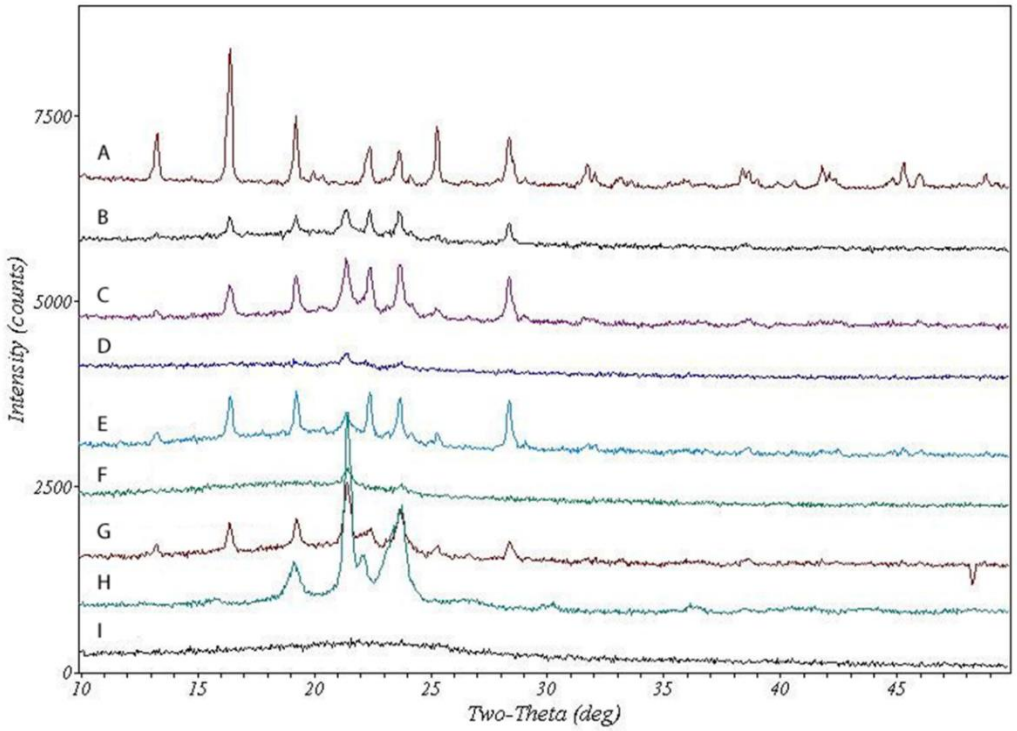

Figure 4.3 *– Powder X-ray diffraction pattern for RES-loaded NPs, physical mixtures (PM) and individual component used in the formulation of nanoparticles. Native RES (A), RES-loaded NPs R_{16} (B), RES-loaded NPs R_{11} (C), RES-loaded NPs R_2 (D), blank NPs R_{16}+RES physical mixture (E), blank NPs R_{16} (F), RES+PLGA+PCL-PEG physical mixture (G), PCL-PEG (H), PLGA (I).*

4.3.3 Effect of the cryoprotectants on the physical stability of resveratrol-loaded nanoparticles

As shown in **Figure 4.4**, all the tested cryoprotectants were able to minimize the NPs mean diameter changes after freeze-drying. The results also indicated that the cryoprotectant effectiveness was type- and concentration-dependent. For example, 1% w/v mannitol was correlated with low S_f/S_i value (≈1.5), whereas at higher concentrations of mannitol (15%, w/v), the S_f/S_i was increased up to 2.20±0.01. Compared to the other tested cryoprotectants, the PDI_f/PDI_i values were higher when stabilized with mannitol.

The cryoprotective effectiveness of sucrose, lactose and trehalose increased with concentration. At 1% w/v of cryoprotectant, the S_f/S_i values were 1.64±0.10 and 1.51±0.01 for sucrose and lactose, respectively. This value was significantly increased at 1% w/v of trehalose (1.79±0.07, $p<0.05$).

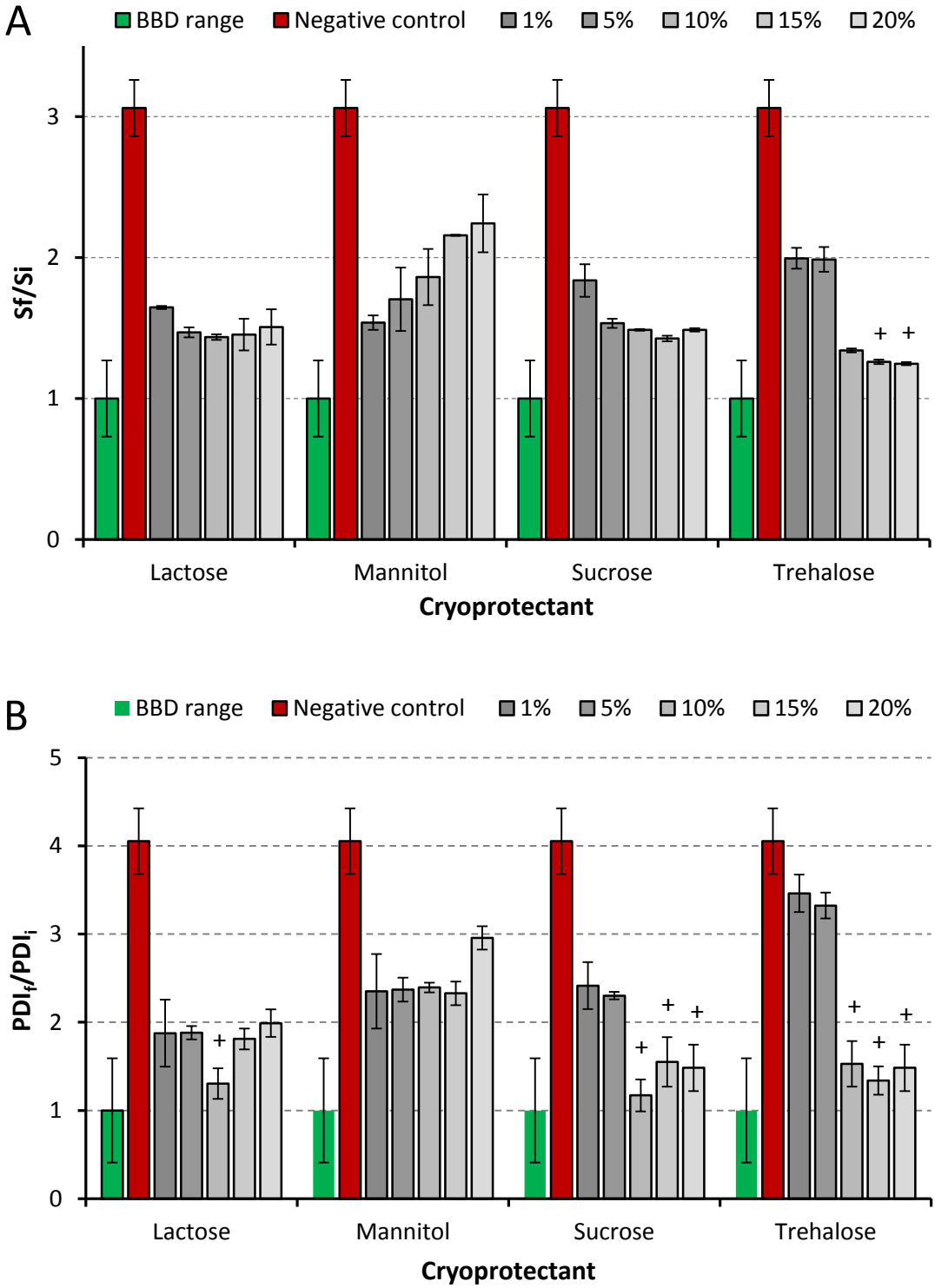

Figure 4.4 *– Effect of cryoprotectant types and concentration on (A) particle mean diameter and (B) PDI of RES-loaded NPs during freeze-drying. Data are presented as average value ± St. Dev. (n=3),* $^{+}$ *when* S_f/S_i *and* PDI_f/PDI_i *are in BBD model variability.*

However, at 15% w/v of trehalose, the S_f/S_i value was found to be 1.28±0.02, which was lower than that of sucrose (1.36±0.02; p=0.01). Similar results were observed for PDI_f/PDI_i. By comparing the S_f/S_i trend from 1% w/v to 15% w/v of disaccharides, a difference was found. The effectiveness of lactose did not change (p=0.21), while a significant improvement of the NPs stability was observed with sucrose (p=0.04) and trehalose (p=0.01). However, the data showed that only trehalose (15%, w/v) was able to maintain the NP and PDI change in the model space. Therefore, it was selected for the preparation of further R_{16} batches.

4.3.4 Morphology of resveratrol-loaded nanoparticles

The results obtained from SEM analysis showed RES-loaded NPs morphology with a high dependency on the type of cryoprotectant (**Figure 4.5**). In the absence of cryoprotectant, the roundness of RES-loaded NPs was reduced. A similar result was obtained with mannitol (data not shown). Spherical particles with a mean diameter of 1 µm were detected in the presence of lactose, sucrose or trehalose. These spherical particles were also shown to be embedded in the solid matrix of cryoprotectant.

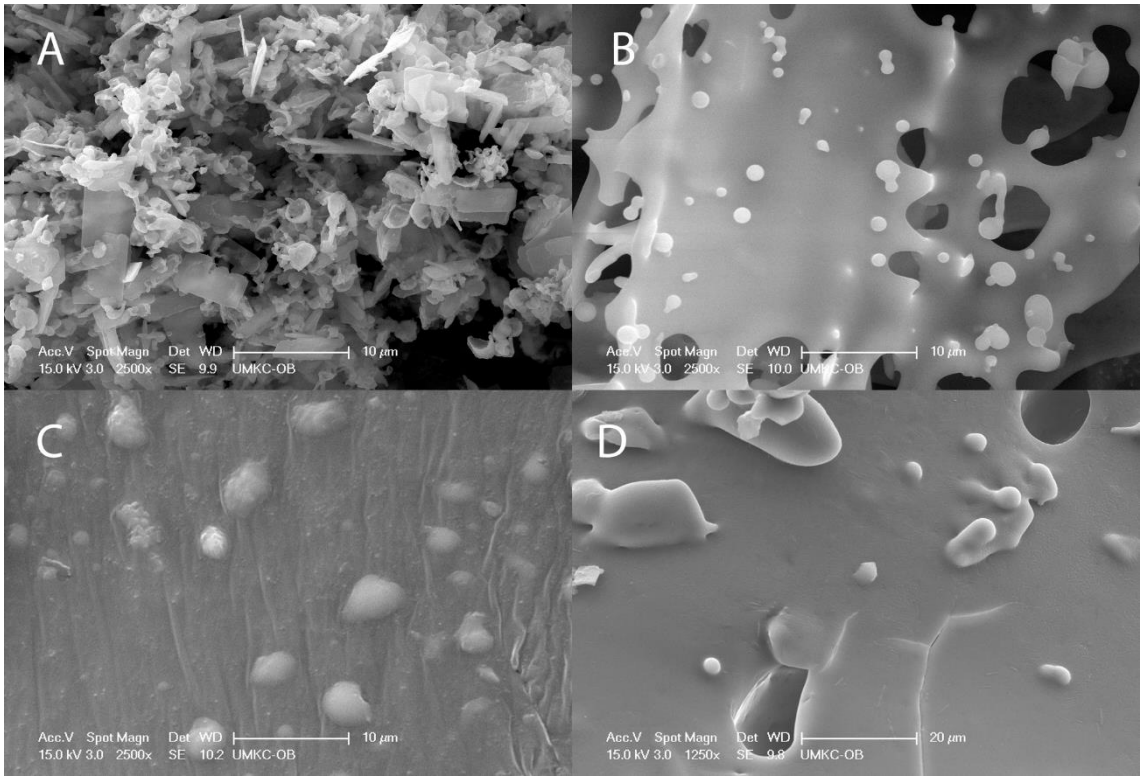

Figure 4.5 *– Resveratrol-loaded NPs (R_{16}) images obtained by scanning electron microscopy (SEM) (A) without or with 15% w/v cryoprotectant: (B) lactose, (C) sucrose, and (D) trehalose.*

4.3.5 In vitro drug release kinetics from resveratrol-loaded nanoparticles

The *in vitro* drug release kinetics from different RES-loaded NPs was compared to that of RES nanocrystals (**Figure 4.6**). Although Zambito et al. [25] have shown that the dialysis bag was not the gold standard method for studying the drug release from nanosystems; the method was only applied to compare formulation performances. From all tested formulations, 1 hour was required to observe detectable amount of RES in the outer phase. After that, the amount of RES nanocrystals increased until 100% of release after 50 h (drug release rate: 1.99±0.02 μg/h). The NPs formulations released RES within 8 h and then achieved a plateau phase (drug release rate: ≤0.2 μg/h). However, the percent-cumulated amount of RES released from NPs was lower than 50%. For example, the RES released from the optimal formulation R_{16} was lower than 20% of loaded amount.

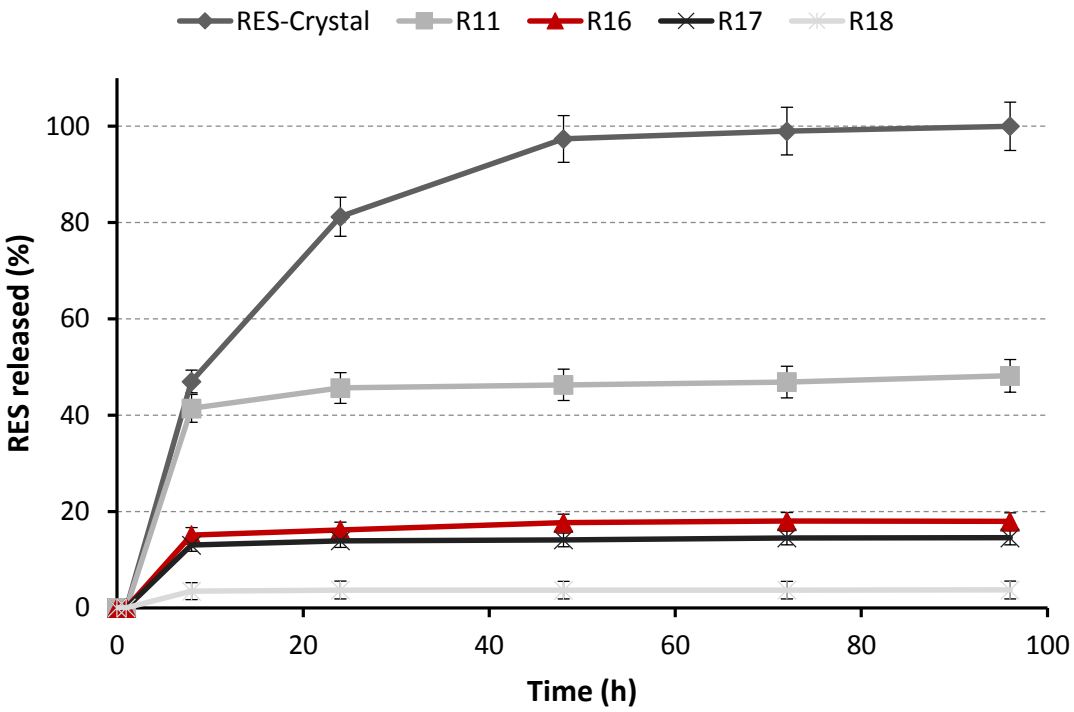

Figure 4.6 *– Resveratrol released (%) from RES nanocrystals within 96 h (control), RES-loaded NPs R_{11}, R_{16} (red line), R_{17}, R_{18}. Data are reported as average value ± St. Dev. (n=3).*

4.3.6 In vitro toxicity of resveratrol, blank and resveratrol-loaded nanoparticles

As shown in **Figure 4.7**, the percentage of cytotoxicity induced by native RES and RES-loaded NPs was negligible in both cell lines in comparison with blank control ($p<0.05$). However, the results from blank NPs showed no-toxicity at lower concentration, whereas cell-dependent cytotoxicity at higher concentration at higher ones.

At high concentration of NPs (600 μg/mL), HEI-OC1 cells seemed to be more sensitive to blank NPs than SVK-1 cells. Indeed, the percentage of cell death in HEI-OC1 cells achieved 58% when treated with 1000 μg/mL of blank NPs (**Figure 4.7**).

On the other hand, the cell viability was affected in a concentration-dependent manner in both cell lines (**Figure 4.8**). At concentrations equal to 50 μM of RES, the cell viability was decreased down slightly to 87% in HEI-OC1 cells. After incubation with 500 μM of RES, the decrease of the cell viability was around 27%, which was similar to positive control results in both cell lines ($p>0.05$). In the case of blank NPs, the results showed the same trend of cytotoxicity in HEI-OC1 cells. At concentration higher than 800 μg/mL of blank NPs, the viability of HEI-OC1 cells decreased, achieving 56% at 1000 μg/mL.

Finally, RES-loaded NPs were shown to affect the cell viability in HEI-OC1. A significant effect on the cell viability was observed at concentrations higher than 25 μg/mL of RES-loaded NPs, corresponding to 50 μM of RES. However, the decrease of the cell viability was less intense with RES-loaded NPs (90%) than with native RES ($p<0.05$).

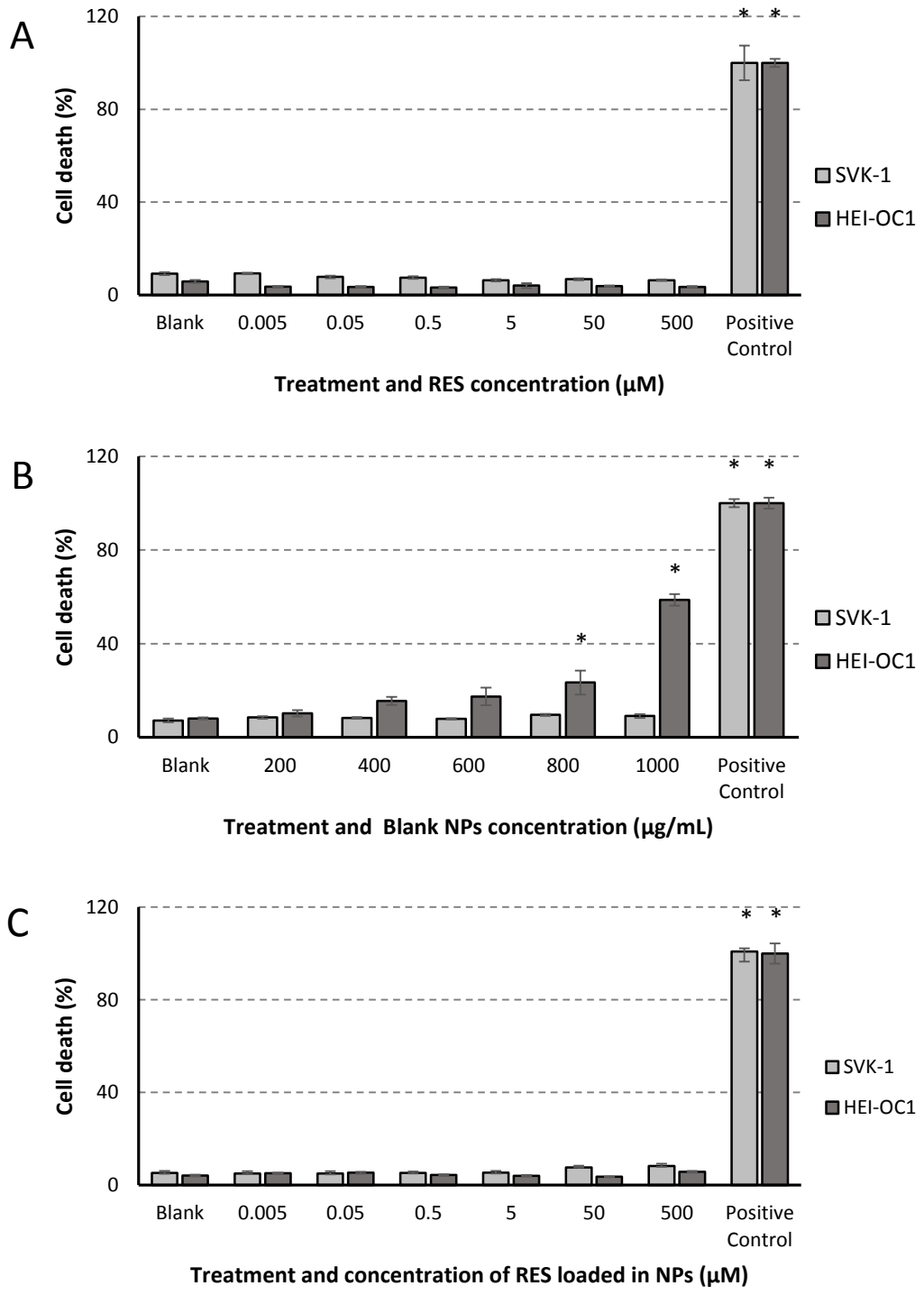

Figure 4.7 *– Cytotoxic effect of native RES (A), Blank NPs (B) and RES-loaded NPs (C) in SVK-1 and HEI-OC1 cells after 24h exposure. Concentrations of RES-loaded NPs are expressed in amount of RES loaded (µM). Data are presented as the average value ± SEM (n=5). * P<0.05 when compared with control by Student's t-test.*

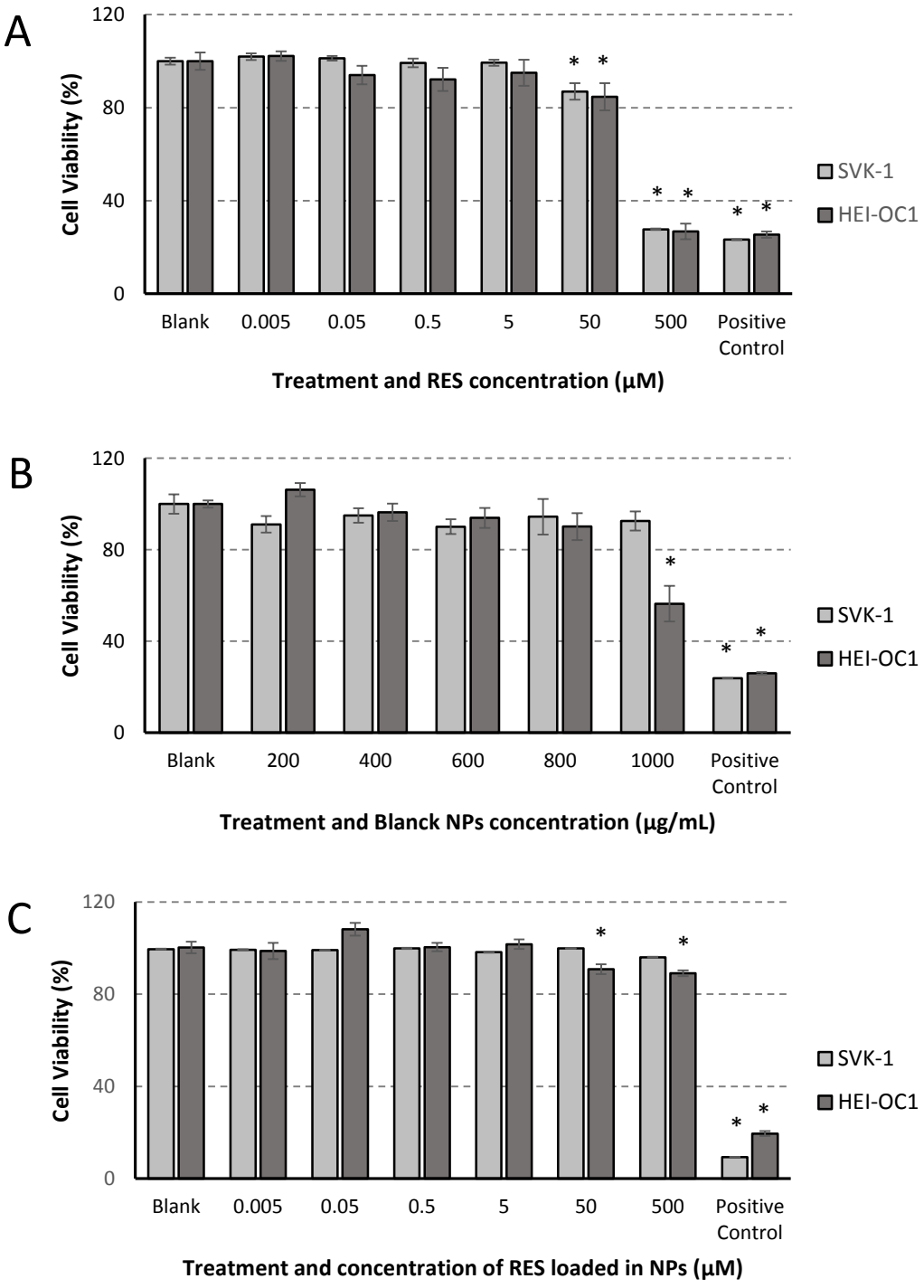

Figure 4.8 *– Viability of SVK-1 and HEI-OC1 cells of native RES (A), Blank NPs (B) and RES-loaded NPs (C) after 24h exposure. Concentrations of RES-loaded NPs are expressed in amount of RES loaded (µM). Data are presented as the average value ± SEM (n=5). * P<0.05 when compared with control by Student's t-test.*

4.4 Discussion

The present study showed that the solvent-diffusion method was suitable for the production of the proposed RES-loaded NPs. Moreover, all the NPs formulation prepared showed consistency with other similar nanoparticle systems reported in literature [26]. The use of BBD as a tool for the design of experiment allowed creating a statistical model for selecting the optimal formulation. The data obtained from checkpoint analyses (**Table 4.2**) and Monte Carlo simulation (**Figure 4.2**) demonstrated the accuracy and robustness of the model prediction. Moreover, the BBD model could well describe how the factors influenced the physiochemical properties of the RES-loaded NPs.

The results indicated that the amount of PLGA (X_2) could directly influence the particle mean diameter (Y_1) and the NPs structure as well. As shown in a previous study, the PLGA concentration might influence the viscosity of the organic internal phase [27]. In the presence of PLGA, an increase of the viscosity tended to increase the size of acetone nanodroplets dripped into the water phase, thus inducing an increase of the NPs diameter.

On the other hand, PXRD analyses showed that the crystalline diffraction peaks of PCL-PEG were attenuated in the NPs, suggesting that the PCL-PEG chains were dispersed in the PLGA matrix. Moreover, the BBD results revealed that PCL-PEG has a significant influence on NPs surface. In addition, the amount of PLGA seemed to decrease the zeta-potential of RES-loaded NPs (**Figure 4.1**, **4.2**), whereas PCL-PEG tended to neutralize it. Since zeta-potential has been defined as the potential difference between the aqueous medium and the stationary layer of fluid attached to the dispersed particle [28], it was likely to be influenced by the nature of NP surface. Therefore, the shift of the neutralization of zeta-potential due to PCL-PEG suggested that negative charges of the PLGA carboxylic group were shielded by the presence of the PCL-PEG molecules on the surface of the NPs at physiological pH.

Moreover, the BBD results indicated that NPs, made of PCL-PEG and PLGA, were able to load RES with high EE% (**Table 4.2**). Since the EE% (Y_4) was mainly influenced by the amount of PCL-PEG, it is possible to speculate that PCL-PEG increased the hydrophobicity of the NPs core (**Figure 4.2**). This hypothesis was also supported by published results of other nanosystems made of PCL-PEG [29, 30]. It is also interesting to note that the EE% values were higher than 100% for DL higher than 30% (*e.g.*, R_{11}:

DL 37%, EE% 141.35%; **Table 4.2**). Indeed, the amount of drug-loaded in the NPs matrix depends on thermodynamic equilibrium [31, 32]. Moreover, Weigiel et al. have indicated the RES/polymer ratio as a critical parameter for the avoidance of the drug crystallization [23]. Therefore, NPs were not able to load RES above the thermodynamic limit of the selected polymer mixture (close to 30% of DL); otherwise, the drug crystallization might occur. Indeed, the PXRD analyses showed that RES was molecularly dispersed in the NP formulations at low EE% (*e.g.*, R_2), whereas the typical RES crystal peaks appeared in the formulations at high EE% (*e.g.*, R_{11}).

The significant effect of RES on the zeta-potential (**Figure 4.1**) suggested that drug crystallization might occur on the surface of the NPs. This evidence also justified the difference observed between formulations in percent of burst effect during the release studies (**Figure 4.6**). Indeed, formulations with high EE% correlated well with high burst effect. For example, the formulation R_{11} (EE%: 141.35%) exhibited the highest burst effect (48.2%), whereas the lowest (3.7%) was detected with the formulation R_{18} (EE%: 75.32%).

Regardless to the burst effect, release studies showed that RES-loaded NPs were able to prevent the release in the ethanol solution for more than 96 h. In comparison with other published studies on RES-loaded micelles [29] or other RES-loaded NPs [33], experimental results suggested that the PLGA matrix could better control the release of RES. Indeed, if 60% of RES was released from the PCL-PEG micelles after 120 h, less than 20% of RES was released after 96 h (R_{16}). Moreover, the burst effect of R_{16} (< 20%) was lower than that from PCL-PEG micelles (≈35%).

Indeed, the proposed NP system might be advantageous for the delivery of RES in the cytoplasm of cochlear cells. This conclusion considers both low burst effect and negligible amount of RES released into the physiological fluids before the cellular uptake.

Overall results indicated that RES-loaded NPs were unstable after the freeze-drying ($S_f/S_i \geq 1.69$; **Table 4.2**). Therefore, the utilization of cryoprotectants was required to preserve the particle integrity [22]. The tested cryoprotectants did not show the same effectiveness in maintaining S_f/S_i and PDI_f/PDI_i values within the variability described by BBD (**Figure 4.4**). For example, mannitol was not able to minimize the physical

instability of the NPs, whereas the cryoprotective effectiveness of lactose, sucrose, and trehalose was concentration-dependent (**Figure 4.4**).

According to the literature, a slow crystallization of mannitol has occurred after freeze-drying at temperatures near to its glass transition (T_g), which was comparable to the freezing temperature used during the freeze-drying process [34]. On the other hand, disaccharides have inhibited the growth of ice crystal by the formation of cluster, thus increasing the physical stability of the frozen compound [35]. Among the tested disaccharides, only trehalose (> 15%, w/v) maintained the S_f/S_i and PDI_f/PDI_i values in the desirable BBD variability range. Therefore, trehalose might be considered as the most effective cryoprotectant in minimizing the growth of ice crystals.

The evaluation of the NP toxicity has been very challenging over the last years [36, 37]. Hoire et al. have shown that PLGA microparticles loaded with lidocaine did not affect the auditory and vestibular functions after their application to the round-window membrane in guinea pigs [38]. However, the *in vitro* studies have shown a dosage-dependent toxicity of nanocapsules on primary cochlear and mouse fibroblast cells, particularly for concentration higher than 785 μg/mL [39].

In line with literature, the proposed blank NPs showed a concentration- and cell-dependent toxicity. As showed in **Figure 4.7**, blank-NPs induced a significant cytotoxicity in HEI-OC1 cells at higher concentrations (> 800 μg/mL). However, the cytotoxicity and the cell viability were not affected by the blank NPs in SVK-1 cells (**Figure 4.7** and **4.8**).

This difference in cell sensitivity might be attributed to specific characteristics of the cell lines. HEI-OC1 cells are immortalized and derived from murine organ of Corti and can be a specific tool to test the ototoxicity of drugs [13], whereas SVK-1 cells have been derived from murine *Stria Vascularis* [14]. Since the organ of Corti cells required a specific environmental condition to modulate the hearing process, high NPs concentrations might alter the osmotic balance of the environment. This alteration might be stressful for HEI-OC1 cells causing the decrease of cell viability and increase cytotoxicity.

On the other hand, SVK-1 cell line exhibits the morphology of epithelial cells and builds the barrier between endolymph and blood [14]. Therefore, these cells were expected to be more resistant than HEI-OC1 cells to stressful factors and osmotic modification induced by nanoparticles.

The toxicity of RES was also evaluated in cochlear cell lines. Any cytotoxic effect was observed in both cell lines at low and medium concentrations of RES (**Figure 4.7**). However, the cell viability decreased in both cell lines when incubated with 100 µL of complete medium containing higher concentrations of RES (> 50 µM; **Figure 4.8**). This finding was due to a direct effect of RES on the functionality of cell mitochondria. Lagouge et al. have shown that 50 µM of RES could increase oxidative phosphorylation and mitochondrial biogenesis [40]. Moreover, RES concentrations higher than 100 µM have been found to induce apoptosis and mitochondrial dysfunction in the human hepatoblastoma cell model [41].

According to these facts and experimental results (**Figure 4.8**), it is reasonable to conclude that RES concentrations below 50 µM did not affect the viability of HEI-OC1 and SVK-1 cells. Moreover, the results of RES-loaded NPs are consistent with those obtained with native RES. RES concentrations higher than 50 µM significantly affected the cell viability, especially the HEI-OC1 cells. Therefore, it is possible to exclude that the effect of RES-loaded NPs on the cell viability was not due to modification of cell environment. Indeed, the highest RES-loaded concentration tested (< 300 µg/mL) was far from lowest cytotoxic concentration of blank NPs (600 µg/mL). Overall results suggested that RES-loaded NPs might be taken up by the cochlear cells and release the RES into the cytoplasm.

4.5 Conclusion

The present study investigated the critical aspect involved in the preparation of RES-loaded NPs intended for cochlear delivery. The application of Box-Behnken Design allowed understanding deeply the effect of the formulation composition on the NPs properties. Furthermore, the Monte Carlo simulation showed the robustness of optimal formulation and highlighted which NPs properties are more sensitive to unintended errors in the manufacturing process. Therefore, the use of Monte Carlo simulation in combination with BBD permitted both optimizing the formulation and selecting the most critical parameters of RES-loaded NPs. The use of trehalose (>15%, w/v) was required to minimize the physical instability of RES-loaded NPs during the freeze-drying. The results revealed that blank NPs could affect the viability of HEI-OC1 cells at concentrations higher than 600 μg/mL. On the other hand, the results showed that RES was able to decrease cell viability at concentrations higher than 50 μM. A similar pharmacological effect was also observed when RES was loaded in NPs. These results suggested that RES-loaded NPs were uptaken into the cells and released RES.

However, future works are required to study deeply the cell uptake mechanism and cellular release of RES. Moreover, the effect of RES on the mitochondrial oxidative phosphorylation should be studied to find out the effective concentration of RES that is able to protect cochlear cells from cisplatin-induced ototoxicity.

4.6 References

[1] Rybak, L. P., Whitworth, C. A., Mukherjea, D., and Ramkumar, V., 2007, "Mechanisms of cisplatin-induced ototoxicity and prevention," Hear. Res., 226(1–2), pp. 157-167.

[2] Knight, K. R., Kraemer, D. F., and Neuwelt, E. A., 2005, "Ototoxicity in children receiving platinum chemotherapy: underestimating a commonly occurring toxicity that may influence academic and social development," J. Clin. Oncol., 23(34), pp. 8588-8596.

[3] Bragado, P., Armesilla, A., Silva, A., and Porras, A., 2007, "Apoptosis by cisplatin requires p53 mediated p38α MAPK activation through ROS generation," Apoptosis, 12(9), pp. 1733-1742.

[4] Alam, S. A., Ikeda, K., Oshima, T., Suzuki, M., Kawase, T., Kikuchi, T., and Takasaka, T., 2000, "Cisplatin-induced apoptotic cell death in Mongolian gerbil cochlea," Hear. Res., 141(1–2), pp. 28-38.

[5] Rybak, L. P., Whitworth, C., and Somani, S., 1999, "Application of antioxidants and other agents to prevent cisplatin ototoxicity," Laryngoscope, 109(11), pp. 1740-1744.

[6] Yumusakhuylu, A. C., Yazici, M., Sari, M., Binnetoglu, A., Kosemihal, E., Akdas, F., Sirvanci, S., Yuksel, M., Uneri, C., and Tutkun, A., 2012, "Protective role of resveratrol against cisplatin induced ototoxicity in guinea pigs," Int. J. Pediatr. Otorhinolaryngol., 76(3), pp. 404-408.

[7] Erdem, T., Bayindir, T., Filiz, A., Iraz, M., and Selimoglu, E., 2011, "The effect of resveratrol on the prevention of cisplatin ototoxicity," Eur. Arch. Otorhinolaryngol., 269(10), pp. 2185-8

[8] Baur, J. A., and Sinclair, D. A., 2006, "Therapeutic potential of resveratrol: the in vivo evidence," Nat. Rev. Drug Discov., 5(6), pp. 493-506.

[9] Amri, A., Chaumeil, J. C., Sfar, S., and Charrueau, C., 2012, "Administration of resveratrol: What formulation solutions to bioavailability limitations?," J. Control. Release, 158(2), pp. 182-193.

[10] Rathore, A. S., and Winkle, H., 2009, "Quality by design for biopharmaceuticals," Nature biotechnology, 27(1), pp. 26-34.

[11] Meng, J., Sturgis, T. F., and Youan, B.-B. C., 2011, "Engineering tenofovir loaded chitosan nanoparticles to maximize microbicide mucoadhesion," Eur. J. Pharm. Sci., 44(1–2), pp. 57-67.

[12] Box, G. E. P., and Behnken, D. W., 1960, "Some New Three Level Designs for the Study of Quantitative Variables," Technometrics, 2(4), pp. 455-475.

[13] Kalinec, G. M., Webster, P., Lim, D. J., and Kalinec, F., 2003, "A cochlear cell line as an in vitro system for drug ototoxicity screening," Audiol. Neurootol., 8(4), pp. 177-189.

[14] Rivolta, M. N., and Holley, M. C., 2002, "Cell lines in inner ear research," J. Neurobiol., 53(2), pp. 306-318.

[15] Fessi, H., Puisieux, F., Devissaguet, J. P., Ammoury, N., and Benita, S., 1989, "Nanocapsule formation by interfacial deposition following solvent displacement," Int. J. Pharm., pp. 55:R51-R54.

[16] List, M., and Sucker, H., 1988, "Pharmaceutical injectable hydrosols containing water-insoluble active agents," Sandoz S. A., Switz. . p. 26 pp.

[17] Kappele, W. D., "Setting robust process specifications using design of experiments and Monte Carlo techniques," Proc. 2010 AIChE Spring Meeting and 6th Global Congress on Process Safety, 10AIChE.

[18] Hackley, V., and Ferraris, C., 2001, "The use of nomenclature in dispersion science and technology, NIST Recommended Practice Guide: SP."

[19] Youm, I., Murowchick, J. B., and Youan, B. B., 2012, "Entrapment and release kinetics of furosemide from pegylated nanocarriers," Colloids Surf. B Biointerfaces, 94, pp. 133-142.

[20] Chen, X., He, H., Wang, G., Yang, B., Ren, W., Ma, L., and Yu, Q., 2007, "Stereospecific determination of cis- and trans-resveratrol in rat plasma by HPLC: application to pharmacokinetic studies," Biomed. Chromatogr., 21(3), pp. 257-265.

[21] Kalinec, G. M., Webster, P., Lim, D. J., and Kalinec, F., 2003, "A Cochlear Cell Line as an in vitro System for Drug Ototoxicity Screening," Audiol. Neurootol., 8, pp. 177-189.

[22] Abdelwahed, W., Degobert, G., Stainmesse, S., and Fessi, H., 2006, "Freeze-drying of nanoparticles: formulation, process and storage considerations," Adv. Drug Deliv. Rev., 58(15), pp. 1688-1713.

[23] Wegiel, L. A., Mauer, L. J., Edgar, K. J., and Taylor, L. S., 2013, "Crystallization of amorphous solid dispersions of resveratrol during preparation and storage-Impact of different polymers," J. Pharm. Sci., 102(1), pp. 171-184.

[24] Zhang, X.-P., Le, Y., Wang, J.-X., Zhao, H., and Chen, J.-F., 2013, "Resveratrol nanodispersion with high stability and dissolution rate," LWT - Food Science and Technology, 50(2), pp. 622-628.

[25] Zambito, Y., Pedreschi, E., and Di Colo, G., 2012, "Is dialysis a reliable method for studying drug release from nanoparticulate systems?-A case study," International journal of pharmaceutics, 434(1-2), pp. 28-34.

[26] Riley, T., Govender, T., Stolnik, S., Xiong, C. D., Garnett, M. C., Illum, L., and Davis, S. S., 1999, "Colloidal stability and drug incorporation aspects of micellar-like PLA–PEG nanoparticles," Colloids Surf. B Biointerfaces, 16(1–4), pp. 147-159.

[27] Mondal, N., Samanta, A., Pal, T. K., and Ghosal, S. K., 2008, "Effect of different formulation variables on some particle characteristics of poly (DL-lactide-co-glycolide) nanoparticles," Yakugaku Zasshi, 128(4), pp. 595-601.

[28] McNaught, A. D., and Wilkinson, A., 1997, IUPAC. Compendium of Chemical Terminology, Blackwell Scientific Publications, Oxford.

[29] Lu, X., Ji, C., Xu, H., Li, X., Ding, H., Ye, M., Zhu, Z., Ding, D., Jiang, X., Ding, X., and Guo, X., 2009, "Resveratrol-loaded polymeric micelles protect cells from Aβ-induced oxidative stress," Int. J. Pharm., 375(1-2), pp. 89-96.

[30] Kim, B. K., Lee, J. S., Oh, J. K., and Park, D. J., 2009, "Preparation of resveratrol-loaded poly(ε-caprolactone) nanoparticles by oil-in-water emulsion solvent evaporation method," Food Science and Biotechnology, 18(1), pp. 157-161.

[31] Kumar, V., and Prud'homme, R. K., 2008, "Thermodynamic limits on drug loading in nanoparticle cores," J. Pharm. Sci., 97(11), pp. 4904-4914.

[32] Vijay, N., Murowchick, J. B., and Youan, B. B., 2010, "Thermodynamics of drug nanoencapsulation: case study of phenytoin-poly (D, L-lactide) nanocarrier," Curr. Drug Deliv., 7(5), pp. 343-354.

[33] Sanna, V., Siddiqui, I. A., Sechi, M., and Mukhtar, H., 2013, "Resveratrol-Loaded Nanoparticles Based on Poly(epsilon-caprolactone) and Poly(d,l-lactic-co-glycolic acid)–Poly(ethylene glycol) Blend for Prostate Cancer Treatment," Mol. Pharm., 10(10), pp. 3871-3881.

[34] Kim, A. I., Akers, M. J., and Nail, S. L., 1998, "The physical state of mannitol after freeze-drying: effects of mannitol concentration, freezing rate, and a noncrystallizing cosolute," J. Pharm. Sci., 87(8), pp. 931-935.

[35] Tsutomu Uchida, S. T. M. N. a. K. G., 2012, "Freezing Properties of Disaccharide Solutions: Inhibition of Hexagonal Ice Crystal Growth and Formation of Cubic Ice," Crystallization and Materials Science of Modern Artificial and Natural Crystals, E. Borisenko, ed., InTech.

[36] Hu, Y. L., and Gao, J. Q., 2010, "Potential neurotoxicity of nanoparticles," Int. J. Pharm., 394(1-2), pp. 115-121.

[37] FDA, 2011, "Investigation of Potential Toxic Effects of Engineered Nanoparticles and Biologic Microparticles in Blood and Their Biomarker Applications.."

[38] Horie, R. T., Sakamoto, T., Nakagawa, T., Tabata, Y., Okamura, N., Tomiyama, N., Tachibana, M., and Ito, J., 2010, "Sustained delivery of lidocaine into the cochlea using poly lactic/glycolic acid microparticles," Laryngoscope, 120(2), pp. 377-383.

[39] Zhang, Y., Zhang, W., Löbler, M., Schmitz, K. P., Saulnier, P., Perrier, T., Pyykkö, I., and Zou, J., 2011, "Inner ear biocompatibility of lipid nanocapsules after round window membrane application," Int. J. Pharm., 404(1-2), pp. 211-219.

[40] Lagouge, M., Argmann, C., Gerhart-Hines, Z., Meziane, H., Lerin, C., Daussin, F., Messadeq, N., Milne, J., Lambert, P., Elliott, P., Geny, B., Laakso, M., Puigserver, P., and Auwerx, J., 2006, "Resveratrol Improves Mitochondrial Function and Protects against Metabolic Disease by Activating SIRT1 and PGC-1α," Cell, 127(6), pp. 1109-1122.

[41] Ma, X., Tian, X., Huang, X., Yan, F., and Qiao, D., 2007, "Resveratrol-induced mitochondrial dysfunction and apoptosis are associated with Ca2+ and mCICR-mediated MPT activation in HepG2 cells," Mol. Cell. Biochem., 302(1-2), pp. 99-109

4.7 Appendix 4.1: Ferrocene-loaded nanocarrier as probe for cochlear biodistribution study

The contents of this appendix was presented as poster at the 2013 AAPS Annual Meeting and Exposition; November 10-14, 2013; San Antonio TX, USA; Poster W4103.

Purpose: The fate of drug nanocarriers (NCs) in the inner ear remains elusive. The aim of the work is to develop ferrocene (FER)-loaded NCs to elucidate the cochlear biodistribution of such NCs.

Methods: FER-NCs were prepared by surfactant free solvent-diffusion technique using a mixture of PLGA/PCL-PEG (ratios 1/1, 1/2) dissolved in acetone. FER-NCs were washed and freeze-dried. TEM analyses were carried out to study the FER-NC morphology. Lactose, mannitol, sucrose were tested at different cryoprotectant/nanocarrier ratios (0/1, 1/1, 3/1, 5/1) to stabilize FER-NCs during freeze-drying. The stability of the FER-NCs was checked by measuring particle size and zeta-potential (ZP) immediately after water dispersion and after 12 days. FER-NCs were placed in the round window (RW) niche of the middle ear in guinea pigs. After 48 hours, the animals were sacrificed, the cochlea isolated and prepared for TEM.

Results: The Ferrocene-loaded NCs had a mean diameter of 201.2±57.7, PDI of 0.328±0.074 and ZP of -20.2±4.8mV. PLGA/PCL-PEG NCs of 1/2 allowed higher EE% (85.50±11.15) than ones made with 1/1 ratio (42.93±3.65). The FER-NCs appeared spherical with smooth surface. All cryoprotectants increased RES-NCs stability during the freeze-drying process. However, lactose, especially when used in 3/1 ratio, was more effective than other ones after dispersion and during 12-day stability studies. FER-NCs crossed the RW membrane and were found adjacent or in the cells lining the scala tympani of the cochlea (**Figure 4.A.1**). Hearing was normal after RW placement of NCs (**Figure 4.A.2**).

Conclusion: FER-NCs were successfully prepared by emulsion-diffusion technique and the 1/2 PLGA/PLC-PEG ratio was selected in term of best encapsulation efficiency. Moreover, lactose (3/1 cryoprotectant/NCs ratio) guaranteed FER-NCs stability during freeze-drying process and maintained FER-NCs stable in suspension for at least 12 days. When placed into the RW niche, FER-NCs enter the cochlea and do not appear to cause hearing loss.

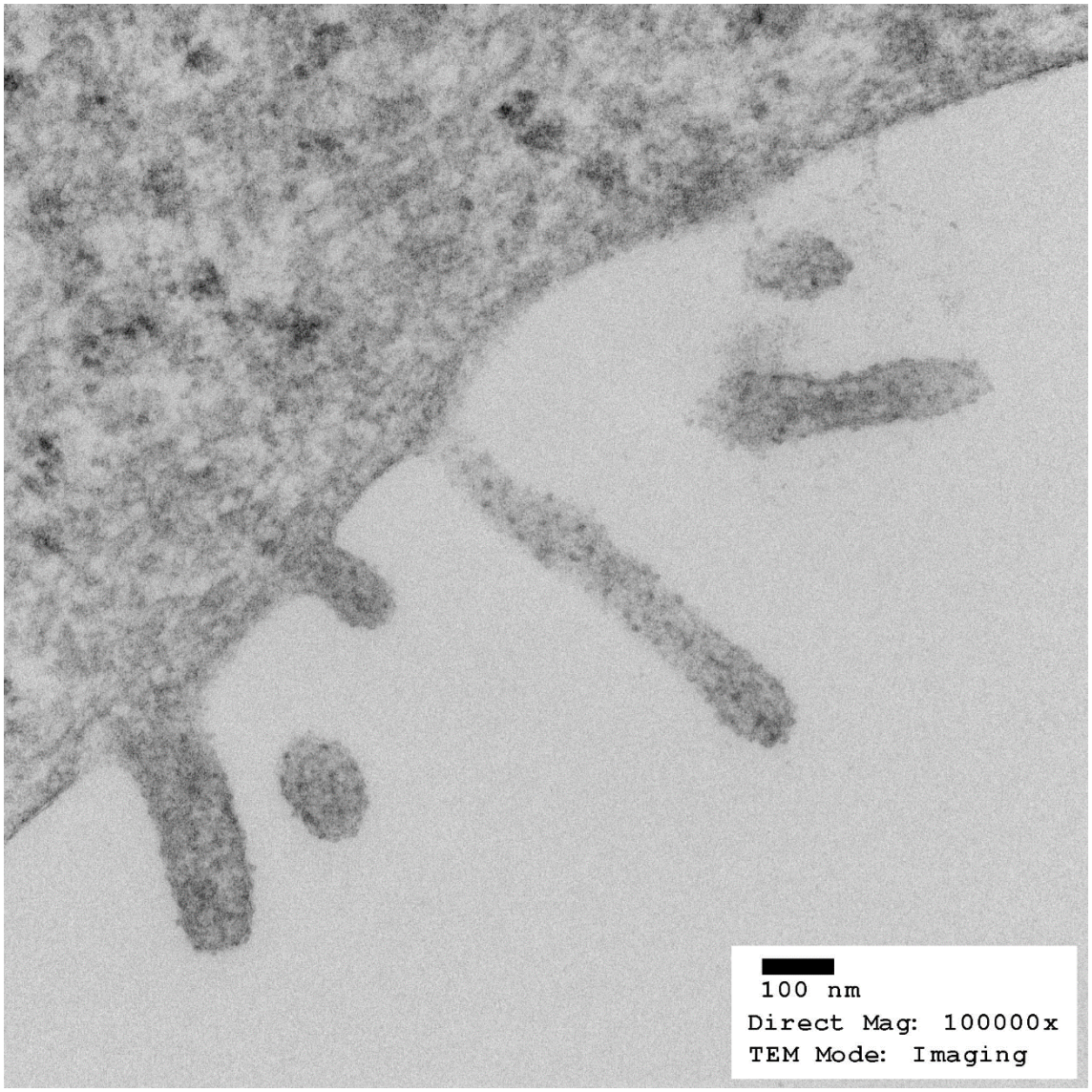

Figure 4.A.1 *- Distribution of FER-loaded NCs in cochlear tissue (Guinea pig).*

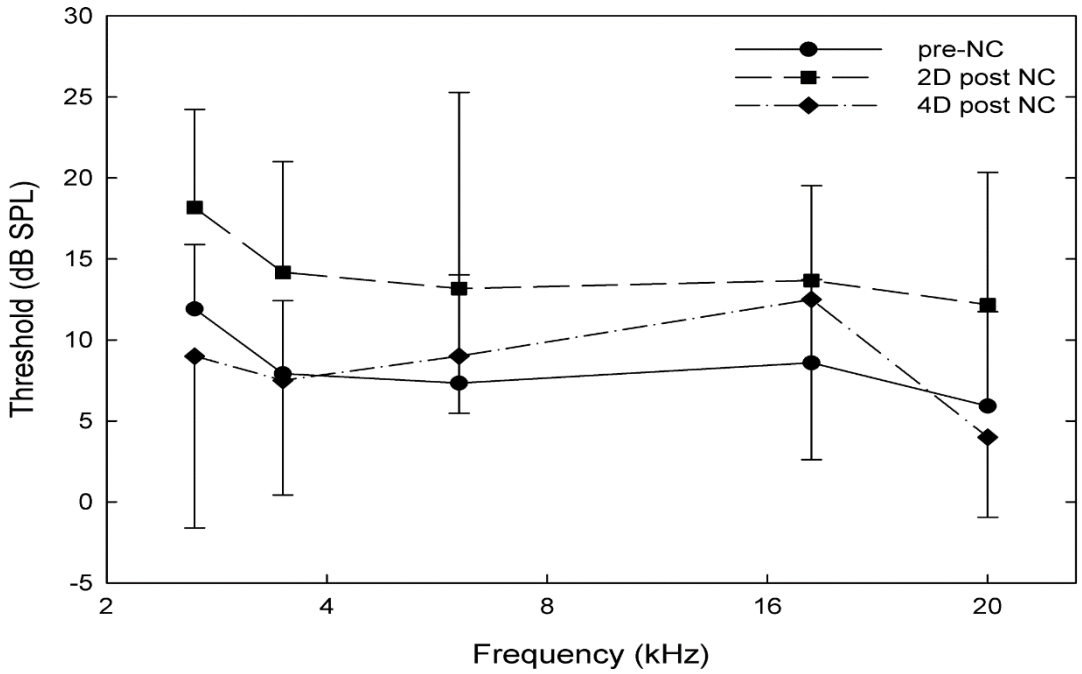

Figure 4.A.2 *- Hearing thresholds by auditory brainstem responses (ABRs) after FER-loaded NC injection into the middle ear (Guinea pig).*

The formulative studies were carried out in the Laboratory of Future Nanomedicines and Theoretical Chronopharmaceutics directed by prof. Bi-Botti C. Youan, Division of Pharmaceutical Sciences, University of Missouri Kansas City, 2464 Charlotte St., Kansas City, MO 64108, USA.

The in vivo biodistribution study was carried out in the laboratory directed by prof. Michael Anne Gratton, Department of Otolaryngology-Head and Neck Surgery, School of Medicine, Saint Louis University, 3635 Vista Ave, St. Louis, MO 63110,USA.

5 Dermal and transdermal delivery of morphine derivatives: a qualitative structure-penetration relationship

5.0 Abstract

Opioids have been used widely for pain management in patients with degenerative or neoplastic diseases. Recent studies showed that opioids are also effective in the treatment of cutaneous lesions. Aiming to select the most suitable candidate for cutaneous painful syndromes, the *in vitro* permeability of eight different morphine derivatives (morphine, codeine, hydromorphone, hydrocodone, oxymorphone, oxycodone) through human epidermis was studied to elucidate the influence of four different substituents (*e.g.*, 3-methoxyl, 6-carbonyl, 14-hydroxyl, 7,8-didehydro) on the drug permeation and retention. The *in vitro* permeation studies were performed using the Franz diffusion cells. The donor phases were aqueous saturated solutions of morphine derivatives. At the end of experiment (*i.e.*, 24 h), the maximum flux (J_{max}), the permeation coefficient (pK_p), the drug concentration in the epidermis at the steady state (Epi Q_{ss}) and normalized by drug solubility ($R_{Q/S}$) were calculated and a statistical analysis of possible structure-permeability relationship was performed. In particular, the statistical analyses indicated that 3-methoxyl group played a key role in governing the skin penetration of morphine derivatives through human skin, since it increased the permeation flux and decreased the drug retention. Moreover, the retention/permeation affinity index confirmed morphine as suitable candidate and suggested hydromorphone as an alternative drug for treating cutaneous painful symptomatology.

The synthesis of morphine derivatives was carried out in the Laboratory directed by prof. Marco De Amici, Department of Pharmaceutical Sciences, University of Milan, via Mangiagalli, 25 – 20133, Milan (Italy).

The penetration study was carried out in the Laboratory directed by prof. Luisa Montanari, Department of Pharmaceutical Sciences, University of Milan, via G. Colombo, 71 – 20133, Milan (Italy).

Abbreviations

AcOEt	Ethyl acetate
CH_2Cl_2	Dichloromethane
$CHCl_3$	Chloroform
$CDCl_3$	Deuterochloroform
CH_3CN	Acetonitrile
DMSO-d_6	Hexadeuterodimethyl sulfoxide
Et_2O	Diethyl ether
EtOH	Ethanol
HCl	Hydrochloric acid
*i*PrOH	Isopropanol
KCl	Potassium chloride
KOH	Potassium hydroxide
MeOH	Methanol
Na_2CO_3	Sodium carbonate
$NaHCO_3$	Sodium bicarbonate
NaN_3	Sodium azide
Na_2SO_4	Sodium sulfate
oct	Octan-1-ol
T_g	Glass transition temperature
THF	Tetrahydrofuran
rt	Room temperature

5.1 Introduction

Opioids are widely and commonly used in pain relief therapies of degenerative diseases or neoplastic pathologies. Indeed, WHO guidelines indicate their systemic administration as first line drugs for controlling moderate to severe pain [1].

Recent studies have shown that opioids are also locally effective in the treatment of inflammatory pain in wounds [2, 3] by activation of opioid receptors in the human skin [4]. However, no information are available on the ability of human skin to retain morphine derivatives. The skin penetration studies reported in literature are mainly focused on fentanyl and its derivatives [5, 6] or buprenorphine [7], which are administered by transdermal patches to obtain systemic activity.

Aiming to rationalize the selection of the most suitable morphine derivative in local pain relief therapy, the present study investigated the effect of four different substituents (*i.e.*, 3-methoxyl, 6-carbonyl, 14-hydroxyl groups and 7,8-didehydro; **Figure 5.1**) on skin penetration of eight morphine derivatives.

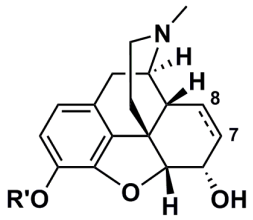

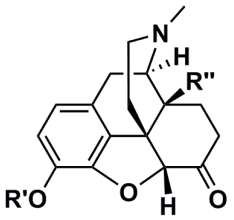

R' = H, (7,8-didehydro)	(**1**) Morphine	R' = H, R'' = OH	(**3**) Oxymorphone
R' = H	(**2**) Dihydromorphine	R' = H, R'' = H	(**4**) Hydromorphone
R' = CH_3, (7,8-didehydro)	(**5**) Codeine	R' = CH_3, R'' = OH	(**7**) Oxycodone
R' = CH_3	(**6**) Dihydrocodeine	R' = CH_3, R'' = H	(**8**) Hydrocodone

Figure 5.1 *- Structures of morphine derivatives.*

Therefore, the skin penetration parameters, namely the drug maximum flux and the skin-retained amount, were determined *in vitro* using human epidermis as a membrane. The impact of substituents was studied in the attempt to minimize the skin permeation and maximize the skin retention. Then, possible relationships between the skin penetration data and the chemical structure or some physicochemical parameters related to drug lipophilicity and/or polarity were screened by stepwise backward statistical analyses.

Most of the models in literature demonstrated the correlation between diffusion through the human skin and the drug lipophilicity (log *P*) and molecular weight [8, 9]. In other models, log *P* was more explicitly represented introducing the terms of dipolarity, polarizability, hydrogen bond donor and acceptor activity, and molar refractivity [10]; whereas further parameters related to the permeant solubility were also taken into consideration [11].

Unlike permeation process, the drug retention in the human skin has not been widely investigated. On the best of our knowledge, only few papers proposed to model skin retention of specific classes of molecules like alcohols and steroids [12, 13].

However, Cross and Robert demonstrated that drug retention was significantly affected by dermal clearance [13]. The authors compared the concentration of different alcohols and steroids in the viable epidermis obtained from two physiological models of blood flow in human skin, namely the full-thickness skin and the epidermal membrane. The former represents an *in vivo* infinite dermal vasoconstriction (low dermal clearance), whereas the latter is a model of *in vivo* infinite dermal perfusion (high dermal clearance). The published results showed that full thickness skin permitted to achieve higher drug concentration in the epidermis layer than other model, suggesting that epidermis retention was increased by low dermal clearance.

In the present study, the epidermis was selected as model membrane for the retention study of morphine derivatives, because it permitted to better clarify the effects of chemical structure on retention process in comparison to other skin models with higher dermal clearance.

5.2 Materials and methods

5.2.1 Materials

Morphine hydrochloride, codeine phosphate, dihydrocodeine bitartrate and oxycodone hydrochloride were purchased from SALAARS S.p.A. (Como, Italy). Standard KOH (0.5 N) and HCl (0.5 N) were prepared from Titrisol volumetric vials purchased from VWR International PBI s.r.l. (Milan, Italy). All other reagents and solvents were used as received without further purification.

5.2.2 Preparation and characterization of the morphine derivatives

5.2.2.1 Synthesis

The progress of reactions was monitored by TLC analyses performed on commercial silica gel 60 F254 aluminum sheets (Merck KGaA, Darmstadt, Germany); spots were visualized by UV detection and further evidenced by spraying with a dilute alkaline potassium permanganate solution or phosphomolybdic acid in ethanol solution, and the Dragendorff reagent. ^{1}H NMR and ^{13}C NMR spectra were recorded with a Varian Mercury 300 (^{1}H, 300.063; ^{13}C, 75.451 MHz) spectrometer at 20°C; the deuterated solvents were indicated for each compound. Chemical shifts (δ) are expressed in ppm and coupling constants (J) in Hz. ESI-MS spectra were obtained on a Varian 320 LC–MS/MS instrument; data are reported as mass-to-charge ratio (m/z) of the corresponding positively charged molecular ions.

Morphine [(5α,6α)-7,8-didehydro-4,5-epoxy-17-methylmorphinan-3,6-diol, ***1****]*. Commercially available morphine hydrochloride (1.000 g, 3.108 mmol) was dissolved in Na_2CO_3 aq. sat. and vigorously extracted with $CHCl_3$/*i*PrOH (9:1, 50 mL x 5). The organic phases were collected, dried over anhydrous Na_2SO_4 and evaporated under reduced pressure to afford a viscous yellow oil that was recrystallized from Et_2O to give pure morphine base (**1**). Yield: 0.822 g (93%); white solid; ^{1}H NMR, ^{13}C NMR and MS spectra were identical to those reported in the literature [14].

Dihydromorphine [3,6-dihydroxy-(5α,6α)-4,5-epoxy-17-methylmorphinan, ***2****]*. A stirred suspension of morphine hydrochloride (1.031 g, 3.204 mmol) and 10% Pd/C (50 mg) in MeOH (25 mL) was evacuated and hydrogenated under pressure (50 psi) in a Parr apparatus for 4 h. The reaction mixture was then passed through a pad of Celite® and the filtrate was concentrated under reduced pressure. This crude material was dissolved in $NaHCO_3$ aq. sat. and extracted with $CHCl_3$/*i*PrOH (9:1, 30 mL x 5), the organic phases were collected, dried over anhydrous Na_2SO_4 and evaporated under reduced pressure to afford a yellow oil which was recrystallized from CH_3CN to give pure dihydromorphine (**2**). Yield: 0.830 g (90%); pale yellow solid, R_f = 0.23 (CH_2Cl_2/MeOH = 7:3); ^{1}H NMR (300 MHz, $CDCl_3$): δ = 6.66 (d, 1H, J = 8.0 Hz), 6.55 (d, 1H, J = 8.0 Hz), 4.60 (d, 1H, J = 5.2 Hz), 4.00 (m, 1H), 3.15 (m, 1H), 2.97 (d, 1H, J = 18.4 Hz), 2.59 (dd, 1H, J = 12.4, 3.8 Hz), 2.42 (s, 3H), 2.40 (dd, 1H, J = 18.4, 6.0 Hz), 2.28 (m, 2H), 1.95 (dt, 1H, J = 12.4, 5.2 Hz), 1.69 (ddd, 1H, J = 12.4, 3.8, 1.9 Hz), 1.45 (m, 3H), 1.08 (m, 1H) ppm; ^{13}C NMR (75 MHz, DMSO-d_6): δ = 146.03, 137.98, 130.07,

125.19, 117.98, 116.69, 89.94, 66.11, 58.92, 46.03, 42.77, 42.01, 38.19, 37.25, 25.61, 19.61, 19.48 ppm; ESI-MS: *m/z* $[M+H]^+$ calcd for $[C_{17}H_{22}NO_3]^+$ 288.16, found 288.1. ^1H NMR, ^{13}C NMR and MS spectra were identical to those reported in the literature [15, 16].

*Oxymorphone [4,5-α-epoxy-3,14-dihydroxy-17-methylmorphinan-6-one, **3**]*. This compound was synthesized from commercially available oxycodone hydrochloride following a procedure already reported in the literature [17]. Yield: 0.799 g (93%) from 1.004 g of oxycodone hydrochloride; white solid; R_f = 0.45 (CH_2Cl_2/MeOH = 9:1); ^1H NMR (300 MHz, $CDCl_3$): δ = 6.72 (d, 1H, *J* = 8.0 Hz), 6.61 (d, 1H, *J* = 8.0 Hz), 5.30 (bs, 2H), 4.68 (s, 1H), 3.15 (d, 1H, *J* = 18.4 Hz), 3.04 (dt, 1H, *J* = 5.2, 14.4 Hz), 2.88 (d, 1H, *J* = 5.6 Hz), 2.56 (dd, 1H, *J* = 6.0, 18.8 Hz), 2.46 (m, 5H), 2.31 (dt, 1H, *J* = 2.8, 14.4 Hz), 2.21 (m, 1H), 1.88 (ddd, 1H, *J* = 3.2, 5.2, 13.6 Hz), 1.64 (m, 2 H) ppm; ^{13}C NMR (75 MHz, DMSO-d_6): δ = 208.7, 143.5, 139.5, 129.2, 119.1, 117.2, 89.3, 70.0, 63.9, 49.6, 45.2, 42.3, 39.9, 35.6, 31.0, 29.9, 21.5 ppm; ESI-MS: *m/z* $[M+H]^+$ calcd for $[C_{17}H_{20}NO_4]^+$ 302.14, found 302.1. ^1H NMR, ^{13}C NMR and MS spectra were identical to those reported in literature [18].

*Hydromorphone [4,5-α-epoxy-3-hydroxy-17-methyl morphinan-6-one, **4**]*. This compound was prepared starting from morphine base (**1**) by a known procedure [19]. Yield: 1.089 g (82%) from 1.324 g of morphine; white solid; R_f = 0.22 (CH_2Cl_2/MeOH = 3:7); ^1H NMR (300 MHz, $CDCl_3$): δ = 6.71 (d, 1H, *J* = 8.3 Hz), 6.61 (d, 1H, *J* = 8.3 Hz), 4.66 (s, 1H), 3.30 (m, 1H), 3.04 (d, 1H, *J* = 18.7 Hz), 2.69 (m, 2H), 2.48 (s, 3H), 2.40 (m, 2H), 2.27 (m, 2H), 1.83 (m, 2H), 1.25 (m, 2H) ppm; ^{13}C NMR (75 MHz, DMSO-d_6): δ = 209.1, 144.0, 139.4, 127.6, 124.6, 119.4, 117.1, 90.5, 58.4, 46.5, 46.3, 42.7, 41.5, 40.0, 34.9, 25.2, 19.6 ppm; ESI-MS: *m/z* $[M+H]^+$ calcd for $[C_{17}H_{20}NO_3]^+$ 286.14, found 286.1. ^1H NMR, ^{13}C NMR and MS spectra were identical to those reported in literature [20, 21].

*Codeine [(5α,6α)-7,8-didehydro-4,5-epoxy-3-methoxy-17-methylmorphinan-6-ol, **5**]*. Commercially available codeine phosphate (1.6209 g, mmol) was dissolved in Na_2CO_3 aq. sat. and extracted with AcOEt (50 mL x 3). The organic phases were collected, dried over anhydrous Na_2SO_4 and evaporated under reduced pressure to afford a viscous oil which was recrystallized from Et_2O to give pure codeine base (**5**). Yield: 0.959 g (78%); white solid; ^1H NMR, ^{13}C NMR and MS spectra were identical to those reported in literature [22].

*Dihydrocodeine [4,5-α-epoxy-3-methoxy-17-methylmorphinan-6-ol, **6**]*. Commercially available dihydrocodeine bitartrate (1.119 g, 2.479 mmol) was dissolved in Na_2CO_3 aq. sat. and extracted with AcOEt (50 mL x 3). The organic phases were collected, dried over anhydrous Na_2SO_4 and evaporated under reduced pressure to afford a viscous yellow oil which was triturated with Et_2O to give pure dihydrocodeine base (**6**) as a white glassy solid. Yield: 0.720 g (96%); white solid; ^{1}H NMR, ^{13}C NMR and MS spectra were identical to those reported in literature [23].

*Oxycodone [4,5-α-epoxy-14-hydroxy-3-methoxy-17-methylmorphinan-6-one, **7**]*. Commercially available oxycodone hydrochloride (0.598 g, 1.702 mmol) was dissolved in Na_2CO_3 aq. sat. and vigorously extracted with AcOEt (35 mL x 3). The organic phases were collected, dried over anhydrous Na_2SO_4 and evaporated under reduced pressure to afford a viscous oil that was recrystallized from Et_2O to give pure oxycodone base (**7**). Yield: 0.482 g (90%); white solid; ^{1}H NMR, ^{13}C NMR and MS spectra were identical to those reported in literature [24].

*Hydrocodone [4,5-α-epoxy-3-methoxy-17-methylmorphinan-6-one, **8**]*. To a solution of dihydrocodeine base (**6**) (0.734 g, 2.435 mmol) in dry CH_2Cl_2 (20 mL) Dess-Martin periodinane (1.033 g, 2.435 mmol) was added at 0°C and the reaction mixture was stirred for 30 min, whereupon it was allowed to warm to rt and stirred for further 2 h. The reaction mixture was diluted with CH_2Cl_2, acidified with 1 N HCl and washed with Et_2O (30 mL x 3). The acidic aqueous layer was then basified with Na_2CO_3 and extracted with CH_2Cl_2 (30 mL x 3). The organic phases were collected, dried over anhydrous Na_2SO_4 and evaporated under reduced pressure to afford a yellow oil which was recrystallized from Et_2O to provide pure hydrocodone (**8**). Yield: 0.649 g (89%); pale yellow solid; R_f = 0.35 (CH_2Cl_2/MeOH = 85:15); ^{1}H NMR (300 MHz, $CDCl_3$): δ = 6.69 (d, 1H, J = 8.1 Hz), 6.62 (d, 1H, J = 8.1 Hz), 4.64 (s, 1H), 3.88 (s, 3H), 3.22 (m, 1H), 3.02 (d, 1H, J = 18.3 Hz), 2.62 (m, 2H), 2.43 (s, 3H), 2.39 (m, 1H), 2.30 (m, 1 H), 2.17 (m, 2H), 1.83 (m, 2H), 1.24 (m, 2H) ppm; ^{13}C NMR (75 MHz, $CDCl_3$): δ = 208.1, 145.6, 143.1, 127.4, 126.4, 120.0, 114.7, 91.6, 59.5, 56.9, 53.7, 47.1, 43.1, 42.8, 40.4, 35.6, 25.8, 20.2 ppm. ESI-MS: m/z $[M+H]^+$ calcd for $[C_{18}H_{22}NO_3]^+$ 300.16, found 300.1. ^{1}H NMR, ^{13}C NMR and MS spectra were identical to those reported in the literature [23].

5.2.2.2 Determination of ionization constants and lipophilicity

The water-saturated octan-1-ol (partition-coefficient grade) was used in all partition experiments. The KOH was standardized by titration with potassium hydrogen phthalate, while pH electrode standardization was performed daily by titrating a known amount of HCl with standardized KOH. The titration instrument Sirius PCA200 (Sirius Analytical Instruments, Forrest Row, UK) was employed to perform the pK_a and log *P* assays (25.0±0.1 °C under argon atmosphere). It was equipped with a semi-micro Ross-type pH electrode, quartz precision dispensers for titrant addition, a temperature probe and a micro mechanical stirrer. The operational pH scale was converted to the concentration scale using a four-parameter equation [25].

Alkalimetric sample titrations were performed in 0.15M KCl employing sample concentrations in the low mM-high µM range. All compounds (**1**-**8**) were sufficiently water soluble to perform normal aqueous titrations. All octan-1-ol/water volume ratios were optimized to allow partitioning in the octan-1-ol phase and a proper shift of the aqueous titration curve. The weighting scheme and the iterative least squares refinement of the titration curves both in water and in octan-1-ol/water biphasic partition system have been reported previously [26].

The aqueous ionization constants (pK_a) were estimated from the Bjerrum difference plots and they were refined by a non-linear multi titration-set least squares procedure [26]. The partition coefficient (log *P*) was determined from the difference between the aqueous pK_a of the species and the apparent pK_a (p$_o$$K_a$) estimated from a titration in the presence of the partition solvent. The log *P* constants were refined using data from three or more titrations, each with a different octan-1-ol/water volume ratio and are reported together with their standard deviations.

5.2.2.3 DSC analyses

Thermal stability was estimated using Differential Scanning Calorimetry (DSC1, Mettler Toledo, Greifensee, Switzerland). Samples of about 2.5 mg were loaded into a standard aluminum pan and scanned from 0 to 300°C at a heating constant rate of 20°C/min under constant purging of nitrogen at a rate of 80 mL/min.

5.2.2.4 Water solubility

Saturated solutions of opioids were made in HPLC-grade water. Briefly, a known amount of opioids (about 40 mg) was suspended in 2 mL of solvent under constant stirring at 32°C for 24 h. Then, the suspension was centrifuged at 5000 rpm, 32°C, for 20 min

(Universal 30RF, Hettich Holding GmbH & Co., Kirchlengern, Germany) and then the supernatant was withdrawn, opportunely diluted and analyzed by HPLC.

5.2.2.5 Quantitative determination

The concentration of each opioid derivative was determined by HPLC (HP 1100 ChemStations, Agilent Technologies, Santa Clara, USA). Compound separation was carried out using reverse-phase column (Hypersil Gold C8, 5 μm, 150 x 4.6 mm, Thermo Fisher Scientific Inc., Waltham, USA) and 0.02 M phosphate pH 8 buffer/acetonitrile (75/25) as mobile phase. The flow rate was 1.0 mL/min and the injection volume was 10 μL. The retention time of all opioid derivatives was between 3 and 10 min. The drug concentration was determined at 210 nm by UV spectrophotometer from calibration curves in the range of 0.1-10 μg/mL (R^2<0.999).

5.2.3 In vitro penetration studies

Human epidermis was selected as membrane for the skin permeation studies. The skin used in the permeation studies was obtained from the abdominal skin of two donors, who underwent cosmetic surgery.

Skin samples were prepared following an internal standard procedure [27]. The full-thickness skin was sealed in evacuated plastic bags and frozen at –20°C within 6 h after removal. Prior to experiments, the skin was thawed at room temperature, and the excess of fat was carefully removed. The skin sections were cut into squares of about 2.5 cm^2 and, after immersing the skin in water at 60°C for 1 min, the epidermis was gently separated from the remaining tissue with forceps and carefully inspected by light microscopy for any defects. Afterward, the epidermis was mounted on the Franz diffusion cell whose receptor compartment was filled with degassed phosphate buffer pH 6.5 containing 100 mg/mL NaN_3 as preservative. Special care was given to avoid air bubbles between the buffer and the epidermis in the receptor compartment. The upper and lower parts of the Franz cell were sealed with Parafilm® (Pechiney Plastic Packaging Company, Chicago, USA) and fastened together by means of a clamp, with the epidermis acting as seal between the donor and receptor compartments. Then, the donor compartment was filled with 0.4 mL saturated solution opioids. The system was kept at 37°C with a

circulating water bath, so that the epidermis surface temperature was at 32±1 °C throughout the experiment.

At predetermined times (1, 3, 5, 8, 24 h), 200 µL samples were withdrawn from the receiver compartment and replaced with fresh receiver medium. Sink conditions were maintained throughout the experiments. Samples were analyzed by HPLC according to the method described above. The values were the averages of parallel experiments performed in triplicate using epidermis sheet from two donors (n=6).

At the end of the permeation experiments, the opioid amount retained into epidermis was quantified according to the following procedure. The epidermis sheet was removed from Franz diffusion cell and each side was gently washed with 5 mL of methanol in order to wash out the unabsorbed drug. Subsequently, sample was dried, sliced thinly and placed in 5 mL of fresh methanol. The suspension was soaked in a sonicator for 30 min and then maintained for 24 h at 2-8°C. Finally, the supernatant was 0.45 µm filtered and analyzed by HPLC. The opioid amount retained by the epidermis after 24 h (Epi Q_{ss}) was expressed as micrograms of opioid in milligrams of epidermis.

5.2.4 Data analysis

The cumulative amount permeated through the skin per unit area was calculated from the drug concentration in the receiving medium and plotted as a function of time. The steady state flux (J_{max}) was determined as the slope of the linear portion of the plot. The permeability coefficient was calculated according to the modified Fick's first law of diffusion (**Eq. 5.1**):

$$pK_p = -\log\frac{Jmax}{S} \qquad \textbf{Eq. 5.1}$$

where pK_p (cm/h) is the permeability coefficient and S is the drug donor concentration (µg/cm^3), corresponding to the drug solubility in the vehicle at 32°C.

The concentration in the epidermis at the steady state (Epi Q_{ss}) was expressed as drug concentration in the epidermal layer (µg/mg). In order to exclude the influence of drug solubility on the retention, the Epi Q_{ss} was normalized by drug solubility in the donor phase (S) [13, 28], as showed in **Eq. 5.2**:

$$R_{Q/S} = \frac{Epi\ Q_{ss}}{S}$$ **Eq. 5.2**

The epidermis/transdermal selectivity index ($I_{E/T}$ value) was also calculated for each drug as the ratio between the Epi Q_{ss} and J_{max}. According to Lin et al., $I_{E/T}$ value can be used as descriptor of the molecule affinity to be retained or permeate through human epidermis [28]: the higher $I_{E/T}$ value, the greater affinity of the drug for epidermis (**Eq. 5.3**).

$$I_{E/T}\ value = \frac{Epi\ C_{ss}}{J_{max}}$$ **Eq. 5.3**

5.2.5 Statistical analyses

The effects of substituents (*i.e.*, 3-methoxyl, X_1; 6-carbonyl, X_2; 14-hydroxyl, X_3; 7,8-didehydro, X_4;) on permeation/retention parameters (Log $J_{max,}$ Y_1; Log Epi Q_{ss}, Y_2; pK_p, Y_3; - Log $R_{Q/S}$, Y_4) and solubility (S, Y_5) of the tested drugs were evaluated by JMP 10.0 software (SAS Institute, Cary, USA). Polynomial equations of interactive terms were built in for each dependent variable, as shown by **Eq. 5.4**:

$$Y_i = b_o + b_1X_1 + b_2X_2 + b_3X_3 + b_4X_4 + b_{1,2}X_1X_2 + b_{1,3}X_1X_3 + b_{1,4}X_1X_4 + b_{2,3}X_2X_3 + b_{3,4}X_3X_4$$ **Eq. 5.4**

where Y_i is the dependent variable, b_0 the arithmetic mean response of the runs and b_i the estimated coefficient for the categorical factor X_i. The interaction between carbonyl (X_2) and 7,8-didehydro (X_4) was not considered in the statistical analyses, since it was not present in the considered dataset of molecules.

The main effects represent the average results of changing one factor at a time from its low (absence: - 1) to high level (presence, +1), as represented in **Table 5.1**. The interaction terms (*e.g.*, X1*X2) show how the response changes when two factors are simultaneously changed.

The estimated coefficient of each interaction was calculated according to a symmetric matrix 2x2 made plotting all possible combinations of two substituents. Due to the symmetry of the matrix, two possible cases were taken into consideration in the model: a) the level of substituents was the same (-1, -1; +1, +1) or b) the opposite (-1, +1; +1, -

1). Consequently, the interaction coefficient estimated by the model in case b) had opposite sign vs case a).

For each dependent variable, stepwise backward analyses were built in to exclude negligible terms from the statistical model (p-value to leave: 0.051).

Even if the inter-donor variability might affect the results of statistical analyses, the t-student tests were carried out on each of the considered permeation/retention parameters. The results did not highlight any significant differences. Therefore, the epidermis donor was not considered as block variable.

***Table 5.1** – Chemical substituents present on the chemical structure of morphine derivatives. The code +1 indicates the substituent presence, whereas -1 its absence.*

Compound	**3-methoxyl (X_1)**	**6-carbonyl (X_2)**	**14-hydroxyl (X_3)**	**7,8-didehydro (X_4)**
Morphine	-1	-1	-1	+1
Dihydromorphine	-1	-1	-1	-1
Oxymorphone	-1	+1	+1	-1
Hydromorphone	-1	+1	-1	-1
Codeine	+1	-1	-1	+1
Dihydrocodeine	+1	-1	-1	-1
Oxycodone	+1	+1	+1	-1
Hydrocodone	+1	+1	-1	-1

5.3 Results

5.3.1 Chemistry

Morphine (**1**), codeine (**5**), dihydrocodeine (**6**) and oxycodone (**7**) were purchased as salts and converted into the corresponding free bases by an organic solvent extraction from the basic aqueous solutions and subsequent crystallization or trituration. The syntheses of opioid derivatives (**2**), (**3**), (**4**), (**8**) were accomplished as shown in **Figure 5.2**.

Dihydromorphine (**2**) was obtained in high yield by a palladium-catalyzed high-pressure hydrogenation of morphine hydrochloride in methanol at room temperature. In our conditions, the hydrogenation reaction proceeded in a very satisfactory manner without

any significant undesired isomerization of morphine, despite what described by Metzger [29, 30] and Weiss and Weiner [31].

Indeed, such type of isomerization reactions seems to be promoted by the presence of large amounts of the noble metal catalyst, heating and strong acidic solutions. It is likely that the high ratio starting material/metal catalyst and the high hydrogen pressure employed favored the double bond hydrogenation respect to any other side reaction, providing dihydromorphine (**2**) in high yield. Oxymorphone (**3**) was prepared in very good yield from oxycodone hydrochloride by a standard procedure of *O*-demethylation with boron tribromide in dichloromethane [17].

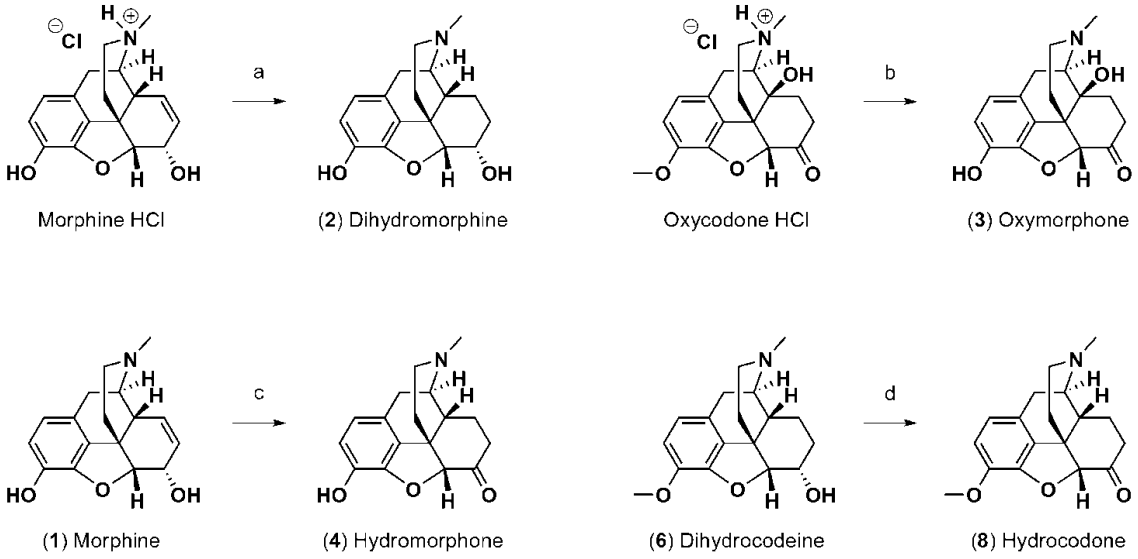

***Figure 5.2** – Reagents and conditions: a) 50 psi H_2, 10% Pd/C, MeOH; b) 1 M BBr3/n-hexane, CH_2Cl_2, 0°C to rt; c) Ru black, H_2SO_4, H_2O, EtOH, 75°C; d) Dess-Martin periodinane, CH_2Cl_2, 0°C to rt.*

Hydromorphone (**4**) was synthesized by refluxing an acidic solution of morphine (**1**) in ethanol and water in the presence of ruthenium as catalyst, following a procedure known from the literature [19]. Finally, hydrocodone (**8**) was obtained in high yield via Dess-Martin oxidation of dihydrocodeine (**6**). The same procedure was described in a recent work by Varghese and Hudlicky [23]. All the free bases synthesized were obtained in a pure form by methods of extraction and crystallization or trituration from organic solvents.

5.3.2 Physicochemical characterization

The solubility at saturation, log *P* and melting temperature (T_m) of the tested compounds are reported in **Table 5.2**. The codeine derivatives were more water-soluble than morphine ones: dihydrocodeine had the highest solubility, whereas morphine the lowest. Among codeine derivatives, oxycodone was an exception, since its solubility was near to morphine one (p=0.64). It is noteworthy that 7,8-didehydro absence increased the solubility of both morphine and codeine. Indeed, the solubility of dihydromorphine was 6-fold higher than morphine. The presence of 3-methoxyl also increased the lipophilicity of molecules (p<0.0001).

***Table 5.2** – Physicochemical parameters of tested molecules. The results are expressed as mean values ± St. Dev. (n=3).*

Compound	**Solubility (mg cm^{-3})**	**Amine pK$_a$**	**log *P***	**T$_m$ (°C)**
Morphine	0.299± 0.006	8.16±0.01	0.89±0.01	256.5±0.1
Dihydromorphine	1.997±0.135	8.46±0.02	0.87±0.01	-[a]
Oxymorphone	4.919±0.501	8.30±0.01	0.74±0.01	245.1±0.0
Hydromorphone	2.652±0.163	8.17±0.01	0.93±0.01	258.6±0.2
Codeine	9.366±0.578	8.28±0.01	1.18±0.01	156.4±0.2
Dihydrocodeine	14.923±2.246	8.87±0.01	1.31±0.01	-[b]
Oxycodone	0.310±0.039	8.89±0.01	1.47±0.01	221.9±0.0
Hydrocodone	3.123±0.250	8.28±0.01	1.41±0.01	176.3±0.2

[a] T_g = 91.1±0.9 °C; [b] T_g = 37.1±1.0 °C

These findings were confirmed by the statistical analyses. The linear multiple regressions suggested that all substituents significantly influenced the water solubility (**Table 5.3**) and the resulting polynomial equation strongly fitted with experimental data (p<0.0001; R^2=1.00; R^2_{Adj}=1.00; F Ratio=706.03; **Eq. 5.5**).

$$LogS = 3.15 + 0.07X_1 - 0.14X_2 - 0.19X_3 - 0.26X_4 - 0.20X_1X_2 - 0.32X_1X_3 + 0.16X_1X_4 \quad \textbf{Eq. 5.5}$$

The statistical model confirmed that 3-methoxyl (X_1) positively influenced molecule solubility (p<0.0001). The regression results also evidenced the synergic effect of 3-

methoxyl and 7,8-didehydro on drug solubility (X_1*X_4: $p<0.0001$). On the contrary, other substituents negatively affected the drug solubility both alone ($p<0.0001$) and in combination with 3-methoxyl ($p<0.0001$).

Finally, T_m of morphine derivatives were in agreement to literature data, with the exception of dihydromorphine and dihydrocodeine. Surprisingly, the thermal analyses showed glassy transitions, whereas melting temperatures were reported in literature [32]. The glass transition temperature (T_g) of dihydromorphine and dihydrocodeine were 91.1±0.9 °C and 37.1±1.0 °C, respectively (**Table 5.2**). Moreover, the lowest T_g value registered for dihydrocodeine justified the highest solubility of such a compound.

***Table 5.3** – Effect of substituents on Log S, Log J_{max}, pK_p, Log Epi Q_{ss}, - Log $R_{Q/Si}$. The interaction effect reported in table is obtained when the level of both substituent is the same (+1, +1; -1, -1). Vice versa, the interaction effect has opposite impact on penetration parameters when substituent level had opposite sign (+1, -1;-1, +1).*

Substituent	**Log S**	**Log J_{max}**	**pK_p**	**Log (Epi Q_{ss})**	**- Log $R_{Q/S}$**
X_1	increase$^{\#}$	increase$^{\#}$	decrease$^{\#}$	decrease$^{\#}$	increase$^{\#}$
X_2	decrease$^{\#}$	decrease*	-	decrease*	-
X_3	decrease$^{\#}$	decrease*	-	decrease$^{\#}$	-
X_4	decrease$^{\#}$	decrease*	-	decrease*	decrease*
Interactions					
X_1*X_2	decrease$^{\#}$	decrease*	-	decrease$^{\#}$	-
X_1*X_3	decrease$^{\#}$	decrease$^{\#}$	-	decrease$^{\#}$	-
X1*X4	increase$^{\#}$	-	increase*	-	-
X_2*X_3	-	-	-	-	-
X_3*X_4	-	-	-	-	-

$^{\#}$ $p<0.001$ by Fisher test. * $p<0.05$ by Fisher test.

5.3.3 In vitro penetration studies

The cumulative amounts of tested compounds permeated through the human epidermis in 24 h are shown in **Figure 5.3**. At a first glance, the permeation profiles evidenced that 3-methoxyl significantly increased the drug diffusion through the human epidermis. Indeed, J_{max} values of codeine derivatives resulted significantly higher than other compounds (**Table 5.4**; $p<0.01$).

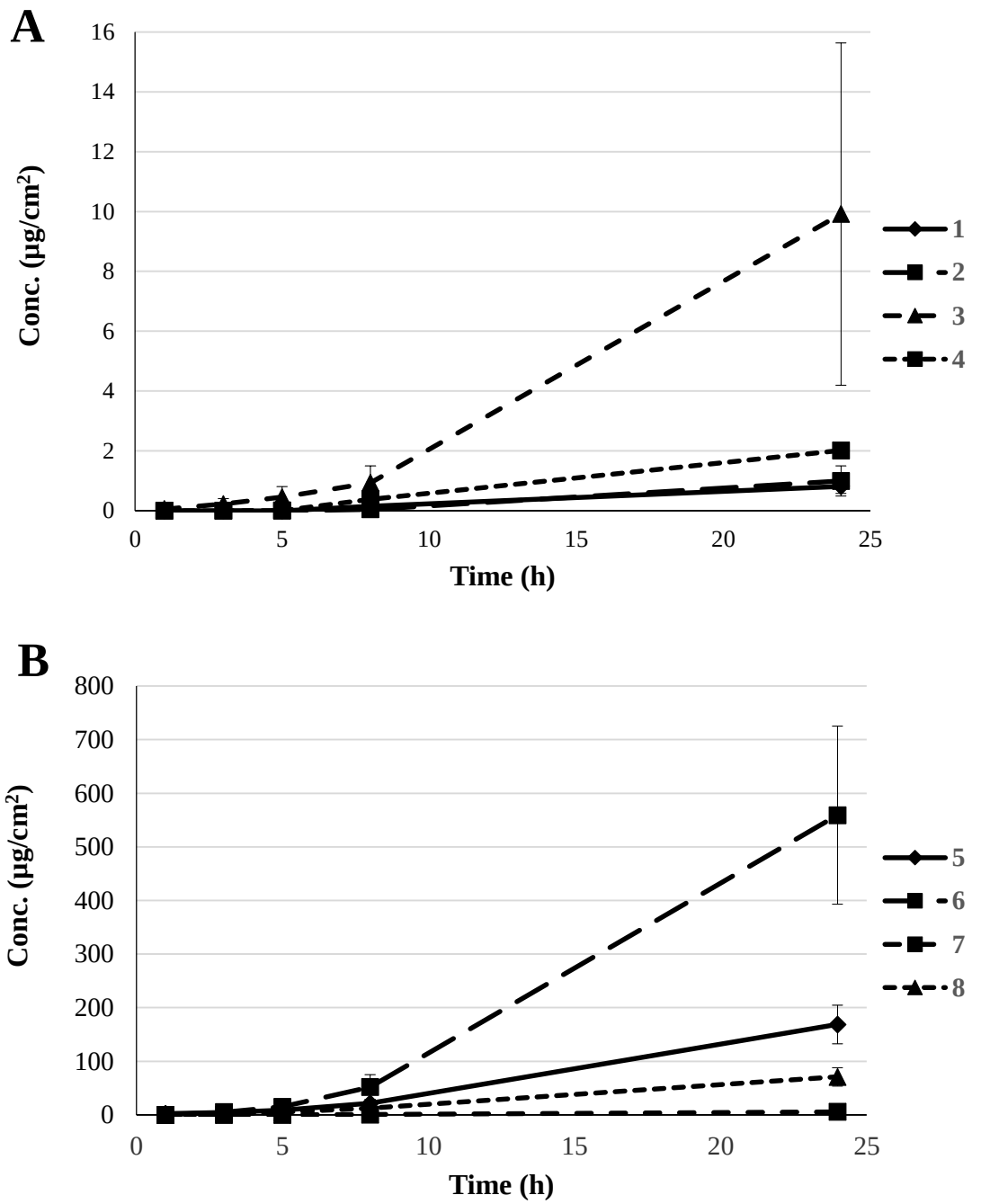

***Figure 5.3** – Permeation profiles of morphine (**A**) and codeine (**B**) derivatives. (n=6, mean value ± SEM.). Morphine derivatives are morphine (**1**), dihydromorphine (**2**), oxymorphone (**3**) and hydromorphone (**4**). Codeine derivatives are codeine (**5**), dihydrocodeine (**6**), oxycodone (**7**) and hydrocodone (**8**).*

The highest J_{max} was reported for dihydrocodeine, whereas the lowest for the morphine. Indeed, J_{max} values calculated for codeine derivatives resulted significantly higher than other compounds (**Table 5.4**; $p<0.01$). J_{max} of oxycodone was the only exception and its

flux value was similar to morphine derivatives. The permeation coefficients confirmed this trend: the pK_p values of codeine derivatives resulted the lowest among the tested molecules.

***Table 5.4** – Penetration data and $I_{E/T}$ values of tested compounds (mean ± sd; donors=2, n=6).*

Compound	J_{max} (µg cm^{-2} h^{-1})	pK_p (cm h^{-1})	Epi Q_{ss} (µg mg^{-1})	- Log $R_{Q/S}$ (cm^3 mg^{-1})	$I_{E/T}$
Morphine	0.05±0.02	3.88±0.29	0.64±0.27	2.72±0.29	12.80
Dihydromorphine	0.21±0.20	4.22±0.55	1.50±0.78	3.16±0.24	7.14
Oxymorphone	0.58±0.70	4.24±0.58	4.68±2.54	3.09±0.25	8.07
Hydromorphone	0.11±0.07	4.47±0.34	2.81±1.64	3.04±0.24	25.55
Codeine	9.60±3.39	3.21±0.15	6.44±2.26	3.18±0.21	0.67
Dihydrocodeine	36.25±14.28	2.64±0.18	8.03±0.89	3.27±0.22	0.22
Oxycodone	0.40±0.41	3.07±0.45	0.10±0.05	3.52±0.26	0.25
Hydrocodone	4.19±1.43	2.90±0.17	2.10±0.82	3.20±0.18	0.50

The polynomial equations (**Eq. 5.6** and **Eq. 5.7**) obtained for permeation parameters fitted with the experimental data (**Figure 5.4**), allowing to identify the significant contribute of each substituent to the permeation process (**Table 5.4**).

$$Log\ J_{max} = -0.90 + 1.36X_1 - 0.60X_2 - 0.39X_3 - 0.60X_4 - 0.44X_1X_2 - 0.96X_1X_3$$

$p<0.0001$; $R^2=0.89$; $R^2_{adj}=0.88$; F ratio=57.32 **Eq. 5.6**

$$pK_p = 3.58 - 0.53X_1 + 0.19X_1X_4$$ **Eq. 5.7**

$p<0.0001$; $R^2=0.76$; $R^2_{adj}=0.74$; F ratio=69.89

The statistical results confirmed the predominant effect of 3-methoxyl (X_1) on the permeation process through the skin. Indeed, 3-methoxyl determined an increase of J_{max} ($p<0.0001$) and a significant decrease pK_p values ($p<0.0001$), suggesting that its effect on diffusion process was due to an improvement of epidermal diffusivity of the molecule through the human epidermis other than to the increase of drug solubility.

The presence of other substituents on molecule backbone had an opposite effect on J_{max} (X_2, p=0.0012; X_3, p=0.0317; X_4, p=0.0013) and resulted ineffective on pK_p values, suggesting that, conversely to 3-methoxyl, they influenced only the concentration gradient. Moreover, the 3-methoxyl/6-carbonyl (X_1*X_2; p=0.0056) or 3-methoxyl/14-hydroxyl (X_1*X_3; p<0.0001) interactions had a detrimental effect on the flux (**Eq. 5.6**). These findings were in agreement with the highest J_{max} of dihydrocodeine, having only 3-methoxyl among the considered substituents, and the lowest values of morphine (**Table 5.4**).

The trend observed in the case of J_{max} and pK_p were significantly different from that observed in the case of the amount retained from the skin at the end of experiments (Epi Q_{ss}). In this case, the highest Epi Q_{ss} values were found in the case of dihydrocodeine, codeine, and oxymorphone. Furthermore, the retention seemed to be correlated to drug solubility, as shown by **Eq. 5.8**.

$$Log(Epi\ Q_{ss}) = -6.81 + 0.94LogS \qquad \textbf{Eq. 5.8}$$

p<0.0001; R^2=0.75; R^2_{adj}=0.74; F ratio=136.86

However, the experimental results cannot be explained considering only water solubility as the key parameter for partition of the morphine derivative from the donor solution to the human epidermis. As an example, Epi Q_{ss} for morphine resulted about 6-fold higher than that of oxycodone (**Table 5.4**), although the solubility was comparable (**Table 5.2**).

In the case of Epi Q_{ss}, the statistical analysis evidenced that all considered substituents influenced the drug amount retained by the epidermis (**Eq. 5.9**)

$$Log(Epi\ Q_{ss}) = 0.06 - 0.42X_1 - 0.21X_2 - 0.63X_3 - 0.29X_4 - 0.56X_1X_2 - 0.89X_1X_3 \qquad \textbf{Eq. 5.9}$$

p<0.0001; R^2=0.89; R^2_{adj}=0.88; F ratio=56.90

In particular, all significant factors determined a decrease of drug concentration in epidermis. It should be also underlined that among the main factors, 14-hydroxyl (X_3) along with interactions between 3-methoxyl and 6-carbonyl (X_1*X_2) or 14-hydroxyl (X1*X3) showed the greater coefficients and the most significant effect (p<0.0001),

justifying the lowest Epi Q_{ss} values determined in the case of oxycodone, which has all these substituents.

On the contrary, the most of the significant effects observed in **Eq. 5.9** became negligible when – Log $R_{Q/S}$ was used as retention descriptor (**Eq. 5.10**).

$$-LogR_{Q/S} = 3.08 + 0.14X_1 - 0.13X_4 \qquad \textbf{Eq. 5.10}$$

$p<0.0001$; $R^2=0.41$; $R^2_{adj}=0.38$; F ratio=15.44

The stepwise backward analyses showed that 3-methoxyl and 7,8-didehydro were the only effects to remain significant when – Log $R_{Q/S}$ was used as retention descriptor. In particular, the presence of 3-methoxyl (X_1; $p<0.0001$) increased the – Log $R_{Q/S}$, whereas the 7,8-didehydro (X_4; $p<0.0013$) had an opposite effect. Since the low correlation of **Eq. 5.10**, the results of stepwise backward analyses were checked by one-way ANOVA analyses. These further tests confirmed 3-methoxyl (X_1; $p<0.0003$) and 7,8.-didehydro (X_4; $p<0.0057$) to be significant for drug retention, suggesting that the influence of both substituents on the drug retention was independent of the drug solubility in the donor phase.

The estimated X_1 coefficient in **Eq. 5.10** is consistent with the value in **Eq. 5.9**, showing that 3-methoxyl negatively affected the drug retention in the human epidermis. On the other side, the coefficients of X_4 had an opposite effect of 7,8-didehydro according to the retention descriptor taken into account (**Table 5.3**). When Epi Q_{ss} was considered, the results of statistical analyses showed that 7,8-didehydro decreased the drug concentration in the human epidermis (b_4 = - 0.29; **Eq. 5.9**). On the contrary, its negative effect on – Log $R_{Q/S}$ suggested that X_4 increased drug retention (b_4 = - 0.13; **Eq. 5.10**). This incongruity might be explained considering that drug solubility influenced only Epi Q_{ss} and not –Log $R_{Q/S}$. Thus, the negative effect of X_4 on Epi Q_{ss} was related to the decrease of drug solubility in the donor phase (**Table 5.3**). These findings are in agreement with the experimental data. For example, the lower solubility of codeine justified its lower Epi Q_{ss} in comparison to dihydrocodeine values (**Table 5.2** and **Table 5.4**). Moreover, no differences were observed in – Log $R_{Q/S}$ values of both molecules, suggesting that lower Epi Q_{ss} of codeine was only due to drug solubility.

Therefore, **Eq. 5.10** better described the influence of 7,8-didehydro on the drug retention than **Eq. 5.9**, since it exclude the ancillary effect of drug solubility.

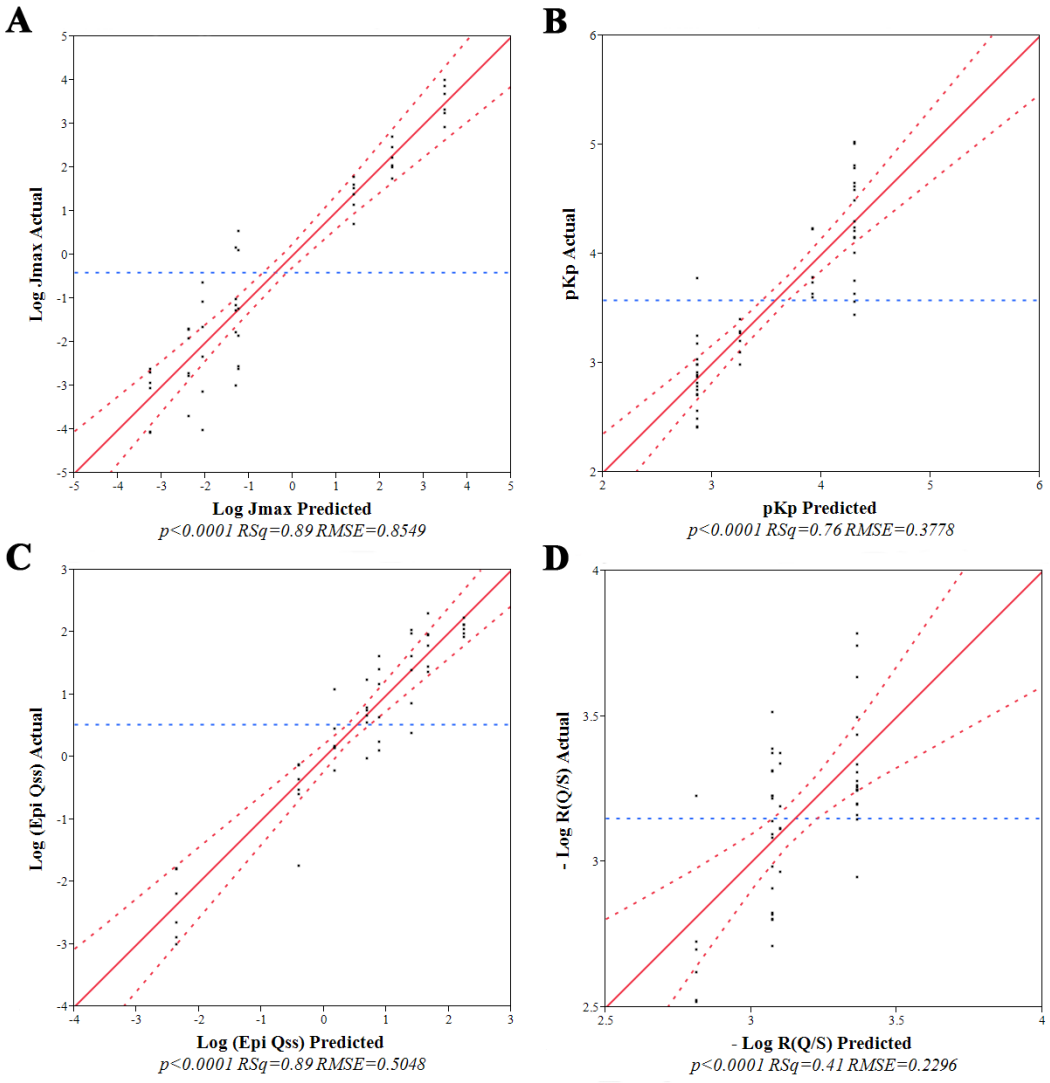

***Figure 5.4** – Actual and predicted plot of the linear multiple regression analyses on the substituent effect on Log J_{max} **(A)**, pK_p **(B)**, Epi Q_{ss} **(C)** and – Log $R_{Q/S}$ **(D)**.*

5.4 Discussion

The permeation data were consistent with those reported in literature, confirming that morphine derivatives slowly permeated through human skin [33]. Statistical analyses revealed significant correlations between chemical modifications on morphine structure and the permeation process. At a first glance, the gradient concentration between donor and receiver compartments seemed to govern the passive diffusion of these molecules through the human epidermis. In other words, the higher the water solubility, the higher the flux ($p<0.0001$; $R^2=0.72$, $R^2_{adj}=0.72$; $F=119.82$).

However, 3-methoxyl determined an increase of J_{max} and a significant decrease in pK_p values, suggesting that its effect on diffusion process was due to an improvement of epidermal diffusivity of the molecule through the human epidermis other than the increase of the concentration gradient.

In order to evaluate the goodness of linear regression in predicting the drug permeation through human epidermis, the model proposed by Potts and Guy [8] was applied to the experimental data of morphine derivatives. The results showed that the Potts and Guy model fitted well with the dataset ($p<0.0001$; $R^2=0.63$; $R^2_{adj}=0.62$, F ratio=39.10). However, its low R^2_{adj} suggested that such a linear regression model was less accurate in predicting permeation of morphine derivatives than the model described by **Eq. 5.7**. Indeed, the bias between predicted and experimental pK_p values of dihydrocodeine was twice higher when pK_p was calculated by the Potts and Guy equation (17.6%) than by **Eq. 5.7** (8.2%).

The lack of fit of the Potts and Guy model can be explain in term of molecular weight. In the case of morphine derivatives, the considered range was too narrow to influence significantly the drug permeation. Indeed, the statistical analyses emphasized the key role of drug lipophilicity (log *P*) in determining the skin permeation (leverage $p<0.0001$), whereas the effect of molecular weight was negligible (leverage $p=0.6030$).

Moreover, retained drug amount was demonstrated to correlate to the drug concentration gradient as well as permeation process (**Eq. 5.8**). However, the substituent effect on drug retention was not only justified by its effect on solubility, as shown by **Eq. 5.10**. In line with literature data [13, 28], normalizing drug retention by solubility ($R_{Q/S}$) permitted to

discriminate which substituent effect on retention was influenced by solubility. For example, 3-methoxyl (X_1) had a positive influence on the drug solubility (**Eq. 5.5**), whereas it negatively affected the drug retention in epithelial layer. These findings are in agreement with permeation results: since 3-methoxyl was able to improve drug diffusivity through the epidermis, it significantly decrease Epi Q_{ss} and increase – Log $R_{Q/S}$.

The low correlation of the linear regression equation obtained for – Log $R_{Q/S}$ demonstrated that retention process might not be modelled only on the base of chemical structure modifications (**Eq. 5.10**). Furthermore, the use of physicochemical parameters (*i.e.*, molecular weight, log *P*) as model descriptors were linked to a similar lack of fit ($p<0.0001$; $R^2=0.38$; $R^2_{adj}=0.35$; F ratio = 13.75) [13], suggesting that the retention process might be modelled introducing also descriptors based on composition of upper layers of human skin. The stratum corneum barrier function is due to a multi-layered wall-like structure in which flat keratinized corneocytes are embedded in a lipophilic network of ceramides, cholesterol esters and fatty acids. In particular, ceramides are essential since their key-role in the lipophilic network organization [34] and are able to modulate the drug permeation through epidermis according to the relative concentration of the ceramides types in the upper layers of human skin [35]. Therefore, the development of predicting models able combine the physicochemical properties of molecules and their interaction with epidermal constituents might be an challenging solution for solving the lack of fit of proposed modelling approach.

In order to select the most suitable compound for designing a dosage form intended for the local treatment of topical painful syndromes, the minimization of the skin permeation and the maximization of the skin retention are highly desirable. Firstly, the overall results on morphine revealed one of the lowest Epi Q_{ss} value and J_{max}. Although the Epi Q_{ss} data might induce to discard morphine as candidate for topical treatment, the low permeation flux suggested a lower incidence of systemic side effect than other more permeable morphine derivatives. Indeed, $I_{E/T}$ value is an order of magnitude higher than codeine derivatives and it was comparable or slightly lower with respect to the parent compounds.

Furthermore, the results identified hydromorphone as another suitable alternative to be topically applied for cutaneous pain management. Hydromorphone exhibited a very low flux through the human epidermis (*i.e.*, the highest pK_p value) and Epi Q_{ss} was 4-fold

higher than morphine. Therefore, hydromorphone resulted the morphine derivative with the highest affinity for epidermis retention (highest $I_{E/T}$ value, **Table 5.4**) among the considered set of compounds.

5.5 Conclusion

The overall results highlighted that the permeation and retention of morphine derivatives may be modelled according to the small modification on their chemical structure. Such an approach appears accurate in predicting drug permeation. In particular, the statistical analyses indicated that 3-methoxyl group played a key role in governing the skin penetration of morphine derivatives through human skin. In contrary, the low R^2 of linear regression model for – Log $R_{Q/S}$ demonstrated that physicochemical properties of molecules might be not enough for modelling the retention process, suggesting the need to deeply understand the retention process taking in consideration the epithelial features.

Moreover, the retention/permeation affinity index confirmed that morphine was a good candidate for treating cutaneous painful symptomatology, although low Epi Q_{ss}. Interestingly, the statistical results suggested that hydromorphone can represent a good alternative to morphine thanks to its greater affinity for human epidermis as well as a relatively higher potency [36].

Finally, the study also underlined that dihydromorphine and dihydrocodeine bases were not achievable as crystals, but only in amorphous state. These findings justified the higher solubility of such drugs and, therefore, the higher fluxes with respect to the parent compounds, namely morphine and codeine.

5.6 References

[1] Santini, D., Lanzetta, G., Dell'Aquila, E., Vincenzi, B., Venditti, O., Russano, M., Papapietro, N., Denaro, V., Tonini, G., and Ripamonti, C., 2013, "'Old' and 'new' drugs for the treatment of cancer pain," Expert Opin. Pharmacother., 14(4), pp. 425-433.

[2] Graham, T., Grocott, P., Probst, S., Wanklyn, S., Dawson, J., and Gethin, G., 2013, "How are topical opioids used to manage painful cutaneous lesions in palliative care? A critical review," PAIN, 154(10), pp. 1920-1928.

[3] LeBon, B., Zeppetella, G., and Higginson, I. J., 2009, "Effectiveness of Topical Administration of Opioids in Palliative Care: A Systematic Review," J. Pain Symptom Manage., 37(5), pp. 913-917.

[4] Stein, C., and Küchler, S., 2012, "Non-analgesic effects of opioids: Peripheral opioid effects on inflammation and wound healing," Curr. Pharm. Des., 18(37), pp. 6053-6069.

[5] Roy, S. D., and Flynn, G. L., 1990, "Transdermal delivery of narcotic analgesics: pH, anatomical, and subject influences on cutaneous permeability of fentanyl and sufentanil," Pharm. Res., 7(8), pp. 842-847.

[6] Lane, M. E., 2013, "The transdermal delivery of fentanyl," Eur. J. Pharm. Biopharm., 84(3), pp. 449-455.

[7] Stinchcomb, A. L., Paliwal, A., Dua, R., Imoto, H., Woodard, R. W., and Flynn, G. L., 1996, "Permeation of buprenorphine and its 3-alkyl-ester prodrugs through human skin," Pharm. Res., 13(10), pp. 1519-1523.

[8] Potts, R. O., and Guy, R. H., 1992, "Predicting skin permeability," Pharm. Res., 9(5), pp. 663-669.

[9] Magnusson, B. M., Anissimov, Y. G., Cross, S. E., and Roberts, M. S., 2004, "Molecular size as the main determinant of solute maximum flux across the skin," J. Invest. Dermatol., 122(4), pp. 993-999.

[10] Potts, R. O., and Guy, R. H., 1995, "A predictive algorithm for skin permeability: The effects of molecular size and hydrogen bond activity," Pharm. Res., 12(11), pp. 1628-1633.

[11] Lian, G., Chen, L., and Han, L., 2008, "An evaluation of mathematical models for predicting skin permeability," J. Pharm. Sci., 97(1), pp. 584-598.

[12] Roberts, M. S., Cross, S. E., and Anissimov, Y. G., 2004, "Factors affecting the formation of a skin reservoir for topically applied solutes," Skin Pharmacol. Physiol., 17(1), pp. 3-16.

[13] Cross, S. E., and Roberts, M. S., 2008, "Use of in vitro human skin membranes to model and predict the effect of changing blood flow on the flux and retention of topically applied solutes," J. Pharm. Sci., 97(8), pp. 3442-3450.

[14] Koizumi, H., Yokoshima, S., and Fukuyama, T., 2010, "Total Synthesis of (-)-Morphine," Chem. Asian J., 5(10), pp. 2192-2198.

[15] Przybyl, A. K., Flippen-Anderson, J. L., Jacobson, A. E., and Rice, K. C., 2003, "Practical and High-Yield Syntheses of Dihydromorphine from Tetrahydrothebaine and Efficient Syntheses of (8S)-8-Bromomorphide," J. Org. Chem., 68(5), pp. 2010-2013.

[16] Varadi, A., Gergely, A., Beni, S., Jankovics, P., Noszal, B., and Hosztafi, S., 2011, "Sulfate esters of morphine derivatives: Synthesis and characterization," Eur. J. Pharm. Sci., 42(1-2), pp. 65-72.

[17] Kvernenes, O. H., Nygard, A. M., Heggelund, A., and Halvorsen, H., 2007, "Process useful in the preparation of morphinan antagonists," Alpharma Aps, Den. . p. 34 pp.

[18] Kok, G. B., and Scammells, P. J., 2012, "Improved synthesis of 14-hydroxy opioid pharmaceuticals and intermediates," RSC Adv., 2(30), pp. 11318-11325.

[19] Gindelberger, D. E., 2011, "Heterogeneous ruthenium metal catalyst for the production of hydrocodone, hydromorphone or a derivative thereof," Mallinckrodt Inc., USA . p. 32pp.

[20] Smith, P. R., Frohwein, A. K., Hays, P. A., and Lurie, I. S., 2005, "Identification and quantitation of hydromorphone hydrochloride in Palladone (extended time-release) capsules," Microgram J., 3(1-2), pp. 39-45.

[21] Bailey, T. S., Gee, P. S., and Rezaie, R., 2006, "Process for the synthesis of hydromorphone," Australia . p. 10 pp.

[22] Trost, B. M., and Tang, W., 2002, "Enantioselective Synthesis of (−)-Codeine and (−)-Morphine," J. American Chem. Soc., 124(49), pp. 14542-14543.

[23] Varghese, V., and Hudlicky, T., 2013, "Total Synthesis of Dihydrocodeine and Hydrocodone via a Double Claisen Rearrangement and C-10/C-11 Closure Strategy," Synlett, 24(3), pp. 369-374.

[24] Tavakol, H., Esfandyari, M., Taheri, S., and Heydari, A., 2011, "Investigation of structure, vibrational and NMR spectra of oxycodone and naltrexone: A combined experimental and theoretical study," Spectrochim. Acta A Mol. Biomol. Spectrosc., 79(3), pp. 574-582.

[25] Avdeef, A., 1992, "PH-Metric log P. Part 1. Difference plots for determining ion-pair octanol-water partition coefficients of multiprotic substances," Quantitative Structure-Activity Relationships, 11(4), pp. 510-517.

[26] Avdeef, A., 1993, "pH-metric log P. II: Refinement of partition coefficients and ionization constants of multiprotic substances," J. Pharm. Sci., 82(2), pp. 183-190.

[27] Cilurzo, F., Alberti, E., Minghetti, P., Gennari, C. G. M., Casiraghi, A., and Montanari, L., 2010, "Effect of drug chirality on the skin permeability of ibuprofen," Int. J. Pharm., 386(1–2), pp. 71-76.

[28] Lin, C.-F., Hwang, T.-L., Al-Suwayeh, S. A., Huang, Y.-L., Hung, Y.-Y., and Fang, J.-Y., 2013, "Maximizing dermal targeting and minimizing transdermal penetration by magnolol/honokiol methoxylation," Int. J. Pharm., 445(1–2), pp. 153-162.

[29] Metzger, H., 1935, "Dihydromorphinones," Knoll AG Chemische Fabriken, pp. Addn. to 607,931 (C. A. 629, 4030.4034).

[30] Metzger, H., 1936, "Dihydromorphinones," Knoll AG Chemische Fabriken, pp. Addn. to 607,931 (C. A. 629, 4030.4034).

[31] Weiss, U., and Weiner, N., 1949, "The isomerization of morphine to O-desmethylthebainone," J. Org. Chem., 14(2), pp. 194-203.

[32] Goto, K., 1940, "Formation of (+)-dihydrocodeine and (+)-dihydromorphine from sinomenine," Proc. Imp. Acad. (Tokyo), 16, pp. 403-404.

[33] Roy, S., and Flynn, G., 1989, "Transdermal Delivery of Narcotic Analgesics: Comparative Permeabilities of Narcotic Analgesics Through Human Cadaver Skin," Pharm. Res., 6(10), pp. 825-832.

[34] Corbe, E., Laugel, C., Yagoubi, N., and Baillet, A., 2007, "Role of ceramide structure and its microenvironment on the conformational order of model stratum corneum lipids mixtures: an approach by FTIR spectroscopy," Chem. Phys. Lipids, 146(2), pp. 67-75.

[35] Školová, B., Janůšová, B., Zbytovská, J., Gooris, G., Bouwstra, J., Slepička, P., Berka, P., Roh, J., Palát, K., Hrabálek, A., and Vávrová, K., 2013, "Ceramides in the Skin Lipid Membranes: Length Matters," Langmuir, 29(50), pp. 15624-15633.

[36] Barnett, M., 2001, "Alternative opioids to morphine in palliative care: A review of current practice and evidence," Postgrad. Med. J., 77(908), pp. 371-378.

6 *Final remarks*

This doctoral thesis dealt with the critical delivery aspects of three loco-regional cancer-related syndromes and proposed technological solutions for rationalizing the drug delivery. In particular, the experimental work permitted (1) to develop a mucoadhesive formulation to guarantee a prolonged drug penetration in the buccal cavity; (2) to optimize a nanoparticle system intended for the resveratrol delivery to cochlea; (3) to rationalize the dermal delivery of morphine derivatives on the base of their chemical structure and identify the best opioid candidate for skin permeation and retention among the most used morphine derivatives in clinics.

The mucoadhesive microparticle suspension (MMS) was proposed as a technological platform for delivering drugs intended for the treatment of oral mucositis (**Chapter 2**). The MMS combined the advantages of liquid and semisolid drug products intended for buccal delivery. First of all, it can be easily handled as liquid solution and it might avoid the fast elimination of drugs by swallowing as well as semisolid dosage forms. Moreover, being made with alginate, microparticles were conveniently prepared in one-step process. The selection of poly-acrylates as bioadhesive polymers permitted to obtain microparticles with a reproducible morphology and satisfactory mucoadhesive properties. The loading of drugs with different physicochemical properties showed that MMS is a robust technological platform for the delivery of several candidates intended for treating oral mucositis (OMs). Moreover, the *in vitro* studies showed that the use of MMS might be more advantageous than other conventional dosage forms for buccal delivery. In fact, the *in vitro* increase of the drug penetration in mucosa suggested that MMS might allow the *in vivo* reduction of the drug dose and regimen.

Resveratrol-loaded nanoparticles were proposed for treating cisplatin-induced ototoxicity (**Chapter 4**). Such technological platform has the double advantage to be theoretically suitable both for intra-tympanic and systemic administration. Indeed, the same nanoparticle system was able to diffuse through round window membrane in guinea pigs (**Appendix 4.1**). The PLGA-based matrix could also control the drug release better than other similar delivery systems published in literature, reducing the drug amount released before the intracellular uptake. Preliminary uptake studies revealed a significant effect of

resveratrol on mitochondrial metabolism suggesting that it might be released in the cellular environment. Furthermore, the *in vitro* toxicity studies indicated that nanosystem was safe for cochlear cell lines.

In both cases, Design of Experiments (DoE) was efficiently applied for rationalizing the development of the proposed delivery systems. Since DoE was introduced in academic and pharmaceutical industry, its application allows to better understand the effect of formulative and process parameters on the final product properties. In particular, the use of a 2^3 factorial design permitted to screen the influence of poly-acrylate polymer and air pressure setting on the microparticle morphology and *in vitro* clobetasol mucosal penetration (**Chapter 3**). The Box-Behnken Design (BBD) was applied to the development of resveratrol-loaded nanoparticles (**Chapter 4**). It allowed to clarify the influence of nanoparticle composition on the morphology and other critical properties and to identify an optimal formulation. Moreover, the Monte Carlo simulations showed how much robust the features of optimal formulation were to stochastic errors in the preparation process. Such an approach showed the importance of combining DoE and simulation tools for the improvement of the model accuracy and robustness in drug product development.

Finally, the experimental work provided useful data for the selection of opioid molecules intended for dermal delivery (**Chapter 5**). According to literature, the effectiveness of opioids in the treatment of cutaneous painful syndromes was demonstrated by empirical evaluation of clinical cases, rather than deep investigation of their pharmacological activity or skin permeation profiles. The current investigation highlighted that permeation and retention were influenced by presence and/or absence of specific substituents on the chemical structure of the considered morphine derivatives. In particular, the overall results suggested that the phenolic ring substitution might be critical for the modulation of the drug affinity to permeate or be retained in the human skin. Among the eight morphine derivatives, hydromorphone resulted as the most promising compound for obtaining a local effect in the human skin. Indeed, due to the highest retention/permeation index ($I_{E/T}$ value), the hydromorphone had the highest affinity to the epidermal layer among tested molecules, one of the lowest flux through the human epidermis and a relative potency higher than morphine.

Acknowledgements

I would like to acknowledge the many people who have trusted and supported me during my PhD program.

First of all, I would like to thank prof. Paola Minghetti, prof. Luisa Montanari and prof. Bi-Botti Youan for being an example for me and for pushing me in this challenging adventure.

I would like to thank dr. Antonella Casiraghi, dr. Francesco Cilurzo, dr. Chiara M.G. Gennari, dr. Francesca Selmin for the teachings, the support, the help and the patience they have had with me in these years.

I would like to dr. Ibrahima Youm, dr. Ezoulin Miezan, dr. Tao Zhang, Vivek Agrahari, Jianing Meng, Albert N'Go, Fohona Coulibaly for introducing me in the nanoscale world and for making my visiting period at UMKC School of Pharmacy great.

I would like to thank dr. Clelia Dallanoce, dr. Carlo Matera and all member of laboratory of prof. De Amici for their work on the synthesis of the morphine derivatives and for supporting me in the preparation of Chapter 5.

Last but not least, I would like to thank a lot all my colleagues and friends for sharing their time and personal experience with me: you helped making these three years in via C. Colombo 71 fantastic.

Thank to Marco Colombo, Paolo Gerosa and Silvia Locati for the friendship and for helping me in the experimental work of Chapter 2, 3, 5.

Thanks to Elena M., Federica C., Giustino D.P., Ilaria F., Iolanda P., Laura M., Paolo R., Silvia F., Ardita N., Clara P., Doriana P., Federica A.C., Laura R., Alessandro D.G., Andrea M., Anna B., Caterina P., Cristina B., Diana Y., Halvin B., Ilaria L., Leonardo S., Luca B., Marco B., Martina A., Martina M., Matteo F., Michele N., Paolo C., Rossella S., Ruggero T., Simona P., Stefano R., Valentina C., Valeria D.N., Zhyljeta G.